From Structure, to Function, to Pathogenesis: Understanding the Immunological Consequences of The Unique Peptidoglycan of *Borrelia burgdorferi*

Marisela M. Davis

Thesis submitted to the faculty of the Virginia Polytechnic Institute and State University in partial fulfillment of the requirements for the degree of

Master of Science
In
Life Sciences

Brandon L. Jutras (chair)
Caroline N. Jones
Zhijian (Jake) Tu

May 7th, 2020
Blacksburg, Virginia

Keywords: Lyme disease, *Borrelia burgdorferi*, peptidoglycan, innate/adaptive immunity

From Structure, to Function, to Pathogenesis: Understanding the Immunological Consequences of The Unique Peptidoglycan of *Borrelia burgdorferi*

Marisela M. Davis

Scientific Abstract

The bacterial pathogen responsible for Lyme disease — *Borrelia burgdorferi*— is an atypical Gram-negative spirochete that is transmitted to humans via the bite of an infected *Ixodes* tick. Like all Gram-negative bacteria the structural portion of the cell envelope known as peptidoglycan (PG) is sandwiched between the inner and outer membranes. Unlike virtually all bacteria, this PG layer is unique in *B. burgdorferi* in that the amino acid structure differs from most Gram-negative and Gram-positive bacteria by the addition of an Ornithine residue to the third amino acid location in the crosslinking structure. This unique motif is hypothesized to be responsible for the unusual clinical manifestations seen in Lyme disease, specifically Lyme arthritis, the most common late stage symptom of the disease in the United States. Peptidoglycan is only one component of the cell envelope in *B. burgdorferi* though; other portions of the cell envelope remain understudied specifically when viewed through the lens of the immune response they may elicit in addition to that of PG. The combined immunological effect of the unique bacterial antigen found in *B. burgdorferi* PG, as well as other potentially associated proteins contained within the cell wall, are explored here. These studies further our understanding of the *B. burgdorferi* cell envelope and provide critical information that underlies the elusive pathogenesis of Lyme disease.

From Structure, to Function, to Pathogenesis: Understanding the Immunological Consequences of The Unique Peptidoglycan of *Borrelia burgdorferi*

Marisela M. Davis

General Audience Abstract

Lyme disease is a growing health concern, namely for the countries in the Northern Hemisphere. The bacterium responsible for this illness is *Borrelia burgdorferi. B. burgdorferi* can survive in the human body and is a threat in that as it replicates in the human host, it sheds pro-inflammatory fragments of its unique cell wall into the environment. This thesis will explore the consequences of this cell wall shedding and how the human immune response differs from the response seen in other more common bacteria. Additionally, I have found that the cell envelope fragments shed from *B. burgdorferi* may contain more than meets the eye. There is evidence here to support the discovery of a moonlighting protein that is bound to a portion of the cell wall in *B. burgdorferi*. This protein acts to bolster the structural integrity of the cell while also acting to modulate the host immune response.

Acknowledgements

"Trust in the Lord with all your heart and lean not on your own understanding;

In all your ways acknowledge Him and He shall make your path straight."

Proverbs 3:5-6

Chandler, Mom, Dad, Migs, and Melina, thank you for loving me, supporting me, and praying for me. You all are my support system and I wouldn't be here without ya'll.

David Lally, thank you for believing in me and opening up doors for me to walk through, you helped me find opportunities to succeed in, and I am forever thankful for that.

Dr. Jutras, you taught me everything know about being a scientist, a GOOD scientist. Thank you for taking me in, teaching me, guiding me, and standing with me throughout this journey. I am forever grateful to you and the family that I have made while in the Jutras lab.

Onward

Table of Contents

List of Figures

List of Tables

List of Abbreviations

PG	Peptidoglycan
LA	Lyme arthritis
Osp	Outer surface protein
OM	Outer membrane
IM	Inner membrane
PAP	Peptidoglycan associating protein
Mur*NA*c	N-acetylmuramic acid
Glc*NA*c	N-acetylglucosamine
mDAP	*meso*-diaminopimelic acid
NLR	NOD-like receptors
TLR	Toll-like receptors
PAMP	Pathogen associated molecular pattern
NOD	Nucleotide binding oligomerization domain
NapA	Neutrophil attracting protein A
PBMC	Peripheral blood mononuclear cell
GO	Gene ontology
KEGG	Kyoto encyclopedia of genes and genomes
DO	Disease ontology
OMV	Outer membrane vesicle
SDS	Sodium dodecyl sulfate
Dps	DNA binding protein from starved bacteria

CHAPTER 1

Literature Review

Lyme Disease Epidemiology

Lyme disease is the most common vector borne illness in the United States with an increase in incidence of over 2000% in the last twenty years (1, 2). Lyme disease is localized to the Northeastern coast of the country with the most heavily affected states being Connecticut, Vermont, Pennsylvania, New Hampshire, and Rhode Island (1, 2). Regardless of this apparent localization, the trend in cases appears to be incrementally moving into areas in both the Midwest and Southwest portion of the country each year. This spread has had a particular impact here, in the New River Valley of Virginia, where local cases have increased in the counties of Giles, Pulaski, Floyd and Montgomery (3). Unfortunately, these counties also maintain the highest incidence in the state (3). The rise in confirmed cases may be attributed to a few different factors including 1) warmer annual temperatures; 2) geographical spread of the tick vector; 3) deforestation; 4) increase in public awareness; and 5) increased social outings during the summer months (2).

Lyme disease is also endemic to Europe and other parts of the world. According to the European Centres for Disease Prevention and Control, there have been over 360,000 cases diagnosed in the last ten years (4), once again establishing Lyme disease as the most common vector borne illness in the European Union(4). Lyme disease case numbers may also be lower than reported in the European Union, as it is not mandatory to report as is the case in the United States (5). A closely related vector also harbors similar bacterium in parts of Russia and extends

through areas in Asia (2), further expanding the geographical reach of Lyme borreliosis and other related vector borne illnesses.

The universal rise in cases of Lyme disease in the Northern Hemisphere over the recent decade indicates that Lyme disease is indeed a prominent health crisis. Each year, as temperatures continue to rise, and the winters become more bearable, the tick vectors that carry the agent of Lyme disease — *Borrelia burgdorferi* — are able to survive and travel further, incidentally infecting more human hosts in the process. Given the number of complex variables contributing to ascendency of Lyme disease, this disease is likely to remain an imminent health concern in the future.

The Enzootic Cycle of Borrelia burgdorferi

The causative agent of Lyme disease is the Gram-negative spirochete *Borrelia burgdorferi.* This bacteria lives within the mid gut of the *Ixodes spp* tick, which experiences a multitude of changes in its environment throughout its life cycle, these stages include the larvae, nymph and adult stages (2, 6). When an *Ixodes* tick at any of these stages feeds on an infected vertebrate host, it can acquire many bacterium including *B. burgdorferi.* The spirochetes travel through the digestive tract of the tick and end up in the mid gut where they grow and replicate. When it is time for the tick to feed on a blood meal, the bacteria travel from the gut to the salivary glands where they are primed for infection of the next host. These infected ticks, most often nymphs (2), will then go on to infect other vertebrates, including humans. While transitioning through the life stages, living in the tick mid gut, and vertebrate host, *B. burgdorferi* undergoes many physiological changes to adapt to these new environments (7). For example, one of these adaptations can be illustrated by the regulation of the two the outer surface proteins (Osp) Osp A and Osp C. The protein OspA is expressed while in the tick and once a blood meal

has been initiated, OspA is downregulated and Osp C is upregulated to promote the transition to the host (8, 9).

While experiencing changes in host environment, *B. burgdorferi* is also subject to many stressors. Host innate and adaptive immunity target *B. burgdorferi*, yet the pathogen has evolved ways to adapt to these responses, of which will be covered in later sections. Starvation for the host incites physiological changes in *B. burgdorferi* (7). If the tick has not partaken in a blood meal, the oxidative stress pathways for *B. burgdorferi* are activated, although the exact methodology is not well studied. Oxidation, metal levels, pH, and temperature all fluctuate in the transition back and forth between the tick vector and vertebrate host, all of which are met with genetic changes in *B. burgdorferi,* to ensure survival and propagation to the next generation (8, 10-13).

Borrelia burgdorferi Physiology

B. burgdorferi maintains unique cellular characteristics that distinguish it from other bacteria. For example, despite being a diderm, *B. burgdorferi* does not produce Lipopolysaccharide (LPS), a potent immune system stimulant (6, 14, 15). The outer membrane (OM) contains host-derived cholesterol (16, 17) and more than 100 different lipoproteins (18). Under normal physiological conditions, *B. burgdorferi* produces outer membrane vesicles (OMVs); blebs pinched off from the OM that contain all sorts of cell envelope contents (19). Flagella are not extruded from the envelope, but rather are contained entirely in the periplasmic space (20, 21). Among the differences there are a few that are specifically relevant to pathogenicity which include 1) the addition of the diamine L-Ornithine to the peptidoglycan (PG) structure (22, 23); 2) the lack of the PG recycling pathway (24) ; and 3) the apparent lack of

peptidoglycan associating proteins (PAPs), all of which will be covered in the following sections.

Peptidoglycan is a vital structure for the bacterial cell. This polymeric mesh surrounds the cell and mainly functions to keep it from bursting from osmotic stress and turgor pressure (25). The typical PG structure observed among bacterium consists of glycan strands crosslinked by short peptides. Virtually all glycan strands are composed of two repeating sugars, N-acetylglucosamine (Glc*NA*c) and N-acetylmuramic acid (Mur*NA*c) (26, 27). However, some variability exists in the composition of the peptide stems. For example, Gram-negative bacteria typically possess *meso*-diaminopimelic acid (mDAP) in the third position of the peptide, while most Gram-positive peptides carry lysine (Lys) at the analogous position. Given the differences at this particular position it is perhaps not surprising that several mammalian pattern recognition receptors have evolved to discriminate bacteria based on the identity of the diamine in this position. In a reversed perspective, it is also not surprising that some bacteria have evolved to avoid pattern recognition from the immune system by altering their PG structure at the amino acid level (28). These such bacteria such as *Bacillus subtilis,* that although is classified as a Gram-positive bacterium, maintains an amidated form of mDAP in the third amino acid position from the Mur*NA*c sugar, thus avoiding classical pattern recognition (29-31). Interestingly, *B. burgdorferi* has neither mDAP or Lys in this position, but rather forms the sugar-peptide crosslink via an Ornithine residue, which remains an atypical alteration to the structure (22, 23).

The PG layer of *B. burgdorferi* is between the inner and outer membranes (IM/OM). Although the structure is unique from other more common bacteria, due to its location, the PG should not directly interact with host immunity. However, this is not necessarily the case. The *B. burgdorferi* genome lacks the genes encoding the proteins required for the peptidoglycan recycling

pathway, an alteration seen in some Gram-negative bacteria (23, 28). Growth of the cell requires that the PG is broken down and remodeled, a process known as PG turnover. These broken-down portions of the PG or muropeptides, are either reused via the peptidoglycan recycling pathway or in the case of *B. burgdorferi*, excised from the cell. Due to the lack of this pathway in *B. burgdorferi*, on average the cell loses about 45% of Ornithine linked muropeptides per generation (23). Note that it is still unknown exactly how the muropeptides escape the cell however, I present and support a method for muropeptide release discussed later in this thesis.

Peptidoglycan associating proteins (PAPs) are among the most common scaffolding proteins in bacteria. These proteins most often are bound to either the IM or the OM and linked to the PG layer to provide additional structural support to the cell envelope. As an example, Braun's lipoprotein in *E. coli* is the most abundant protein in the cell (32), solidifying its importance in the cell envelope structure. Bacteria unable to produce PAPs, have severe defects in cell 1) growth; 2) division; 3) morphology; 4) communication; and 5) ability to withstand exogenous stress (33, 34). Interestingly, many of these seemingly structural cell wall components moonlight as virulence factors that contribute to bacterial pathogenicity (33, 35, 36). Prior to the studies outlined in this thesis, there have been no PAPs reported in *B. burgdorferi.*

Lyme Disease Pathogenesis

If an infected *Ixodes* tick partakes in an uninterrupted human blood meal, the tick may be able to transmit enough *B. burgdorferi* to cause disease. The number of spirochetes required to cause persistent infection is estimated to be anywhere from 1-100 organisms and the ideal location for bacterium dissemination is in the skin (37). The disease state can be broken up into two stages, the acute and the late stage. In the acute stage, patients typically present with indiscriminate flu like symptoms, arthralgia, and fatigue. The one discriminating symptom in the

acute stage used to diagnose Lyme disease is *erythema migrans* or the bullseye rash. This rash typically indicates where the tick bite occurred and can appear anywhere from a few days to months after the initial tick bite (2, 38). If the patient is left improperly or completely untreated, the bacteria, as well as bacterial byproducts such as released muropeptides, will disseminate to other parts of the body resulting in a variety of late stage symptoms. Late stage infection can occur in the heart, the central nervous system, and most notably in the synovial fluid of large joints (39). Namely, Lyme arthritis (LA)—proliferative synovitis of one or more large joints—the most common late stage manifestation of Lyme disease in the United States (2, 38).

The current treatment for Lyme disease is a 3-week course of antibiotic treatment with either doxycycline, amoxicillin or cefuroxime depending on the age and medical history of the patient (40). Unfortunately, according to the CDC there are about 10-20% of patients that, despite undergoing antibiotic treatment, still present with chronic symptoms (39, 41, 42). A plausible explanation for this phenomenon has recently been proposed and stands on three immunological findings

1) humans mount a specific immune response to *B. burgdorferi* PG; 2) *B. burgdorferi* PG is found in the synovial fluid of antibiotic treated Lyme arthritis patients, and; 3) purified PG from *B. burgdorferi* elicits an inflammatory response resulting in arthritis of the ankle joint in the mouse model (23). Based on the notion that the PG from *B. burgdorferi* is a unique antigen, this thesis will continue to explore the mechanisms and reasons behind why the body responds the way it does when exposed to it.

The innate immune response to Borrelia burgdorferi

As soon as the tick latches onto the human host and begins the exchange of foreign tick material for human blood, the innate immune response arrives on scene. The cell types outlined

here are major contributors (although not all the cells contributing) to the overall responses seen to *B. burgdorferi* and include neutrophils, macrophages, and dendritic cells. All cells of the innate immune system are covered in innate receptors that will be discussed later. The organization of the innate immune response is critical for the initiation of the adaptive response, which will also be covered in the next section.

The first responders are the neutrophils that act to fight off invaders while also orchestrating the secondary response from other innate cell types. During the initial stages of infection, neutrophils phagocytize *B. burgdorferi*, utilize lethal enzymes and destroy bacterial cells using neutrophil extracellular traps (NETs) (43-45). In preparation for this assault, enzymes in the tick saliva have been shown to dampen the efforts of neutrophils. These enzymes can suppress overall neutrophil functionality, namely through manipulation, enzyme production, and chemotaxis (43, 46). In this way, the two-systems wage war with one another both attempting to establish dominance in the host.

Macrophages also phagocytize *B. burgdorferi* and destroy bacterial cells utilizing oxygen radicals in the phagosome. Ingestion of whole *B. burgdorferi* often causes macrophages and their precursors, monocytes, to rupture in apoptosis (43); however, the consequences of this apoptosis are still under investigation. Innate cell lysis removes majority of the bacterial cell from the extracellular environment but may also lead to expulsion of robust and inflammatory bacterial products such as muropeptides. Macrophages are also the main contributors of innate cytokines that lead to inflammation including TNF-α and IFN-ɣ (47).

Dendritic cells (DCs) are the bridge that connects innate and adaptive immunity. These cells ingest *B. burgdorferi* and present antigens on the surface to naïve lymphocytes via both major histocompatibility complexes I and II (43, 48). Miscommunications between the DCs and

lymphocytes results in a faulty adaptive immune response and although the exact mechanisms are still under investigation, it is clear that DCs play a critical role in *B. burgdorferi* infection. This is especially true in that epithelial dendritic cells are among the first to interact with *B. burgdorferi* in the skin during infection and are capable of phagocytosing these bacterium (49, 50). Careful coordination of each of these cell types are crucial in the host response to acute *B. burgdorferi* infection.

The innate receptors of this arm of the immune system are equally as important as the cells themselves and include the NOD-like receptors (NLRs), Toll-like receptors (TLRs) and the peptidoglycan receptor proteins. These receptors may present themselves on the surface of immune cells or intracellularly and are often dependent on the type of ligand they bind. The innate receptors listed here are all responsible for recognizing common bacterial ligands and are thus known as pathogen associated molecular pattern (PAMP) receptors. These PAMPS include those such as LPS, nuclear material, cell surface proteins or cell envelope components. Once a pattern is recognized, a brigade of downstream effectors is activated, often resulting in large scale responses to invaders. These responses include fevers, vasodilation, and inflammation. Notice that these attacks are not specific, as they are in the adaptive immune response which will be covered later, rather are aimed at boosting the overall ability of the body to clear the pathogen.

The nucleotide-binding oligomerization domain (NOD 1/2) receptors are of particular interest in that these are typically how the body distinguishes different types of bacterium. NOD-2 recognizes a portion of the microstructure of PG, in this case the Mur*NA*c sugar linked to L-Ala and D-Glu also known as N-Acetylmuramyl-L-Alanyl-D-Isoglutamine (MDP) (51). This recognition essentially serves the body as a "general," PG detector as this structure is nearly

ubiquitously found in bacterium with PG (Figure 1A). In contrast, NOD-1 only recognizes the third amino acid in many Gram-negative bacteria, mDAP (30) . These patterns in PG structure are essential for recognition by the immune response and thus the body *typically* uses NOD-1 to recognize Gram-negative bacteria and NOD-2 to for Gram-positives (30, 31, 51). As mentioned earlier, in the case of *B. burgdorferi* this presents a unique scenario in that the third amino acid in the peptide chain is the diamine L-Ornithine. *B. burgdorferi* PG stimulates NOD-2, as its structure still contains MDP (23) , however it does not stimulate NOD-1 due to the mDAP substitution with L-Ornithine (31). The immunological consequences of the L-Ornithine substitution are still under investigation and have been partially explored as part of this thesis work.

Toll like receptors also recognize bacterial antigenic patterns. There are 13 TLRs and each one is responsible for binding to a class of microbial ligands (43, 52). Acute infection with *B. burgdorferi* leads to the activation of TLR1, TLR2, and TLR6 (43, 52, 53). There is experimental evidence to support the notion that there are other TLRs that are stimulated by other *B. burgdorferi* bacterial components, however only TLR 1, 2 and 6 will be discussed due to their enhanced relevance to the acute pathogenesis. Outer surface protein A stimulates TLR2 and this has been shown to lead to dimerization of TLR2 with both TLR1/6 (54). This activation leads to downstream activation of the inflammasome, thereby increasing the overall inflammatory response to the presence of *B. burgdorferi*. Interestingly, there is a trend in TLR2 polymorphisms in patients with more severe forms of Lyme disease (55). The arthritic effect seen in the TLR2 deficient mouse model is exacerbated and there are less infiltrating innate immune cells present when compared to control (56) (57). This indicates that the TLR2 innate

receptor plays a critical role in the recruitment of innate immune cells that go on to phagocytize and clear *B. burgdorferi*.

The adaptive immune response to Borrelia burgdorferi

The two large families of cells in adaptive immunity include CD4/8 T and B cells. The role of T cells is to either aid other cell types in differentiation/activation (CD4) or to play a role in physically removing foreign invaders from the body (CD8). Depending on the antigen from *B. burgdorferi* that is presented to the T cell, the T cell may go on to stimulate the production of antibodies from B cells.

Antibody production from B cells occurs in two ways, either T cell dependent or independent. The T cell independent pathway typically consists of activation directly from antigen presenting cells and these antigens are typically simple bacterial constructs that ultimately result in shorter lived antibodies from the B cells they act on. The T cell dependent pathway relies on antigen presentation from T cells and often results in a more robust, lengthier antibody response. Antibodies are classified according to their constant chain and are either IgA, IgG, IgD, IgE, or IgM. IgM is the first antibody produced in an adaptive response and is often the product of a T independent activation of B cells. Within a few weeks, there is a kindling of an IgG response from T cell dependent activated B cells. In a majority of cases, the ratio of IgM to IgG dwindles over time as less IgM antibodies are produced in favor of IgG. Interestingly this is not the case in *B. burgdorferi* infection as often there is a pronounced effect seen from IgM antibodies. Although there is still an IgG response, the overall antibody levels (58, 59) result in high quantities of both antibodies throughout the course of infection, perhaps another mechanism utilized by this pathogen to evade extermination by the immune system.

Borrelia burgdorferi evasion and dissemination

B. burgdorferi maintains nearly as many methods for avoidance of the immune system as the immune system has methods for its destruction and clearance. Although the innate immune system deploys numerous tactics to halt the initial infection with *B. burgdorferi*, the pathogen still manages to disseminate to other parts of the body, wreaking havoc wherever that may be. Travel for *B. burgdorferi* is feasible not only through the blood but also through the lymph where it can interfere with adaptive immune cell generation (58, 59). Thus, dissemination to the heart, central nervous system, and synovial fluid result in late stage symptoms of Lyme disease (39). Components in the tick saliva (60, 61), outer surface protein manipulation (9), suppression of proper antibody production (58, 59), and motility ability (62) are all methods employed by *B. burgdorferi* to evade the host immune response and establish residency.

Irrespective of which arm of the immune response being studied, there is no denying that the two rely heavily on each other for proper elimination of pathogens. The temporal immune response to *B. burgdorferi* is unique in that Lyme disease presents as a biphasic illness. There are a specific set of symptoms that are seen in acute patients and these are drastically different from those seen in the chronically ill. Where does the shift occur from acute symptoms to long term? How early can we detect this shift? What signals are being sent to kickstart it and which ones are designated for dealing with the long-term infection? Armed with the fundamental knowledge that *B. burgdorferi* PG is a unique antigen released during the life cycle of the bacteria and utilizing this antigen as a bio-tool to study the immunological implications for the pathogenesis of Lyme disease, we can truly begin to answer these questions.

The physical and economical burdens Lyme disease places on those it affects are brutal. The economic impact of Lyme costs the US $292 million a year with over 300,000 annual cases

diagnosed in the United States alone (63). Each year the cases continue to rise, the geographical location spreads, and the costs associated follow the same trends.

B. burgdorferi is a unique pathogen in many ways, the architecture of the cell and the resulting physiology presents unique challenges to each system it resides in during the enzootic cycle. Its compact, yet complex, genome encodes anomalies that often times are involved in the unique pathogenesis seen in Lyme disease.

This thesis presents evidence for the distinctive immune response elicited from *B. burgdorferi* PG using RNA sequencing. We uncover that the acute immune response from bacterial PG is fairly similar but also that there are a few distinguishing responses seen only from stimulation with *B. burgdorferi* PG. The PG is only a single component of the cell envelope and the presence of other proteins potentially associated with the PG implies that there may also be implications for the immune response seen. With this in mind, I present work in this thesis that describes the function and perhaps the role that Neutrophil attracting protein A (NapA) plays in *B. burgdorferi*. This protein is the first PAP to have been discovered in *B. burgdorferi* and this thesis provides evidence that NapA not only plays a role in the structural integrity of the cell envelope, but also doubles as an immunomodulatory beacon to the human immune system.

Figure 1: PG structure and differentiation

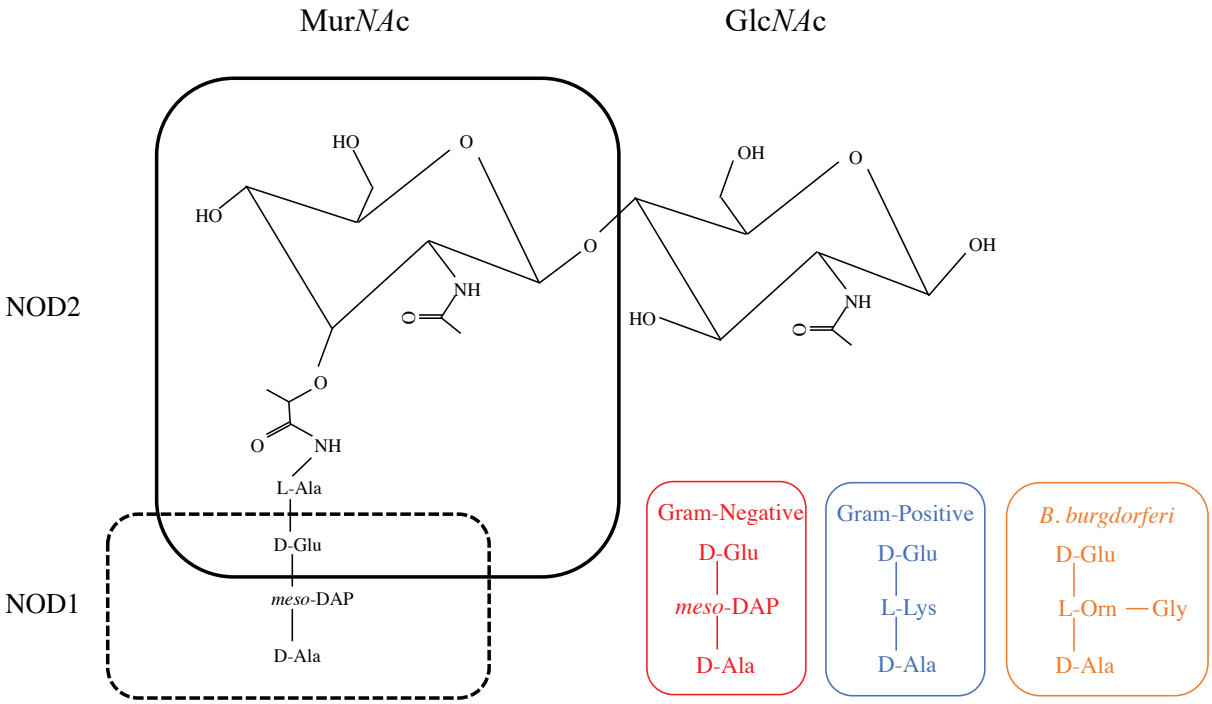

Figure 1: Adapted from Davis et al 2011 (28). The microstructure of PG consisting of repeated Mur*NA*c and Glc*NA*c sugars linked to a chain of altering amino acids. NOD2 and NOD1 ligands shown. The typical Gram-negative, Gram-positive and *B. burgdorferi* side chains in red, blue and orange respectively.

References

1. Prevention CfDCa. Recent Lyme disease surveillance data November 7, 2019 [Available from: https://www.cdc.gov/lyme/datasurveillance/recent-surveillance-data.html.

2. Mead PS. Epidemiology of Lyme disease. Infectious Disease Clinics. 2015;29(2):187-210.

3. Health VDo. 2016 Annual Surveillance Data 2016 [Available from: http://www.vdh.virginia.gov/surveillance-and-investigation/virginia-reportable-disease-surveillance-data/annual-reports/2016-annual-surveillance-data/.

4. Agency EE. Vector-borne diseases 2016 [Available from: https://www.eea.europa.eu/data-and-maps/indicators/vector-borne-diseases-2/assessment.

5. Smith R, Takkinen J. Lyme borreliosis: Europe-wide coordinated surveillance and action needed? Euro Surveill. 2006;11(6):E060622 1.

6. Radolf JD, Caimano MJ, Stevenson B, Hu LT. Of ticks, mice and men: understanding the dual-host lifestyle of Lyme disease spirochaetes. Nat Rev Microbiol. 2012;10(2):87-99.

7. Stewart PE, Rosa PA. Physiologic and Genetic Factors Influencing the Zoonotic Cycle of Borrelia burgdorferi. In: Adler B, editor. Spirochete Biology: The Post Genomic Era. Cham: Springer International Publishing; 2018. p. 63-82.

8. Schwan TG, Piesman J, Golde WT, Dolan MC, Rosa PA. Induction of an outer surface protein on Borrelia burgdorferi during tick feeding. Proc Natl Acad Sci U S A. 1995;92(7):2909-13.

9. Srivastava SY, de Silva AM. Reciprocal expression of ospA and ospC in single cells of Borrelia burgdorferi. J Bacteriol. 2008;190(10):3429-33.

10. Li X, Pal U, Ramamoorthi N, Liu X, Desrosiers DC, Eggers CH, et al. The Lyme disease agent Borrelia burgdorferi requires BB0690, a Dps homologue, to persist within ticks. Mol Microbiol. 2007;63(3):694-710.

11. Boylan JA, Posey JE, Gherardini FC. Borrelia oxidative stress response regulator, BosR: a distinctive Zn-dependent transcriptional activator. Proc Natl Acad Sci U S A. 2003;100(20):11684-9.

12. Carroll JA, Garon CF, Schwan TG. Effects of environmental pH on membrane proteins in Borrelia burgdorferi. Infect Immun. 1999;67(7):3181-7.

13. Stevenson B, Schwan TG, Rosa PA. Temperature-related differential expression of antigens in the Lyme disease spirochete, Borrelia burgdorferi. Infect Immun. 1995;63(11):4535-9.

14. Fraser CM, Casjens S, Huang WM, Sutton GG, Clayton R, Lathigra R, et al. Genomic sequence of a Lyme disease spirochaete, Borrelia burgdorferi. Nature. 1997;390(6660):580-6.

15. Casjens S, Palmer N, van Vugt R, Huang WM, Stevenson B, Rosa P, et al. A bacterial genome in flux: the twelve linear and nine circular extrachromosomal DNAs in an infectious isolate of the Lyme disease spirochete Borrelia burgdorferi. Mol Microbiol. 2000;35(3):490-516.

16. Pappas CJ, Iyer R, Petzke MM, Caimano MJ, Radolf JD, Schwartz I. Borrelia burgdorferi requires glycerol for maximum fitness during the tick phase of the enzootic cycle. PLoS Pathog. 2011;7(7):e1002102.

17. Crowley JT, Toledo AM, LaRocca TJ, Coleman JL, London E, Benach JL. Lipid exchange between Borrelia burgdorferi and host cells. PLoS Pathog. 2013;9(1):e1003109.

18. Zuckert WR. Secretion of bacterial lipoproteins: through the cytoplasmic membrane, the periplasm and beyond. Biochim Biophys Acta. 2014;1843(8):1509-16.

19. Schwechheimer C, Kuehn MJ. Outer-membrane vesicles from Gram-negative bacteria: biogenesis and functions. Nat Rev Microbiol. 2015;13(10):605-19.

20. Wolgemuth CW, Charon NW, Goldstein SF, Goldstein RE. The flagellar cytoskeleton of the spirochetes. J Mol Microbiol Biotechnol. 2006;11(3-5):221-7.

21. Motaleb MA, Corum L, Bono JL, Elias AF, Rosa P, Samuels DS, et al. Borrelia burgdorferi periplasmic flagella have both skeletal and motility functions. Proc Natl Acad Sci U S A. 2000;97(20):10899-904.

22. Beck G, Benach JL, Habicht GS. Isolation, preliminary chemical characterization, and biological activity of Borrelia burgdorferi peptidoglycan. Biochem Biophys Res Commun. 1990;167(1):89-95.

23. Jutras BL, Lochhead RB, Kloos ZA, Biboy J, Strle K, Booth CJ, et al. Borrelia burgdorferi peptidoglycan is a persistent antigen in patients with Lyme arthritis. Proceedings of the National Academy of Sciences. 2019:201904170.

24. Jutras BL, Lochhead RB, Kloos ZA, Biboy J, Strle K, Booth CJ, et al. Borrelia burgdorferi peptidoglycan is a persistent antigen in patients with Lyme arthritis. Proc Natl Acad Sci U S A. 2019;116(27):13498-507.

25. Parry BR, Surovtsev IV, Cabeen MT, O'Hern CS, Dufresne ER, Jacobs-Wagner C. The bacterial cytoplasm has glass-like properties and is fluidized by metabolic activity. Cell. 2014;156(1-2):183-94.

26. Costerton JW, Ingram JM, Cheng KJ. Structure and function of the cell envelope of gram-negative bacteria. Bacteriol Rev. 1974;38(1):87-110.

27. Gan L, Chen S, Jensen GJ. Molecular organization of Gram-negative peptidoglycan. Proc Natl Acad Sci U S A. 2008;105(48):18953-7.

28. Davis KM, Weiser JN. Modifications to the peptidoglycan backbone help bacteria to establish infection. Infect Immun. 2011;79(2):562-70.

29. Arts RJW, Carvalho A, La Rocca C, Palma C, Rodrigues F, Silvestre R, et al. Immunometabolic Pathways in BCG-Induced Trained Immunity. Cell Rep. 2016;17(10):2562-71.

30. Girardin SE, Boneca IG, Carneiro LA, Antignac A, Jehanno M, Viala J, et al. Nod1 detects a unique muropeptide from gram-negative bacterial peptidoglycan. Science. 2003;300(5625):1584-7.

31. Girardin SE, Travassos LH, Herve M, Blanot D, Boneca IG, Philpott DJ, et al. Peptidoglycan molecular requirements allowing detection by Nod1 and Nod2. J Biol Chem. 2003;278(43):41702-8.

32. Asmar AT, Collet JF. Lpp, the Braun lipoprotein, turns 50-major achievements and remaining issues. FEMS Microbiol Lett. 2018;365(18).

33. Kovacs-Simon A, Titball RW, Michell SL. Lipoproteins of bacterial pathogens. Infect Immun. 2011;79(2):548-61.

34. Cascales E, Bernadac A, Gavioli M, Lazzaroni JC, Lloubes R. Pal lipoprotein of Escherichia coli plays a major role in outer membrane integrity. J Bacteriol. 2002;184(3):754-9.

35. Haake DA. Spirochaetal lipoproteins and pathogenesis. Microbiology-Uk. 2000;146:1491-504.

36. Henderson B, Martin A. Bacterial virulence in the moonlight: multitasking bacterial moonlighting proteins are virulence determinants in infectious disease. Infect Immun. 2011;79(9):3476-91.

37. Barthold SW. Infectivity of Borrelia burgdorferi relative to route of inoculation and genotype in laboratory mice. J Infect Dis. 1991;163(2):419-20.

38. Amy M. Schwartz AFH, Paul S. Mead, Sarah A. Hook, Kiersten J. Kuegeler. Surveillance for Lyme Disease - United States, 2008-2015. Centers for Disease Control and Prevention; 2017. Contract No.: 22.

39. Steere AC. Lyme disease. N Engl J Med. 2001;345(2):115-25.

40. Wormser GP, Dattwyler RJ, Shapiro ED, Halperin JJ, Steere AC, Klempner MS, et al. The clinical assessment, treatment, and prevention of Lyme disease, human granulocytic anaplasmosis, and babesiosis: clinical practice guidelines by the Infectious Diseases Society of America. Clinical Infectious Diseases. 2006;43(9):1089-134.

41. Rebman AW, Bechtold KT, Yang T, Mihm EA, Soloski MJ, Novak CB, et al. The Clinical, Symptom, and Quality-of-Life Characterization of a Well-Defined Group of Patients with Posttreatment Lyme Disease Syndrome. Front Med (Lausanne). 2017;4:224.

42. Marques A. Chronic Lyme disease: a review. Infect Dis Clin North Am. 2008;22(2):341-60, vii-viii.

43. Oosting M, Buffen K, van der Meer JW, Netea MG, Joosten LA. Innate immunity networks during infection with Borrelia burgdorferi. Crit Rev Microbiol. 2016;42(2):233-44.

44. Benach JL, Fleit HB, Habicht GS, Coleman JL, Bosler EM, Lane BP. Interactions of phagocytes with the Lyme disease spirochete: role of the Fc receptor. J Infect Dis. 1984;150(4):497-507.

45. Menten-Dedoyart C, Faccinetto C, Golovchenko M, Dupiereux I, Van Lerberghe PB, Dubois S, et al. Neutrophil extracellular traps entrap and kill Borrelia burgdorferi sensu stricto

spirochetes and are not affected by Ixodes ricinus tick saliva. J Immunol. 2012;189(11):5393-401.

46. Hartiala P, Hytonen J, Suhonen J, Lepparanta O, Tuominen-Gustafsson H, Viljanen MK. Borrelia burgdorferi inhibits human neutrophil functions. Microbes Infect. 2008;10(1):60-8.

47. Steere AC, Coburn J, Glickstein L. The emergence of Lyme disease. J Clin Invest. 2004;113(8):1093-101.

48. Mason LM, Veerman CC, Geijtenbeek TB, Hovius JW. Menage a trois: Borrelia, dendritic cells, and tick saliva interactions. Trends Parasitol. 2014;30(2):95-103.

49. Nestle FO, Zheng XG, Thompson CB, Turka LA, Nickoloff BJ. Characterization of dermal dendritic cells obtained from normal human skin reveals phenotypic and functionally distinctive subsets. J Immunol. 1993;151(11):6535-45.

50. Filgueira L, Nestle FO, Rittig M, Joller HI, Groscurth P. Human dendritic cells phagocytose and process Borrelia burgdorferi. J Immunol. 1996;157(7):2998-3005.

51. Girardin SE, Boneca IG, Viala J, Chamaillard M, Labigne A, Thomas G, et al. Nod2 is a general sensor of peptidoglycan through muramyl dipeptide (MDP) detection. J Biol Chem. 2003;278(11):8869-72.

52. Steere AC, Glickstein L. Elucidation of Lyme arthritis. Nat Rev Immunol. 2004;4(2):143-52.

53. Singh SK, Girschick HJ. Toll-like receptors in Borrelia burgdorferi-induced inflammation. Clin Microbiol Infect. 2006;12(8):705-17.

54. Dennis VA, Dixit S, O'Brien SM, Alvarez X, Pahar B, Philipp MT. Live Borrelia burgdorferi spirochetes elicit inflammatory mediators from human monocytes via the Toll-like receptor signaling pathway. Infect Immun. 2009;77(3):1238-45.

55. Strle K, Shin JJ, Glickstein LJ, Steere AC. Association of a Toll-like receptor 1 polymorphism with heightened Th1 inflammatory responses and antibiotic-refractory Lyme arthritis. Arthritis Rheum. 2012;64(5):1497-507.

56. Wooten RM, Ma Y, Yoder RA, Brown JP, Weis JH, Zachary JF, et al. Toll-like receptor 2 is required for innate, but not acquired, host defense to Borrelia burgdorferi. J Immunol. 2002;168(1):348-55.

57. Fikrig E, Narasimhan S, Neelakanta G, Pal U, Chen M, Flavell R. Toll-like receptors 1 and 2 heterodimers alter Borrelia burgdorferi gene expression in mice and ticks. J Infect Dis. 2009;200(8):1331-40.

58. Tracy KE, Baumgarth N. Borrelia burgdorferi Manipulates Innate and Adaptive Immunity to Establish Persistence in Rodent Reservoir Hosts. Front Immunol. 2017;8:116.

59. Tunev SS, Hastey CJ, Hodzic E, Feng S, Barthold SW, Baumgarth N. Lymphoadenopathy during lyme borreliosis is caused by spirochete migration-induced specific B cell activation. PLoS Pathog. 2011;7(5):e1002066.

60. Anguita J, Ramamoorthi N, Hovius JW, Das S, Thomas V, Persinski R, et al. Salp15, an ixodes scapularis salivary protein, inhibits CD4(+) T cell activation. Immunity. 2002;16(6):849-59.

61. Verhaegh D, Joosten LAB, Oosting M. The role of host immune cells and Borrelia burgdorferi antigens in the etiology of Lyme disease. Eur Cytokine Netw. 2017;28(2):70-84.

62. Moriarty TJ, Norman MU, Colarusso P, Bankhead T, Kubes P, Chaconas G. Real-time high resolution 3D imaging of the lyme disease spirochete adhering to and escaping from the vasculature of a living host. PLoS Pathog. 2008;4(6):e1000090.

63. Mac S, da Silva SR, Sander B. The economic burden of Lyme disease and the cost-effectiveness of Lyme disease interventions: A scoping review. PLoS One. 2019;14(1):e0210280.

CHAPTER II

Insights in the Characterization of the Immune Response to *B. burgdorferi* Peptidoglycan

Introduction

Peptidoglycan is a potent immune response stimulant. Fortunately, this structural polymer is only found in bacteria, and there are no homologues to it in the human system, making it a perfect target for destruction by the innate immune system. The molecular patterns found in PG can be extracellularly sensed via outer membrane TLRs or intracellularly via NLRs and in some cases can be sensed vice versa via these same receptors. Either way, the downstream effectors upregulated by the presence of PG, trigger the translocation of transcription factors into the nucleus and act to upregulate pro-inflammatory responses.

The two most broad categories of bacterial PG are the Gram-negative and Gram-positive bacteria that differ in the cross-linking amino acid in the third position be it mDAP or lysine respectively. The model Gram-negative organism is *E. coli*, has the basic Mur*NA*c-Ala-Glu-mDAP PG structure(1,2). Similarly, *Streptococcus mutans* has the typical Gram-positive PG structure Mur*NA*c-Ala-Glu-Lys(3). Structural aberrations to the PG layer are common in bacteria as there has been an evolutionary drive to alter PG structures to enhance structural integrity and avoid immune system stimulation. For example, the Gram-positive *Bacillus subtilis* does not incorporate lysine in its PG structure, but instead has amidated-DAP, a deviation that has proven to dampen immune signaling by the NLRs in vitro (4). *Staphylococcus aureus* is known for two PG structural changes 1) the O-acetylation of the Mur*NA*c sugar, which makes this PG structure resistant to lysozyme (5) and; 2) the presence of a penta-glycine bridge that acts to provide additional structure support to the cell (6).

Perhaps among the most unique and understudied alterations to PG though, is that of *B. burgdorferi.* This structure is different from other more common bacteria in that it does not simply acetylate or amidate preexisting structural moieties, rather has incorporated a completely new amino acid, L-Ornithine (7). The Ornithine alteration is seen in some spirochetes as well as bacteria from the *Thermus*, *Eubacteria*, and *Deinococcus* genera (2, 8, 9). Based on the distinctive properties of this PG structure, the hypothesis of this chapter is that *B. burgdorferi* PG produces a unique response when compared to human immune cells stimulated with other bacterial PG, and that the PG of *B. burgdorferi* is responsible for the pathogenesis of Lyme arthritis. Additionally, we sought to answer the question of whether or not *B. burgdorferi* PG alone could recapitulate the immune response seen when immune cells were stimulated with live *B. burgdorferi*. Insights into the immunological implications of the unique PG structure found in *B. burgdorferi*, compared to those of more well-known bacterium, are presented here using RNA sequencing analysis.

Methodology

Bacterial Strains

The Wild type strains of E. *coli* (K-12 strain MG1655), *B. subtilis* strain (168), *S. mutans* (Clarke), *S. aureus* strain (USA300) and a clone of the *B. burgdorferi* strain B31 were utilized in these experiments. The *B. burgdorferi* was cultured at 37 ^{o}C under 5% CO_2 in BSK II medium supplemented with 6% rabbit serum. *S. mutans* was grown in BHI medium at 37^{o}C. All other bacteria were grown in Luria-Bertaini broth at 37^{o}C to an OD_{600} of 0.6-0.7.

Peptidoglycan Purification

Peptidoglycan from Gram-negative (*E. coli and B. burgdorferi)* bacterium was purified as described previously (7) and was isolated from 1L of culture. Gram-positive (*S. mutans, S. aureus, and B. subtilis*) were isolated according to the same protocol with the following additional steps. Prior to solubilization in 5% SDS, the Gram-positive pellets were aliquoted out into 1mL homogenizing tubes containing small glass beads and shaken in a Mini Bead Beater at 60% power for 2 minutes per tube. The tubes were reconsolidated, and the pellet was then solubilized in 5% SDS. The pellets were subjected to the same ultracentrifugation processing while being washed with deionized water at each step. Following chymotrypsin treatment, the samples were resuspended in 800 µL water and split into two microcentrifuge tubes each holding 400 µL of sample. One hundred microliters of 5M HCl was added and the tubes were placed on a rotating rack at 4^{o}C for 48 hours. The Gram-positive samples were then treated in the same manner as the Gram-negative samples following the protocol listed above. Peptidoglycan concentration was determined by dry weight following lyophilization.

PBMC Culturing

Three, cryopreserved pooled samples of peripheral blood mononuclear cells (PBMCs) at a concentration of 1 x 10^8 cells/mL from Zen-Bio were thawed and pooled into one batch of pooled cells in Lymphocyte culture media (Zen-Bio). These cells were plated in 12 well plates at a concentration of 2 x 10^6 cells/mL and rested for 12 hours prior to stimulation. Following stimulation for 12 or 72 hours with 50 µg/mL PG from each strain, live *B. burgdorferi* strain A3 (5000 cells/mL or 500 cells/mL), or phosphate buffered saline (PBS) the cells were harvested by

centrifugation at 800 x g for 5 min at 15 ºC. The plates along with the supernatants that were collected, and aliquoted were all kept at -80 ºC.

RNA Isolation

Twelve well plates containing PBMCs were thawed on ice for 5 minutes and equilibrated to room temperature for another 2-3 minutes prior to lysis with TRI Reagent (Sigma). RNA was precipitated with isopropyl alcohol and the pellets were washed twice with 75% ethanol before DNAse I (Zymo Research) treatment. The digested samples were further purified using the RNA Miniprep Plus Kit from Zymo Research. RNA quality and quantity were confirmed using Nanodrop. The samples were then frozen at -80 ºC before being shipped on dry ice to NovoGene Co., Ltd (https://en.novogene.com/) for analysis. Names of samples provided to Novogene Co., Ltd are listed in Table 1.1.

RNA Sequencing

Note: All RNA sequencing and the subsequent data analysis was performed by Novogene Co., Ltd. The following are summaries of the company's protocols used and can be found here (10). A complimentary DNA (cDNA) library was constructed and sequencing was done using Illumina, sequencing by synthesis, technology. Novogene performed quality control error rate and GC content distribution on the raw reads. Prior to gene expression analysis, raw reads with the adaptor sequences P5 and P7 (https://en.novogene.com/) were removed as well as reads with uncertain nucleotide sequences greater than 10% or Q-scores of >50%. Quality control checked reads were then aligned to the human genome (USCS hg 38) as the reference genome using the 'Spliced Transcripts Alignment to a Reference' (STAR v2.6.1) software. Read count is

correlated to the counts produced by HTSeq v0.6.1 and these two values were used to calculate the Fragments per kilobase of transcript per million base pairs sequenced (FPKM) to normalize transcript levels.

Differential Gene Expression Analysis

All experimental and control samples groups were composed of two biological replicates. Differential expression analysis was performed using the DESeq2 R Package (v2_1.6.3).

Cluster Analysis

Samples were clustered using the assigned FPKM value and heatmaps were generated using self-organization mapping (SOM) using default parameters in R.

Functional Analysis

Gene ontology enrichment analysis (GO), Kyoto Encyclopedia of Genes and Genomes (KEGG) Human Disease Ontology (DO) and Reactome analysis of differentially expressed genes was performed using clusterProfiler R (v2.4.3) package. Terms with a padj <0.05 are considered significantly enriched when compared to controls. Gene ontology, KEGG, coExpression, and clustering heatmap figures were all produced as part of the analysis performed by Novogene Co., Ltd.

Results

Purified PG Induces an Acute Pro-inflammatory Transcriptomic Profile in PBMCs

Purified PG from *B. burgdorferi (*PG^{Bb}*), E. coli (*PG^{Ec}*), B. subtilis (*PG^{Bs}*), S. mutans (*PG^{Sm}*),* and *S. aureus (*PG^{Sa}*),* were used to stimulate human PBMCs over the course of 12 and 72 hours. Additionally, PBMCs were stimulated with two concentrations of live *B. burgdorferi,* 500 cells/mL, for a ratio of *B. burgdorferi* to PBMCs of 1:4000 or 5000 cells/mL for a ratio of *B. burgdorferi* to PBMCs of 1:400. After stimulation with the PG of interest or live *B. burgdorferi* (referred to as live *Borrelia*), RNA was extracted from the samples, concentration and purity were verified via Nanodrop, and sent to Novogene Co., Ltd. for RNA sequencing analysis. Among all the PGs, there were a total of 10,290 and 10,855 co-expressed genes observed at 12 and 72 hours respectively (Fig. 2A and 2B). In contrast, when PBMCs were stimulated with live *Borrelia* there were 10,808 co-expressed genes shared between the two concentrations used (Fig. 2C). Peptidoglycan from all samples tested at 12 hours, with the exception of *B. subtilis,* caused a statistically significant change in genes involved in leukocyte degranulation, granulocyte activation, neutrophil activation and regulation of the innate immune response according to the Gene Ontology (GO) Enrichment analysis (Fig. 3A). Among some of the most prevalent differentially expressed genes represented in the study were TNFAIP3, IL1A/B, IL6, CXCL2, CXCL12, CXCL5, and IL8, all of which were seen at 12 hours when compared to controls (Figure 4A) (Table 2.1 and 2.2). Kyoto Encyclopedia of Genes and Genomes analysis (KEGG) shows that after acute stimulation with all PGs used, with the exception of *B. subtilis*, there is strong correlation with innate immune signaling pathways including involvement of the TNF

signaling pathway, NOD-like receptor signaling pathway, and the NF-kB signaling pathway (Figure 5A).

Cluster analysis of the differentially expressed genes among all experimental samples shows that there is a 1) distinct difference between PBMCs stimulated for 12 hours versus 72 hours; 2) clustering of coexpressed genes shared between both PG^{Bb}/PG^{Ec} and PG^{Bb}/PG^{Sa}; and 3) PG^{Bs} clusters more closely to controls than to samples stimulated with other PGs (Fig 6A). It is interesting to note that PBMCs stimulated with PG^{Bb}/PG^{Sa} cluster together at both 12 and 72 hours considering the respective differences in PG structure. A similar pattern is shared between PG^{Sm}/PG^{Ec} 72 hours post stimulation. The larger clusters separate the experimental groups by time exposed to the stimulant perhaps suggesting an equally important role for both PG structure and length of time exposed to the PG.

B. burgdorferi PG Initiates a Unique Immune Response in PBMCs

There were a few notable differences in the acute response seen in PBMCs stimulated with PG^{Bb} when compared to the other experimental samples. First, PBMCs stimulated with PG^{Bb} for 12 hours had the highest number of uniquely expressed genes (266) in comparison to the other PG stimuli used (Figure 2A) (Table S1). Interestingly, the number of uniquely expressed genes dropped over 2-fold when cells stimulated with PG^{Bb} for 12 hours were compared to those stimulated for 72 hours (Figure 2B) (Table S2). Secondly, according to the GO analysis, PBMCs stimulated with PG^{Bb} for 12 hours regulate gene products that function in pathways involving the use of ficolin-1-rich granules, a response seen only in PG^{Bb} with a padj value of 1×10^{-15} (Figure 3A). Notable among these genes were TNFAIP6, TGFB1 and FGL2 which function in hyaluronan binding, cell growth/homeostasis, and prothrombinase activity

respectively (11). Ficolin-1 or M-ficolin is produced by neutrophils and monocytes when stimulated with Gram-negative bacterial products. Of note, M-ficolin has been reported to correlate with neutrophil count in rheumatoid arthritis (RA) patients and SNPs in the M-ficolin gene has been connected to susceptibility to RA (12). Connections between these findings present interesting avenues to be explored in future studies.

Dysregulation in the balance between osteoblast (bone forming cells) and osteoclasts (bone resorbing cells) is a prominent feature in rheumatic diseases including RA and osteoarthritis (13). Among the most highly expressed genes in the in the PBMCs stimulated with PG^{Bb} for 12 hours when compared to controls were CSF3, HAS1, and MMP1, all of which function to maintain homeostasis within the cells of the bone marrow, joints, and extracellular matrix respectively (Fig. 4A) (Table 2.1 and 2.2) (11). Note that among the other PGs tested these genes also had similar log2fold changes when compared to controls. After 12 hours of stimulation, PG^{Bb} KEGG pathway analysis in PBMCs showed the second highest correlation with the osteoclast differentiation pathway with 68 differentially expressed genes compared to control and a padj of 2.98×10^{-8} (Fig. 5A far right). Note that this pathway as also seen in the PG^{Ec} and PG^{Sm} at 12 hours post stimulation. Interestingly, this pathway is not seen in PBMCs stimulated with PG^{Bb} for 72 hours although the pathway still remains at the same time point with PG^{Ec} and PG^{Sm} (Fig. 5B). Following the trend, the genes mentioned above are also less prominently expressed among the PGs tested at 72 hours (Fig. 4B).

There is a prominent shift in the response seen from PBMCs when considering the 12- and 72-hour stimulations with PG^{Bb}. The GO enrichment analysis for all other PG samples (with the exception of *S. aureus*) shows the continued involvement of genes correlated to neutrophil degranulation, granulocyte activation, and regulation of innate immunity at 72 hours post

stimulation (Fig. 3B). Although genes involved in these pathways are still represented, PG^{Bb} and PG^{Sa} both show a shift in GO association toward pathways involving cell migration, leukocyte migration, and cell motility (Fig. 3B). For example, the GO pathway "Granulocyte activation" resulting from PBMCs stimulated with PG^{Bb} for 12 hours is composed of 271 genes, this same pathway at 72 hours post stimulation is composed of only 139 genes. Among the genes no longer represented at 72 hours are the potent neutrophil activator CXCL6 (Table 5.1) (11); for comparison, there are no GO pathways representing chemotaxis in PBMCs stimulated with PG^{Bb} for 12 hours (Figure 3A and 3B). At 12 hours post stimulation with PG^{Bb} the KEGG pathways enriched are the innate TNF, NLR, NF-kB, and complement mediated pathways (Fig. 5A). In contrast, in PBMCS stimulated with PG^{Bb} for 72 hours the only innate pathway remaining is the TNF signaling pathway whereas all other PGs maintain at least 2 of the innate pathways seen at 12 post stimulation (Fig. 5B). Reactome Enrichment analysis supports a shift in innate pathways pertaining to neutrophil degranulation in PBMCS stimulated with PG^{Bb} at 72 hours when compared to those at 12 hours with a change in padj from 6.89×10^{-24} to 3.35×10^{-12} and that this change in PBMCs is unique to PG^{Bb} (Table 3.5 and Table 4.5).

B. burgdorferi PG Recapitulates the Overarching Response from PBMCs Stimulated with live *Borrelia*

Peptidoglycan is released from *B. burgdorferi* under normal growth conditions (7). Thus, muropeptides may be free to interact with cellular receptors causing downstream effectors to activate. Although there are is a near 2-fold decrease at 12 hours and a 2-fold increase at 72 hours of differentially expressed genes between PG^{Bb} and live *Borrelia* (Fig.2C) (Table S3, S4), GO, KEGG and Reactome enrichment analysis show similarities in the genes and pathways

invoked by both stimuli. Similar to the GO results from PG^{Bb} at 12 hours, the PBMCs stimulated with live *Borrelia* for 12 hours also upregulated genes responsible for neutrophil degranulation, granulocyte activation, and regulation of innate immunity (Fig. 7A). The aforementioned observed shift in gene function to cell chemotaxis and motility is also seen in the PBMCs stimulated with live *Borrelia* at 72 hours according to GO analysis (Fig. 7B). Innate signaling pathways TNF, NLR, NF-kB and JAK-STAT KEGG pathways are seen in both the 12- and 72-hour samples when stimulated with either PG^{Bb} or live *Borrelia* (Fig. 8A and 8B). Considering the findings in the next chapter, it is also interesting that both stimulants also cause an upregulation in genes involved in the IL-17 pathway 72 hours post stimulation according to KEGG analysis (Fig. 8B). The temporal change in genes corresponding to neutrophil degranulation seen in PG^{Bb} is also seen in the Reactome enrichment analysis of live cells stimulated with live *Borrelia* (Table 6.1 and Table 6.2).

Study Limitations

It should be noted that follow-up experiments were planned to support the findings presented in this study. Real-time reverse transcription PCR studies were planned to confirm the major findings outlined above. In addition, bead array ELISA tests were planned to confirm the RNA transcription levels as they relate to the proteins produced. Due to the current COVID-19 pandemic currently underway, further experiments to be added in this study were placed on hold due to university policy. Additionally, there were two samples that failed initial quality control testing by Novogene Sample A1 and A27 (Table 1.1), these two samples were each one of two biological replicates.

Discussion

The studies outlined here provide supporting evidence for the notion that PG^{Bb} is a potent and unique immune system modulator. Using bulk RNA sequencing technology, we found that PG^{Bb} elicits a similar acute pro-inflammatory transcriptomic profile in PBMCs and that this response is virtually universal among the other PGs used in this study. Although there are many similarities in the acute profile seen in PBMCs stimulated with PG, there are unique differences seen only in those stimulated with PG^{Bb}. These differences carry over into the response seen 72 hours post stimulation with PG^{Bb} and correlate well with the responses seen when PBMCs are stimulated with live *Borrelia* instead of PG.

The PGs used in this study virtually all upregulated acute pro-inflammatory genes and together best correlated to the disease genotype associated with RA according to Disease Ontology (DO) analysis (Table 7.1). This is an interesting finding considering there are a handful of studies correlating bacterial products such as PG with acute synovitis and arthritic phenotypes (7, 5, 9 14-16). These data confirm a strong role for previous bacterial infections with the onset of rheumatic disease, and correlate with the symptoms seen in Lyme arthritis. It is important to note that in these studies there is no evidence of an active bacterial infection at the time of the arthritic onset. Instead, it is hypothesized that the bacterial antigens are the source of the inflammation. More specifically, there is often no evidence of a bacterial infection in RA patients, but there is supporting evidence for small quantities of bacterial DNA in their joints(14). In addition, the condition known as reactive arthritis (ReA) in which patients present with arthralgia, conjunctivitis and urinary tract inflammation, is also often a result of a previously resolved bacterial infection(17). Lyme arthritis shares many features with these other rheumatic diseases in that in about 10% of cases, Lyme arthritis may occur after a patient has

undergone proper antibiotic treatment (18). The genes that play a role in the pathways involved in the DO enrichment analysis are seen when PBMCs are stimulated with both PG^{Bb} and live *Borrelia*. Most notable among these genes are the three with the highest fold change when compared to controls, CSF3, HAS1 and MMP1 (Figure 4A). Colony stimulating factor 3 (CSF3) specifically acts on bone marrow cells to produce granulocytes, such as neutrophils, perhaps to areas of acute inflammation caused by the exposure to PG (11). Hyaluronan synthase 1 (HAS1) is involved in the joint lubrication process and lastly, matrix metallopeptidase 1 (MMP1) belongs to a family of peptidases that remodel the extracellular matrix and collagen, interestingly both are also implicated in rheumatic disease (11). The genes listed here in Figure 4A namely CXCL6, CXCL5, CXL2, IL6 and MMP1 were all recently reported as upregulated in fibroblast-like synoviocytes (FLS) stimulated with *B. burgdorferi* (19), supporting the notion that PG alone is able to recapitulate the transcriptomic phenotype seen when stimulating with *B. burgdorferi*.

The shift in transcriptomic profile expressed by PBMCs stimulated with PG^{Bb} at 12 hours versus 72 hours presents an interesting finding. It is perhaps not coincidental that much like other bacterial PGs tested here, there is an acute onset of pro-inflammatory genes when PG^{Bb} is the stimulus. The intracellular activation of NOD-2 is dependent on the presence of MDP, a ubiquitous structure in PG. Interestingly, there is only a notable change in NOD2 expression in PBMCs that have been stimulated with live *Borrelia* at 12 hours, perhaps indicating that PG alone requires the aid of portions of the *B. burgdorferi* cell/cell envelope to bind to the intracellular NOD receptor (Table 2.3) or that there may be other inflammatory pathways involved here. At 72- hours post PG^{Bb}, and live *Borrelia*, stimulation, there is a decrease in pro-inflammatory innate pathways and an increase in leukocyte migration, cell motility, and chemotaxis as seen in both the GO and KEGG analysis results (Fig. 3B and Fig. 5B). These

pathways are supported by the downregulation of the genes encoding the pro-inflammatory molecules IL-1A, IL-6, and CXCL6 at 72- hours post PG^{Bb} (Fig. 4B). Peptidoglycan from *B. burgdorferi* also appears to suppress the activation of chemotactic cytokines CXCL12 and CXCL10 from PBMCs stimulated at 12 hours, whereas this response is lessened at 72 hours (Fig. 9A and 9B). In a similar manner, stimulation with live *Borrelia* at 12 hours results in an increase in IL1A and IL6 while CXCL12 is downregulated (Fig. 10A). At 72 hours post stimulation with live *Borrelia*, the opposite is seen for these genes (Fig. 10A). The dampening of the classical and robust immune response initially seen with PG^{Bb} could be an attributing factor to the pathogenesis of late stage Lyme symptoms. Perhaps the chronicity of low levels of inflammation driven by the presence of bacterial PG, as well as increased cell signaling for leukocyte infiltration, could correlate with Lyme arthritis which can occur anywhere from days to months after infection(20).

A recent study has shown that after antibiotic treatment, Lyme disease patients that develop Lyme arthritis have PG^{Bb} in their synovial fluid (23). Even after the eradication of the active infection, these bacterial components can still be detected using ELISAs to detect IgG antibodies to PG^{Bb} (7). The mouse model has been used to tie these findings together. When PG^{Bb} is injected in the tail vein of mice, they develop arthritis in their ankle joints 24 hours later (7). This systemic injection of purified PG indicates that the PG can travel through the body and eventually still end up in the synovial fluid, perhaps in a similar manner to the mechanism in the human system. The study above is supported by the RNA sequencing data presented here. The work presented in this chapter supports the hypothesis that PG^{Bb} is indeed capable of inducing inflammatory mediators that may play a role in the pathogenesis of Lyme arthritis.

Table 1.1 RNA Sequencing Sample Names

Raw Sample Name	Novogene NO	Species Latin Name	Sample Description(Treatment etc.)	Sample Name in Report	Group Name
A_1	CKRN200008764-1A	*H. sapien*	*h12*	Ctrl-1	Ctrl12
A_2	CKRN200008765-1A	*H. sapien*	*h12*	Ctrl-2	Ctrl12
A_3	CKRN200008766-1A	*H. sapien*	*h12*	Bb-1	Bb12
A_4	CKRN200008767-1A	*H. sapien*	*h12*	Bb-2	Bb12
A_5	CKRN200008768-1A	*H. sapien*	*h12*	Ec-1	Ec12
A_6	CKRN200008769-1A	*H. sapien*	*h12*	Ec-2	Ec12
A_7	CKRN200008770-1A	*H. sapien*	*h12*	Bs-1	Bs12
A_8	CKRN200008771-1A	*H. sapien*	*h12*	Bs-2	Bs12
A_9	CKRN200008772-1A	*H. sapien*	*h12*	Sm-1	Sm12
A_10	CKRN200008773-1A	*H. sapien*	*h12*	Sm-2	Sm12
A_11	CKRN200008774-1A	*H. sapien*	*h12*	Sa-1	Sa12
A_12	CKRN200008775-1A	*H. sapien*	*h12*	Sa-2	Sa12
A_13	CKRN200008776-1A	*H. sapien*	*h72*	Ctrl-3	Ctrl72
A_14	CKRN200008777-1A	*H. sapien*	*h72*	Ctrl-4	Ctrl72
A_15	CKRN200008778-1A	*H. sapien*	*h72*	Bb-3	Bb72
A_16	CKRN200008779-1A	*H. sapien*	*h72*	Bb-4	Bb72
A_17	CKRN200008780-1A	*H. sapien*	*h72*	Ec-3	Ec72
A_18	CKRN200008781-1A	*H. sapien*	*h72*	Ec-4	Ec72
A_19	CKRN200008782-1A	*H. sapien*	*h72*	Bs-3	Bs72
A_20	CKRN200008783-1A	*H. sapien*	*h72*	Bs-4	Bs72
A_21	CKRN200008784-1A	*H. sapien*	*h72*	Sm-3	Sm72
A_22	CKRN200008785-1A	*H. sapien*	*h72*	Sm-4	Sm72
A_23	CKRN200008786-1A	*H. sapien*	*h72*	Sa-3	Sa72
A_24	CKRN200008787-1A	*H. sapien*	*h72*	Sa-4	Sa72
A_25	CKRN200008788-1A	*H. sapien*	*h72*	Bb-5	Bb1X12
A_26	CKRN200008789-1A	*H. sapien*	*h72*	Bb-6	Bb1X12
A_27	CKRN200008790-1A	*H. sapien*	*h72*	Bb-7	Bb2X72
A_28	CKRN200008791-1A	*H. sapien*	*h72*	Bb-8	Bb2X72
A_29	CKRN200008792-1A	*H. sapien*	*h72*	Bb-9	Bb1X72
A_30	CKRN200008793-1A	*H. sapien*	*h72*	Bb-10	Bb1X72
A_31	CKRN200008794-1A	*H. sapien*	*h72*	Bb-11	Bb2X12
A_32	CKRN200008795-1A	*H. sapien*	*h72*	Bb-12	Bb2X12

Table 2. 1 Differentially Expressed Genes of Interest in PBMCs Stimulated with PG^{Bb} for 12 Hours

Gene ID	Gene Name	log2Fold Change
ENSG00000108342	CSF3	10.325
ENSG00000196611	HAS1	9.1282
ENSG00000105509	MMP1	8.8096
ENSG00000081041	CXCL2	5.1343
ENSG00000163735	CXCL5	4.5347
ENSG00000124875	CXCL6	7.2557
ENSG00000115008	IL11A	7.9102
ENSG00000125538	IL1B	7.2255
ENSG00000136244	IL6	5.9373
ENSG00000169429	IL8	7.1785
ENSG00000142224	IL19	6.8802
ENSG00000136688	IL-36G	8.0504
ENSG00000109320	NFKB1	1.638
ENSG00000137462	TLR2	1.3073
ENSG00000106100	NOD1	-0.424
ENSG00000167207	NOD2	-0.485
ENSG00000118503	TNFAIP3	1.1767
ENSG00000123610	TNFAIP6	2.8911

Table 2. 2 Differentially Expressed Genes of Interest in PBMCs Stimulated with PG^{Bb} for 72 hours

Gene ID	Gene Name	log2Fold Change
ENSG00000108342	CSF3	9.6662
ENSG00000196611	HAS1	5.8353
ENSG00000105509	MMP-1	9.8312
ENSG00000081041	CXCL2	4.6356
ENSG00000163735	CXCL5	11.879
ENSG00000124875	CXCL6	1.2273
ENSG00000115008	IL11A	5.5591
ENSG00000125538	IL1B	7.5753
ENSG00000136244	IL6	5.6878
ENSG00000169429	IL8	7.2734
ENSG00000142224	IL19	2.8319
ENSG00000136688	IL-36G	5.9828
ENSG00000109320	NFKB1	0.345
ENSG00000137462	TLR2	0.706
ENSG00000106100	NOD1	-0.955
ENSG00000167207	NOD2	0.418
ENSG00000118503	TNFAIP3	1.032
ENSG00000123610	TNFAIP6	2.8399

Table 2. 3 Differentially Expressed Genes of Interest in PBMCs Stimulated with Live *Borrelia* for 12 Hours

Gene ID	Gene Name	log2Fold Change
ENSG00000108342	CSF3	0.34004
ENSG00000196611	HAS1	-0.17191
ENSG00000105509	MMP1	0.13029
ENSG00000081041	CXCL2	2.0512
ENSG00000163735	CXCL5	5.6366
ENSG00000124875	CXCL6	0.48111
ENSG00000115008	IL11A	2.3115
ENSG00000125538	IL1B	3.0072
ENSG00000136244	IL6	2.3263
ENSG00000169429	IL8	2.4063
ENSG00000142224	IL19	0.272
ENSG00000136688	IL-36G	0.20953
ENSG00000109320	NFKB1	0.971
ENSG00000137462	TLR2	1.12
ENSG00000106100	NOD1	0.266
ENSG00000167207	NOD2	1.32
ENSG00000118503	TNFAIP3	1.328
ENSG00000123610	TNFAIP6	2.45

Table 2. 4 Differentially Expressed Genes of Interest in PBMCs Stimulated with Live *Borrelia* for 72 Hours

Gene ID	Gene Name	log2Fold Change
ENSG00000108342	CSF3	0.0709
ENSG00000196611	HAS1	-0.0386
ENSG00000105509	MMP1	NA
ENSG00000081041	CXCL2	-0.10144
ENSG00000163735	CXCL5	0.746
ENSG00000124875	CXCL6	0.0629
ENSG00000115008	IL11A	0.025645
ENSG00000125538	IL1B	0.57677
ENSG00000136244	IL6	-0.024473
ENSG00000169429	IL8	0.989
ENSG00000142224	IL19	NA
ENSG00000136688	IL-36G	NA
ENSG00000109320	NFKB1	-0.185
ENSG00000137462	TLR2	0.359
ENSG00000106100	NOD1	-0.406
ENSG00000167207	NOD2	0.616
ENSG00000118503	TNFAIP3	0.012993
ENSG00000123610	TNFAIP6	1.03

Table 3. 1 Reactome Analysis Post 12 Hour PBMC Stimulation with PG^{Sm}

Description	GeneRatio	BgRatio	pvalue	padj	Count
Viral mRNA Translation	64/2450	86/8838	2.14126E-19	2.14543E-16	64
Neutrophil degranulation	211/2450	449/8838	3.40274E-19	2.14543E-16	211
Eukaryotic Translation Elongation	65/2450	89/8838	5.92962E-19	2.49242E-16	65
Nonsense Mediated Decay (NMD) independent of the Exon Junction Complex (EJC)	66/2450	92/8838	1.5183E-18	3.3697E-16	66
Eukaryotic Translation Termination	65/2450	90/8838	1.56292E-18	3.3697E-16	65
Peptide chain elongation	63/2450	86/8838	1.60335E-18	3.3697E-16	63
Selenocysteine synthesis	63/2450	90/8838	6.70848E-17	1.20848E-14	63
SRP-dependent cotranslational protein targeting to membrane	71/2450	109/8838	3.06056E-16	4.8242E-14	71
Formation of a pool of free 40S subunits	66/2450	99/8838	5.96726E-16	7.24524E-14	66
Nonsense-Mediated Decay (NMD)	71/2450	110/8838	6.32019E-16	7.24524E-14	71

Table 3. 2 Reactome Analysis Post 12 Hour PBMC Stimulation with PG^{Sa}

Description	GeneRatio	BgRatio	pvalue	padj	Count
Neutrophil degranulation	134/1261	450/8819	2.71E-18	3.03E-15	134
Interleukin-10 signaling	29/1261	43/8819	2.47E-15	1.38E-12	29
Interferon Signaling	69/1261	189/8819	1.28E-14	4.76E-12	69
Interferon gamma signaling	37/1261	88/8819	1.81E-10	5.06E-08	37
Interferon alpha/beta signaling	30/1261	67/8819	1.56E-09	3.48E-07	30
Interleukin-4 and 13 signaling	39/1261	104/8819	3.21E-09	5.98E-07	39
Class A/1 (Rhodopsin-like receptors)	59/1261	217/8819	3.86E-07	5.52E-05	59
Chemokine receptors bind chemokines	20/1261	43/8819	3.94E-07	5.52E-05	20
Cell surface interactions at the vascular wall	36/1261	115/8819	2.24E-06	0.00027864	36
Phosphorylation of CD3 and TCR zeta chains	12/1261	20/8819	2.87E-06	0.00032146	12

Table 3. 3 Reactome Analysis Post 12 Hour PBMC Stimulation with PG^{Ec}

Description	GeneRatio	BgRatio	pvalue	padj	Count
Neutrophil degranulation	226/2294	453/8824	4.23E-29	5.32E-26	226
Interferon Signaling	97/2294	190/8824	8.05E-14	5.06E-11	97
Interferon gamma signaling	55/2294	89/8824	9.83E-13	4.12E-10	55
Interleukin-10 signaling	33/2294	42/8824	1.40E-12	4.40E-10	33
Interferon alpha/beta signaling	44/2294	67/8824	9.32E-12	2.34E-09	44
Interleukin-4 and 13 signaling	55/2294	100/8824	5.75E-10	1.20E-07	55
Toll-Like Receptors Cascades	73/2294	150/8824	1.62E-09	2.92E-07	73
Immunoregulatory interactions between a Lymphoid and a non-Lymphoid cell	61/2294	123/8824	1.45E-08	2.27E-06	61
Cell surface interactions at the vascular wall	58/2294	116/8824	2.24E-08	3.13E-06	58
Toll Like Receptor 4 (TLR4) Cascade	61/2294	127/8824	6.55E-08	8.23E-06	61

Table 3. 4 Reactome Analysis Post 12 Hour PBMC Stimulation with PG^{Bs}

Description	GeneRatio	BgRatio	pvalue	padj	Count
Eukaryotic Translation Elongation	70/1818	89/8791	7.25E-32	9.07E-29	70
Eukaryotic Translation Termination	70/1818	90/8791	2.62E-31	9.44E-29	70
Peptide chain elongation	68/1818	86/8791	3.02E-31	9.44E-29	68
Viral mRNA Translation	68/1818	86/8791	3.02E-31	9.44E-29	68
Nonsense Mediated Decay (NMD) independent of the Exon Junction Complex (EJC)	70/1818	92/8791	3.05E-30	7.63E-28	70
Selenocysteine synthesis	68/1818	90/8791	4.37E-29	9.10E-27	68
Formation of a pool of free 40S subunits	72/1818	99/8791	6.19E-29	1.10E-26	72
SRP-dependent cotranslational protein targeting to membrane	75/1818	109/8791	1.50E-27	2.35E-25	75
Nonsense-Mediated Decay (NMD)	74/1818	110/8791	3.16E-26	3.95E-24	74
Nonsense Mediated Decay (NMD) enhanced by the Exon Junction Complex (EJC)	74/1818	110/8791	3.16E-26	3.95E-24	74

Table 3. 5 Reactome Analysis Post 12 Hour PBMC Stimulation with PG^{Bb}

Description	GeneRatio	BgRatio	pvalue	padj	Count
Neutrophil degranulation	258/2942	451/8865	5.44E-27	6.89E-24	258
Interferon Signaling	112/2942	190/8865	1.71E-13	1.08E-10	112
Interleukin-4 and 13 signaling	69/2942	101/8865	4.30E-13	1.82E-10	69
Interleukin-10 signaling	36/2942	42/8865	2.55E-12	8.08E-10	36
Interferon gamma signaling	59/2942	89/8865	1.45E-10	3.67E-08	59
Interferon alpha/beta signaling	47/2942	67/8865	5.99E-10	1.26E-07	47
Platelet activation, signaling and aggregation	125/2942	257/8865	1.42E-07	2.57E-05	125
Interleukin-3, 5 and GM-CSF signaling	33/2942	48/8865	4.75E-07	7.52E-05	33
The citric acid (TCA) cycle and respiratory electron transport	86/2942	167/8865	6.36E-07	8.95E-05	86
Signaling by NOTCH	60/2942	109/8865	1.92E-06	0.000242987	60

Table 4. 1 Reactome Analysis Post 72 Hour PBMC Stimulation with PG^{Sm}

Description	GeneRatio	BgRatio	pvalue	padj	Count
Neutrophil degranulation	287/3707	452/8811	4.06E-21	5.15E-18	287
rRNA processing	141/3707	196/8811	1.13E-17	7.20E-15	141
rRNA processing in the nucleus and cytosol	136/3707	188/8811	1.99E-17	8.43E-15	136
Major pathway of rRNA processing in the nucleolus and cytosol	128/3707	178/8811	3.92E-16	1.24E-13	128
Formation of a pool of free 40S subunits	78/3707	100/8811	1.93E-13	4.91E-11	78
Regulation of expression of SLITs and ROBOs	112/3707	162/8811	2.05E-12	3.58E-10	112
Eukaryotic Translation Initiation	87/3707	118/8811	2.25E-12	3.58E-10	87
Cap-dependent Translation Initiation	87/3707	118/8811	2.25E-12	3.58E-10	87
Signaling by ROBO receptors	134/3707	205/8811	9.02E-12	1.27E-09	134
L13a-mediated translational silencing of Ceruloplasmin expression	81/3707	110/8811	1.45E-11	1.85E-09	81

Table 4. 2 Reactome Analysis Post 72 Hour PBMC Stimulation with PG^{Sa}

Description	GeneRatio	BgRatio	pvalue	padj	Count
Interleukin-10 signaling	18/548	43/8794	2.15E-11	9.60E-09	18
Class A/1 (Rhodopsin-like receptors)	42/548	218/8794	2.98E-11	9.60E-09	42
Chemokine receptors bind chemokines	18/548	44/8794	3.43E-11	9.60E-09	18
Interleukin-4 and 13 signaling	26/548	103/8794	4.64E-10	9.73E-08	26
Response to metal ions	9/548	121/8794	2.47E-09	4.15E-07	9
GPCR ligand binding	48/548	311/8794	3.29E-09	4.60E-07	48
Peptide ligand-binding receptors	27/548	123/8794	5.98E-09	7.17E-07	27
Activation of Matrix Metalloproteinases	12/548	27/8794	2.23E-08	2.34E-06	12
Regulation of Insulin-like Growth Factor (IGF) transport and uptake by Insulin-like Growth Factor Binding Proteins (IGFBPs)	23/548	103/8794	5.78E-08	5.39E-06	23
Post-translational protein phosphorylation	21/548	90/8794	9.80E-08	8.22E-06	21

Table 4. 3 Reactome Analysis Post 72 Hour PBMC Stimulation with PG^{Ec}

Description	GeneRatio	BgRatio	pvalue	padj	Count
Neutrophil degranulation	284/3512	451/8779	4.74E-24	6.03E-21	284
Interferon alpha/beta signaling	49/3512	57/8779	8.41E-13	5.34E-10	49
Interferon Signaling	115/3512	181/8779	9.32E-11	3.95E-08	115
Mitotic G1-G1/S phases	92/3512	146/8779	1.30E-08	4.13E-06	92
Interleukin-10 signaling	35/3512	43/8779	3.13E-08	6.77E-06	35
Cell Cycle, Mitotic	255/3512	492/8779	3.20E-08	6.77E-06	255
Interleukin-4 and 13 signaling	67/3512	102/8779	1.23E-07	2.21E-05	67
Interferon gamma signaling	60/3512	89/8779	1.39E-07	2.21E-05	60
Interleukin-1 family signaling	72/3512	115/8779	7.06E-07	9.97E-05	72
Antigen processing-Cross presentation	61/3512	94/8779	8.45E-07	0.0001074	61

Table 4. 4 Reactome Analysis Post 72 Hour PBMC Stimulation with PG^{Bs}

Description	GeneRatio	BgRatio	pvalue	padj	Count
Neutrophil degranulation	139/1417	450/8745	1.19E-15	1.45E-12	139
Interferon Signaling	66/1417	181/8745	1.93E-11	1.17E-08	66
Interferon gamma signaling	38/1417	88/8745	1.63E-09	6.60E-07	38
Interleukin-10 signaling	24/1417	43/8745	3.10E-09	9.42E-07	24
Interleukin-4 and 13 signaling	39/1417	101/8745	4.37E-08	1.06E-05	39
Phosphorylation of CD3 and TCR zeta chains	13/1417	20/8745	1.27E-06	0.00025707	13
Interferon alpha/beta signaling	25/1417	59/8745	1.56E-06	0.00027	25
PD-1 signaling	13/1417	21/8745	2.84E-06	0.000431	13
Translocation of ZAP-70 to Immunological synapse	11/1417	17/8745	9.32E-06	0.00125706	11
Amino acid transport across the plasma membrane	14/1417	26/8745	1.13E-05	0.00137105	14

Table 4. 5 Reactome Analysis Post 72 Hour PBMC Stimulation with PG^{Bb}

Description	GeneRatio	BgRatio	pvalue	padj	Count
Neutrophil degranulation	132/1455	452/8803	3.35E-12	4.03E-09	132
Interferon alpha/beta signaling	31/1455	59/8803	2.06E-10	1.24E-07	31
Interferon Signaling	62/1455	181/8803	3.33E-09	1.34E-06	62
Interleukin-4 and 13 signaling	41/1455	104/8803	1.76E-08	5.28E-06	41
Interleukin-10 signaling	22/1455	43/8803	1.67E-07	4.01E-05	22
Interferon gamma signaling	34/1455	88/8803	5.08E-07	0.00010177	34
Chemokine receptors bind chemokines	21/1455	44/8803	1.41E-06	0.00024162	21
Extracellular matrix organization	71/1455	261/8803	6.90E-06	0.00103777	71
Response to metal ions	9/1455	Dec-03	1.23E-05	0.00163739	9
Phosphorylation of CD3 and TCR zeta chains	12/1455	20/8803	1.36E-05	0.00163739	12

Table 5. 1 GO Analysis "Granulocyte Activation," Pathway

Stimulant	Genes in Pathway	Temporal Difference	Uniquely Expressed Genes
PG^{Bb} 12 hrs	271	132	ABR ACAA1 AGPAT2 ALAD ALDH3B1 ALOX5 ANXA2 APEH ARHGAP9 ARPC5 ARSAASAH1 ATG7 ATP11B ATP6AP2 ATP6V0A1 ATP8A1 B2M BIN2 BRI3 BST1 CAPN1 CAT CD33 CD47 CD63 CDA CFP CLEC4C CLEC4D COTL1 CPPED CRISPLD2 CTSA CTSB CTSD CTSS CTSZ CXCL6 CYBB DBNL DDOST DDX3X DERA DOCK2 DOK3 DPP7 DSP ENPP4 ERP44 FAF2 FTL FUCA2 GDI2 GHDC GLB1 GLIPR1 GMFG GSDMD GUSB GYG1 HEBP2 HK3 HLA-B HLA-C HMGB1 HMOX2 HSP90AA1 HSP90AB1 HSPA1A HSPA6 HSPA8 IQGAP2 ITGAM ITGB2 KCNAB2 KPNB1 LAMP1 LAMP2 LAMTOR1 LAMTOR2 LGALS3 LILRB2 LRG1 LTA4H MANBA MLEC MVP NAPRT1 NBEAL2 NCKAP1L NCSTN NFAM1 NFKB1 NIT2 NPC2 NRAS PAFAH1B2 PDXK PFKL PGM2 PLAC8 PLAU PPIA PRDX4 PREX1 PSAP PSMA5 PSMB1 PSMC2 PSMC3 PTPRC PYGB PYGL RAB10 RAB14 RAB24 RAB27A RAB31 RAB5C RAB6A RAC1 RAP1A RAP1B RAP2C RHOA RHOG S100A11 SERPINB1 SIRPB1 SLC15A4 SLC27A2 SNAP23 SRP14 STOM STX4 STXBP2 SYK TBC1D10C TCIRG1 TIMP2 TMC6 TMEM179B TMEM63A TRAPPC1 TRPM2 TSPAN14 TYROBP UNC13D VAT1 VCL VCP YPEL5
PG^{Bb} 72 hrs	139		ALDOA ALDOC ANO6 ANPEP ATP8B4 C3AR1 CEACAM3 CXCR1 ELANE F2RL1 FCER1G GNS IGF2R IQGAP1 PGM1 PKM PPBP PTPRJ QPCT S100A12 SLC2A5
Live Borrelia 12 hrs	272	188	FGR FUCA2 ENPP4 MPO LAMP2 ALDH3B1 PSMB1 TYROBP MVP SERPINB1 ERP44 RNASET2 VCL HEXB CYBA HEBP2 ATP11B CTSA CNN2 CDK13 PKM ROCK1 ATP11A KCNAB2 STK10 PLD1 STXBP2 PSEN1 HSP90AA1 PPIE RAB10 SCAMP1 B4GALT1 FTL CMTM6 SNAP23 DSP MAPK1 TOM1 ARSA PYGL MMP9 DNAJC5 CTSZ SIRPB1 BPI MAGT1 GLA DNAJC3 HMOX2 PYCARD STX4 GSDMD GPI CD33 VAT1 ALDOC NFKB1 BST1 COMMD9 TCIRG1 MLEC BIN2 PTPN6 FAF2 ARSB QPCT QSOX1 STXBP3 LAMTOR2 CD58 LRMP VAMP8 NPC2 CAT CCR2 PLAU HVCN1 ARHGAP9 NCKAP1L RAP2C ATP8A1 SERPINB6 C3 RAP1B UBR4 FGL2 COPB1 EFCAB4B MOSPD2 GMFG CAP1 ACTR10 LGALS3 CHIT1 AMPD3 DOCK2 CD63 TMBIM1 ACTR2 DNAJC13 IDH1 GLIPR1 GPR84 SLC27A2 IQGAP1 ITGAX TMC6 PFKL CREG1 FCGR2A ILF2 DEGS1 C1orf35 DOK3 DYNLT1 NAPRT1 SURF4 PTGES2 PTPRJ LAMTOR1 DSN1 ALDOA ADAM8 CCT8 EEF1A1 CDA FCER1G CSTB ITGB2 NBEAL2 HK3 PSMC2 ARPC5 CTSS S100A11 S100A12 PTX3 PPBP CXCL1 PRKCD APEH IL15 F2RL1 BRI3 CTSB HGSNAT CYBB VCP PSMC3 CCT2 B2M LAIR1 EEF2 CD300A GHDC FTH1 PAFAH1B2 RAB31 PGM2 AGPAT2 ITGAM GUSB GLB1 PA2G4 FPR2 FPR1 GAA CANT1 PGAM1 HPSE HSPA6 OLR1 PSMD1 TBC1D10C DPP7 ANO6 IMPDH2 RAP2B ATP6AP2 ANXA2 TMEM173 METTL7A LAMP1 BCR SELL HMGB1 TMEM63A MME GM2A CD47 DYNC1H1 ATG7 ELANE SPTAN1 PSAP SIRPA APRT CR1 HSPA1B NRAS DDX3X HLA-B NFAM1 PLEKHO2 DDOST SIGLEC14 MGAM
Live Borrelia 72 hrs	84		MGST1 ALOX5 SLC11A1 RAB27A CD59 CYB5R3 TMEM30A CD93 CFP CD36 GSN CLEC4D CEACAM3 JUP RAB6A GPR97 C19orf59 AP2A2 CD55 LILRB3

Table 6. 1 Reactome Analysis Post 12 Hour PBMC Stimulation with Live *Borrelia*

Description	GeneRatio	BgRatio	pvalue	padj	Count
Neutrophil degranulation	256/3379	448/8775	2.00E-16	2.54E-13	256
Cell Cycle, Mitotic	251/3379	490/8775	2.79E-09	1.77E-06	251
Signaling by Rho GTPases	205/3379	392/8775	1.02E-08	4.32E-06	205
RHO GTPase Effectors	147/3379	269/8775	3.76E-08	1.19E-05	147
Interferon gamma signaling	58/3379	88/8775	1.59E-07	3.90E-05	58
Interferon Signaling	107/3379	188/8775	1.85E-07	3.90E-05	107
Toll-Like Receptors Cascades	86/3379	148/8775	8.89E-07	0.0001609	86
Activated TLR4 signalling	68/3379	114/8775	3.46E-06	0.0005479	68
Toll Like Receptor 3 (TLR3) Cascade	60/3379	98/8775	3.97E-06	0.00055936	60
Toll Like Receptor 4 (TLR4) Cascade	73/3379	125/8775	4.56E-06	0.00056017	73

Table 6. 2 Reactome Analysis Post 72 Hour PBMC Stimulation with Live *Borrelia*

Description	GeneRatio	BgRatio	pvalue	padj	Count
Neutrophil degranulation	76/620	448/8678	4.31E-13	4.01E-10	76
Interferon gamma signaling	25/620	88/8678	1.15E-09	5.35E-07	25
Interferon Signaling	35/620	180/8678	3.77E-08	1.17E-05	35
Interleukin-4 and 13 signaling	24/620	100/8678	9.11E-08	2.12E-05	24
Phosphorylation of CD3 and TCR zeta chains	10/620	20/8678	3.09E-07	5.76E-05	10
Amino acid transport across the plasma membrane	11/620	27/8678	1.03E-06	0.0001594	11
Response to metal ions	7/620	121/8678	5.30E-06	0.00070516	7
PD-1 signaling	9/620	21/8678	6.17E-06	0.00071773	9
Translocation of ZAP-70 to Immunological synapse	8/620	17/8678	8.85E-06	0.00091514	8
Interferon alpha/beta signaling	14/620	58/8678	4.16E-05	0.00387271	14

Table 7. 1 DO Enrichment Analysis

DOID	Description	GeneRatio	BgRatio	padj
DOID:7148	Rheumatoid arthritis	253/2301	492/6514	1.65458970051366e-11
DOID:104	Bacterial infectious disease	137/2301	236/6514	1.43643235991752e-10
DOID:2237	Hepatitis	204/2301	391/6514	4.03222388307199e-10
DOID:3213	Demyelinating disease	99/2301	160/6514	7.2113240873819e-10
DOID:2377	Multiple sclerosis	97/2301	156/6514	7.2113240873819e-10

Figure 2: CoExpresssion Analysis

A

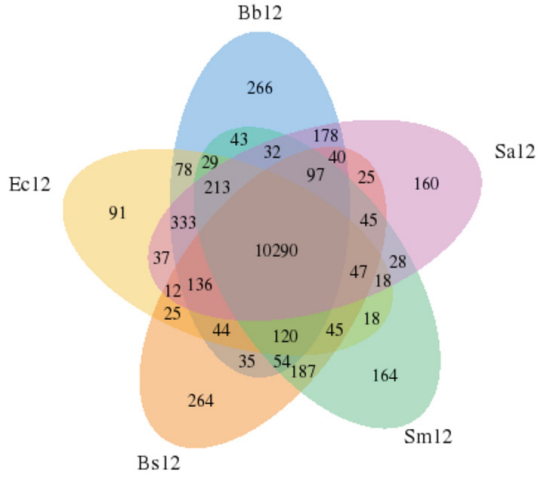

B

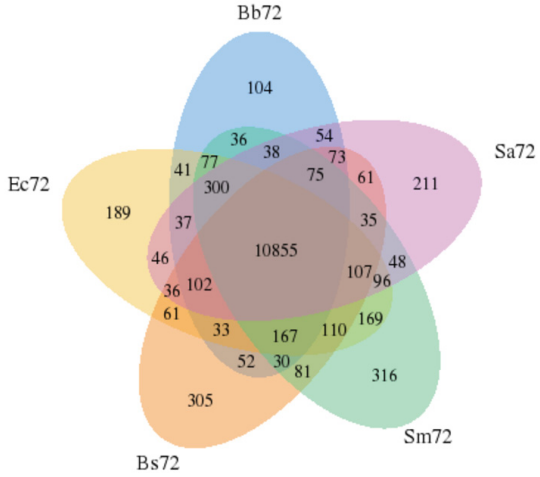

C

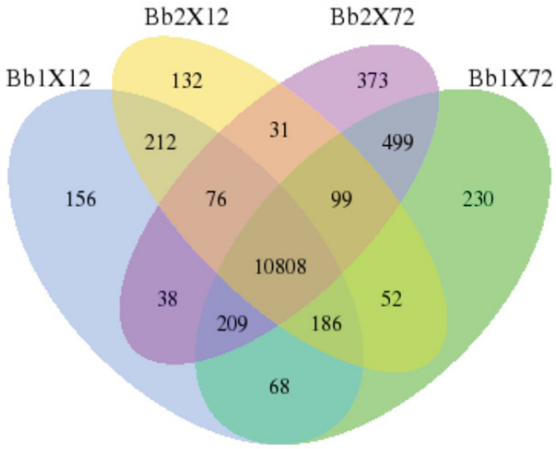

Figure 2: CoExpression Analysis. (A) Coexpression analysis for PBMCs stimulated with PG^{Bb} , PG^{Ec} , PG^{Bs}, PG^{Sm} and PG^{Sa} for 12 hours. **(B)** Coexpression analysis forPBMCs stimulated with PG^{Bb} , PG^{Ec} , PG^{Bs}, PG^{Sm} and PG^{Sa} for 72 hours. **(C)** PBMCs stimulated with live Borrelia at either 500 cells/mL (Bb1X) or 5000 cells/mL (Bb2X) for 12 or 72 hours.

Figure 3: GO Enrichment Analysis Results for the PBMCs Stimulated with Bacterial PGs for 12 and 72 Hours.

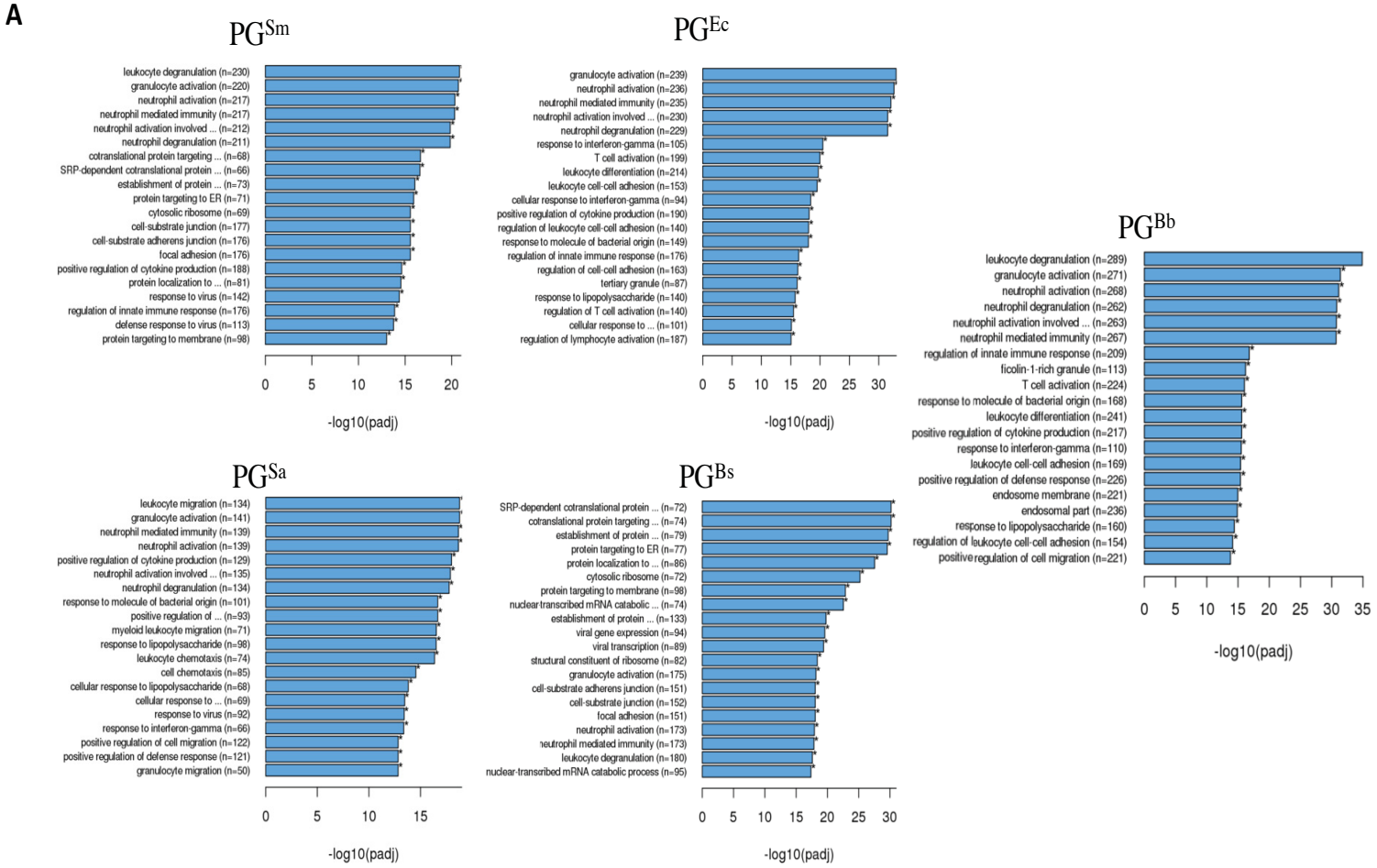

B

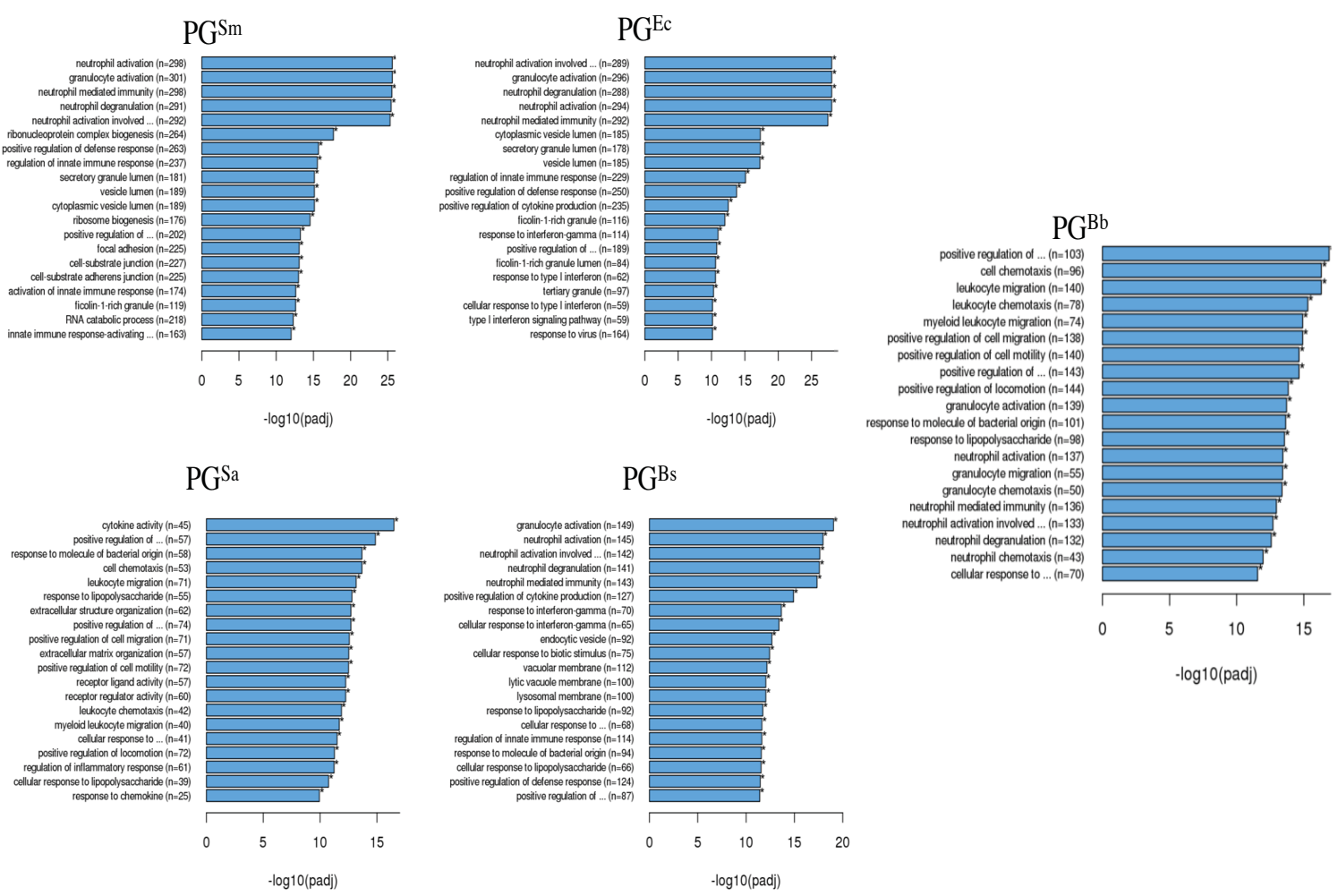
PG^Sm
neutrophil activation (n=298)
granulocyte activation (n=301)
neutrophil mediated immunity (n=298)
neutrophil degranulation (n=291)
neutrophil activation involved ... (n=292)
ribonucleoprotein complex biogenesis (n=264)
positive regulation of defense response (n=263)
regulation of innate immune response (n=237)
secretory granule lumen (n=181)
vesicle lumen (n=189)
cytoplasmic vesicle lumen (n=189)
ribosome biogenesis (n=176)
positive regulation of ... (n=202)
focal adhesion (n=225)
cell-substrate junction (n=227)
cell-substrate adherens junction (n=225)
activation of innate immune response (n=174)
ficolin-1-rich granule (n=119)
RNA catabolic process (n=218)
innate immune response-activating ... (n=163)
0 5 10 15 20 25
-log10(padj)
PG^Ec
neutrophil activation involved ... (n=289)
granulocyte activation (n=296)
neutrophil degranulation (n=288)
neutrophil activation (n=294)
neutrophil mediated immunity (n=292)
cytoplasmic vesicle lumen (n=185)
secretory granule lumen (n=178)
vesicle lumen (n=185)
regulation of innate immune response (n=229)
positive regulation of defense response (n=250)
positive regulation of cytokine production (n=235)
ficolin-1-rich granule (n=116)
response to interferon-gamma (n=114)
positive regulation of ... (n=189)
ficolin-1-rich granule lumen (n=84)
response to type I interferon (n=62)
tertiary granule (n=97)
cellular response to type I interferon (n=59)
type I interferon signaling pathway (n=59)
response to virus (n=164)
0 5 10 15 20 25
-log10(padj)
PG^Bb
positive regulation of ... (n=103)
cell chemotaxis (n=96)
leukocyte migration (n=140)
leukocyte chemotaxis (n=78)
myeloid leukocyte migration (n=74)
positive regulation of cell migration (n=138)
positive regulation of cell motility (n=140)
positive regulation of ... (n=143)
positive regulation of locomotion (n=144)
granulocyte activation (n=139)
response to molecule of bacterial origin (n=101)
response to lipopolysaccharide (n=98)
neutrophil activation (n=137)
granulocyte migration (n=55)
granulocyte chemotaxis (n=50)
neutrophil mediated immunity (n=136)
neutrophil activation involved ... (n=133)
neutrophil degranulation (n=132)
neutrophil chemotaxis (n=43)
cellular response to ... (n=70)
0 5 10 15
-log10(padj)
PG^Sa
cytokine activity (n=45)
positive regulation of ... (n=57)
response to molecule of bacterial origin (n=58)
cell chemotaxis (n=53)
leukocyte migration (n=71)
response to lipopolysaccharide (n=55)
extracellular structure organization (n=62)
positive regulation of ... (n=74)
positive regulation of cell migration (n=71)
extracellular matrix organization (n=57)
positive regulation of cell motility (n=72)
receptor ligand activity (n=57)
receptor regulator activity (n=60)
leukocyte chemotaxis (n=42)
myeloid leukocyte migration (n=40)
cellular response to ... (n=41)
positive regulation of locomotion (n=72)
regulation of inflammatory response (n=61)
cellular response to lipopolysaccharide (n=39)
response to chemokine (n=25)
0 5 10 15
-log10(padj)
PG^Bs
granulocyte activation (n=149)
neutrophil activation (n=145)
neutrophil activation involved ... (n=142)
neutrophil degranulation (n=141)
neutrophil mediated immunity (n=143)
positive regulation of cytokine production (n=127)
response to interferon-gamma (n=70)
cellular response to interferon-gamma (n=65)
endocytic vesicle (n=92)
cellular response to biotic stimulus (n=75)
vacuolar membrane (n=112)
lytic vacuole membrane (n=100)
lysosomal membrane (n=100)
response to lipopolysaccharide (n=92)
cellular response to ... (n=68)
regulation of innate immune response (n=114)
response to molecule of bacterial origin (n=94)
cellular response to lipopolysaccharide (n=66)
positive regulation of defense response (n=124)
positive regulation of ... (n=87)
0 5 10 15 20
-log10(padj)

Figure 3: GO Enrichment Analysis Results for the PBMCs Stimulated with Bacterial PGs for 12 and 72 Hours. Top 20 GO results are reported, those with a padj value of <0.05 represent significant findings. **(A)** GO analysis for PBMCs stimulated with bacterial PG for 12 hours. **(B)** GO analysis for PBMCs stimulated with bacterial PG for 72 hours.

Figure 4: Gene Expression Analysis in PBMCs Stimulated with Bacterial PGs for 12 and 72 Hours.

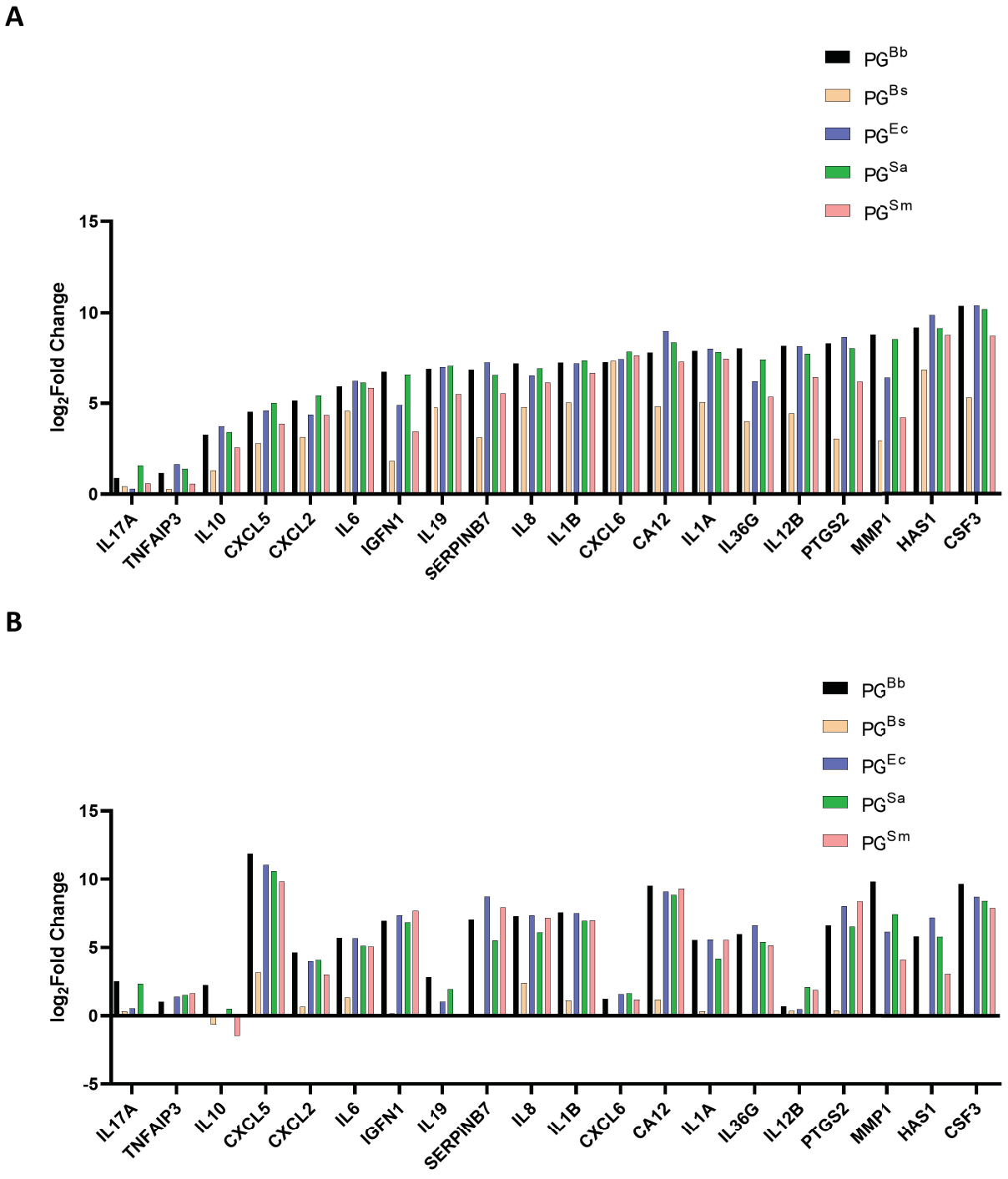

Figure 4: Gene Expression Analysis in PBMCs Stimulated with Bacterial PGs for 12 and 72 Hours. Y-axis is log_2Fold change in gene expression compared to controls, PBMC stimulated with PBS. **(A)** Genes upregulated in response to $PG^{Bb,}$ $PG^{Ec,}$ $PG^{Bs,}$ PG^{Sm} and PG^{Sa} for 12 hours. **(B)** Genes upregulated in response to $PG^{Bb,}$ PG^{Ec} , $PG^{Bs,}$ PG^{Sm} and PG^{Sa} for 72 hours.

Figure 5: KEGG Enrichment Analysis Results for the PBMCs Stimulated with Bacterial PGs for 12 and 72 Hours

A

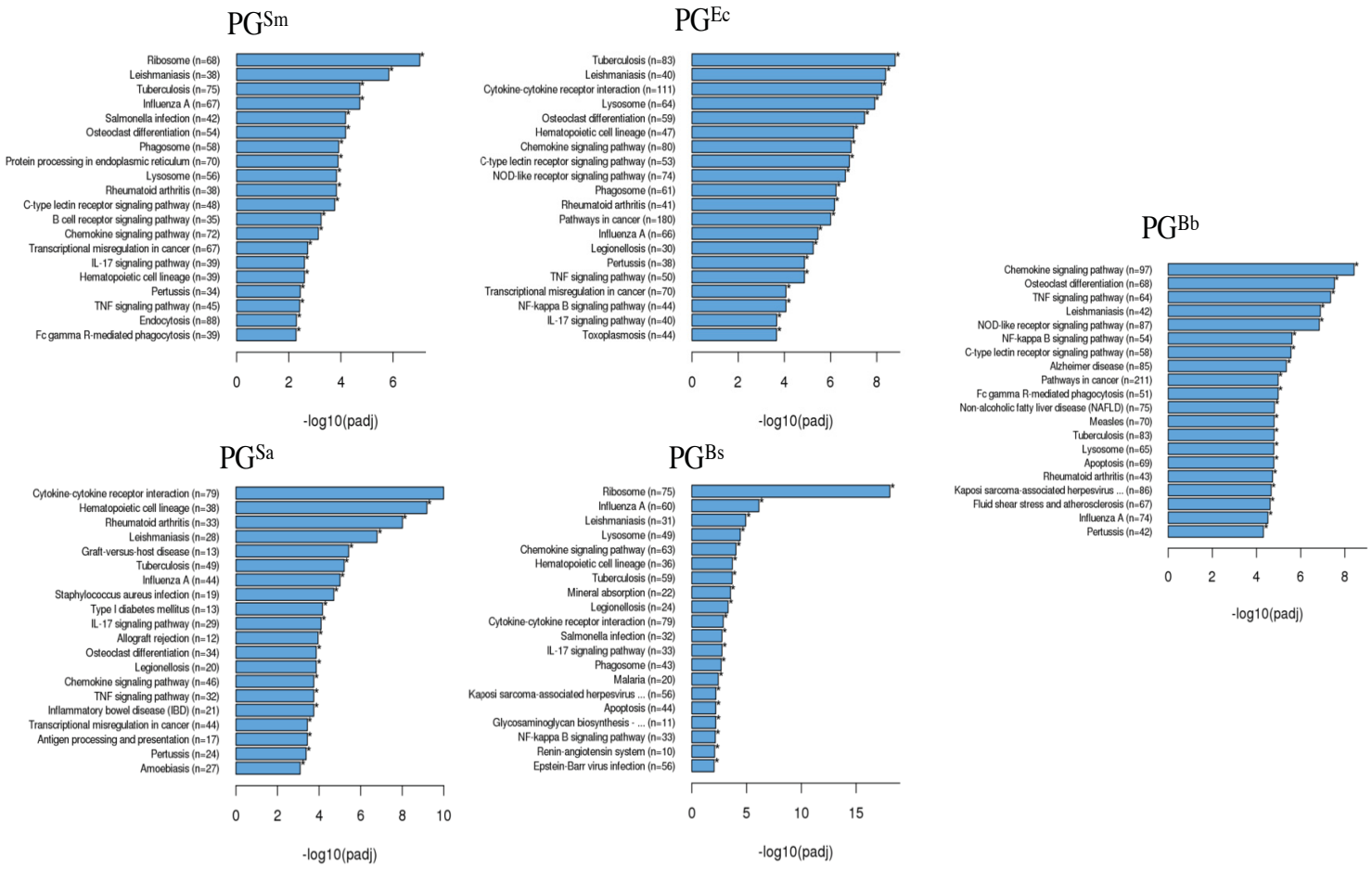

B

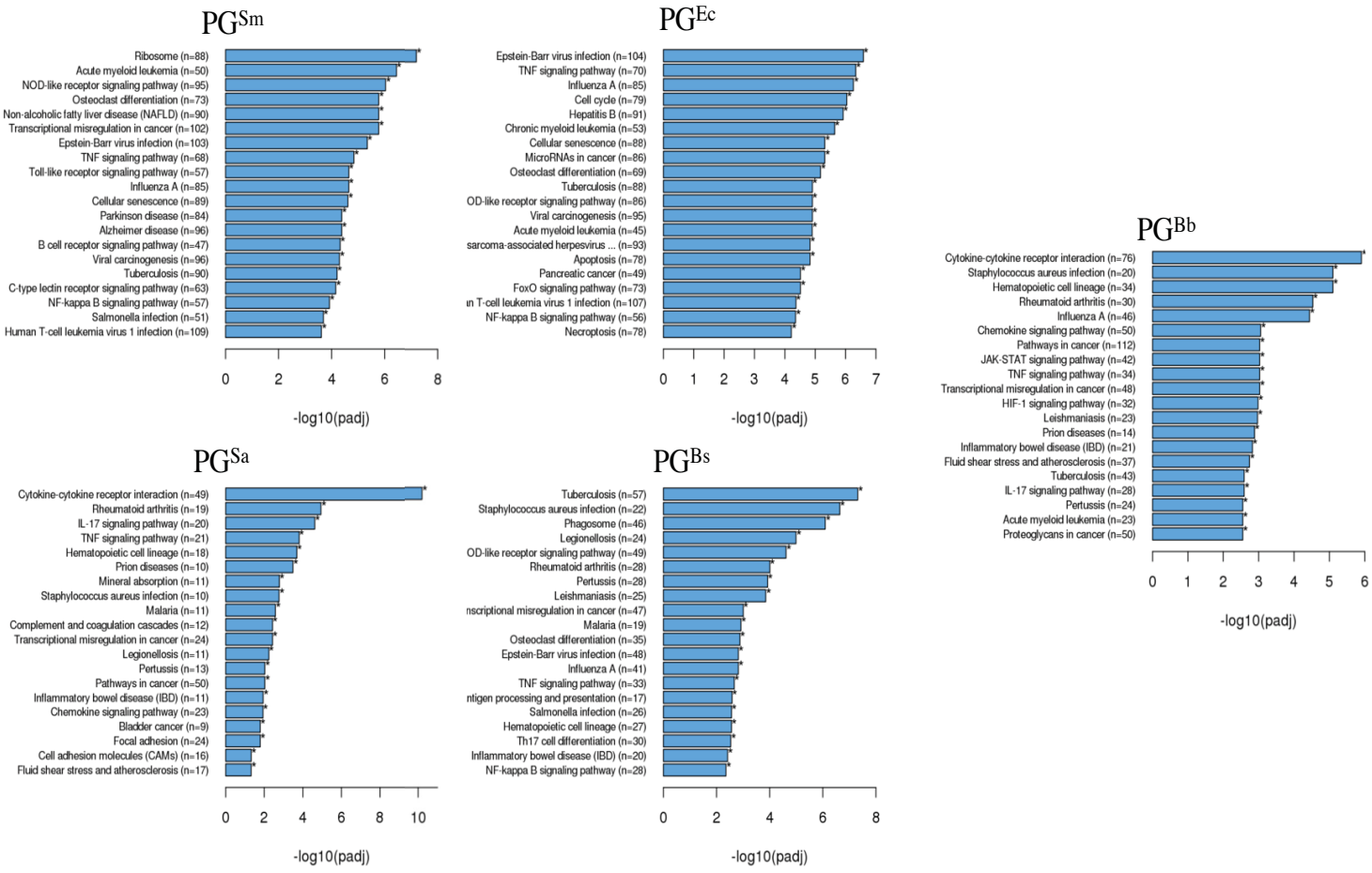
PG^Sm
Ribosome (n=88)
Acute myeloid leukemia (n=50)
NOD-like receptor signaling pathway (n=95)
Osteoclast differentiation (n=73)
Non-alcoholic fatty liver disease (NAFLD) (n=90)
Transcriptional misregulation in cancer (n=102)
Epstein-Barr virus infection (n=103)
TNF signaling pathway (n=68)
Toll-like receptor signaling pathway (n=57)
Influenza A (n=85)
Cellular senescence (n=89)
Parkinson disease (n=84)
Alzheimer disease (n=96)
B cell receptor signaling pathway (n=47)
Viral carcinogenesis (n=96)
Tuberculosis (n=90)
C-type lectin receptor signaling pathway (n=63)
NF-kappa B signaling pathway (n=57)
Salmonella infection (n=51)
Human T-cell leukemia virus 1 infection (n=109)
0 2 4 6 8
-log10(padj)
PG^Ec
Epstein-Barr virus infection (n=104)
TNF signaling pathway (n=70)
Influenza A (n=85)
Cell cycle (n=79)
Hepatitis B (n=91)
Chronic myeloid leukemia (n=53)
Cellular senescence (n=88)
MicroRNAs in cancer (n=86)
Osteoclast differentiation (n=69)
Tuberculosis (n=88)
OD-like receptor signaling pathway (n=86)
Viral carcinogenesis (n=95)
Acute myeloid leukemia (n=45)
sarcoma-associated herpesvirus ... (n=93)
Apoptosis (n=78)
Pancreatic cancer (n=49)
FoxO signaling pathway (n=73)
ın T-cell leukemia virus 1 infection (n=107)
NF-kappa B signaling pathway (n=56)
Necroptosis (n=78)
0 1 2 3 4 5 6 7
-log10(padj)
PG^Bb
Cytokine-cytokine receptor interaction (n=76)
Staphylococcus aureus infection (n=20)
Hematopoietic cell lineage (n=34)
Rheumatoid arthritis (n=30)
Influenza A (n=46)
Chemokine signaling pathway (n=50)
Pathways in cancer (n=112)
JAK-STAT signaling pathway (n=42)
TNF signaling pathway (n=34)
Transcriptional misregulation in cancer (n=48)
HIF-1 signaling pathway (n=32)
Leishmaniasis (n=23)
Prion diseases (n=14)
Inflammatory bowel disease (IBD) (n=21)
Fluid shear stress and atherosclerosis (n=37)
Tuberculosis (n=43)
IL-17 signaling pathway (n=28)
Pertussis (n=24)
Acute myeloid leukemia (n=23)
Proteoglycans in cancer (n=50)
0 1 2 3 4 5 6
-log10(padj)
PG^Sa
Cytokine-cytokine receptor interaction (n=49)
Rheumatoid arthritis (n=19)
IL-17 signaling pathway (n=20)
TNF signaling pathway (n=21)
Hematopoietic cell lineage (n=18)
Prion diseases (n=10)
Mineral absorption (n=11)
Staphylococcus aureus infection (n=10)
Malaria (n=11)
Complement and coagulation cascades (n=12)
Transcriptional misregulation in cancer (n=24)
Legionellosis (n=11)
Pertussis (n=13)
Pathways in cancer (n=50)
Inflammatory bowel disease (IBD) (n=11)
Chemokine signaling pathway (n=23)
Bladder cancer (n=9)
Focal adhesion (n=24)
Cell adhesion molecules (CAMs) (n=16)
Fluid shear stress and atherosclerosis (n=17)
0 2 4 6 8 10
-log10(padj)
PG^Bs
Tuberculosis (n=57)
Staphylococcus aureus infection (n=22)
Phagosome (n=46)
Legionellosis (n=24)
OD-like receptor signaling pathway (n=49)
Rheumatoid arthritis (n=28)
Pertussis (n=28)
Leishmaniasis (n=25)
nscriptional misregulation in cancer (n=47)
Malaria (n=19)
Osteoclast differentiation (n=35)
Epstein-Barr virus infection (n=48)
Influenza A (n=41)
TNF signaling pathway (n=33)
ntigen processing and presentation (n=17)
Salmonella infection (n=26)
Hematopoietic cell lineage (n=27)
Th17 cell differentiation (n=30)
Inflammatory bowel disease (IBD) (n=20)
NF-kappa B signaling pathway (n=28)
0 2 4 6 8
-log10(padj)

Figure 5: KEGG Enrichment Analysis Results for the PBMCs Stimulated with Bacterial PGs for 12 and 72 Hours. Top 20 KEGG results are reported, those with a padj value of <0.05 represent significant findings. **(A)** KEGG analysis for PBMCs stimulated with bacterial PG for 12 hours. **(B)** KEGG analysis for PBMCs stimulated with bacterial PG for 72 hours.

Figure 6: Cluster Analysis of Differentially Expressed Genes

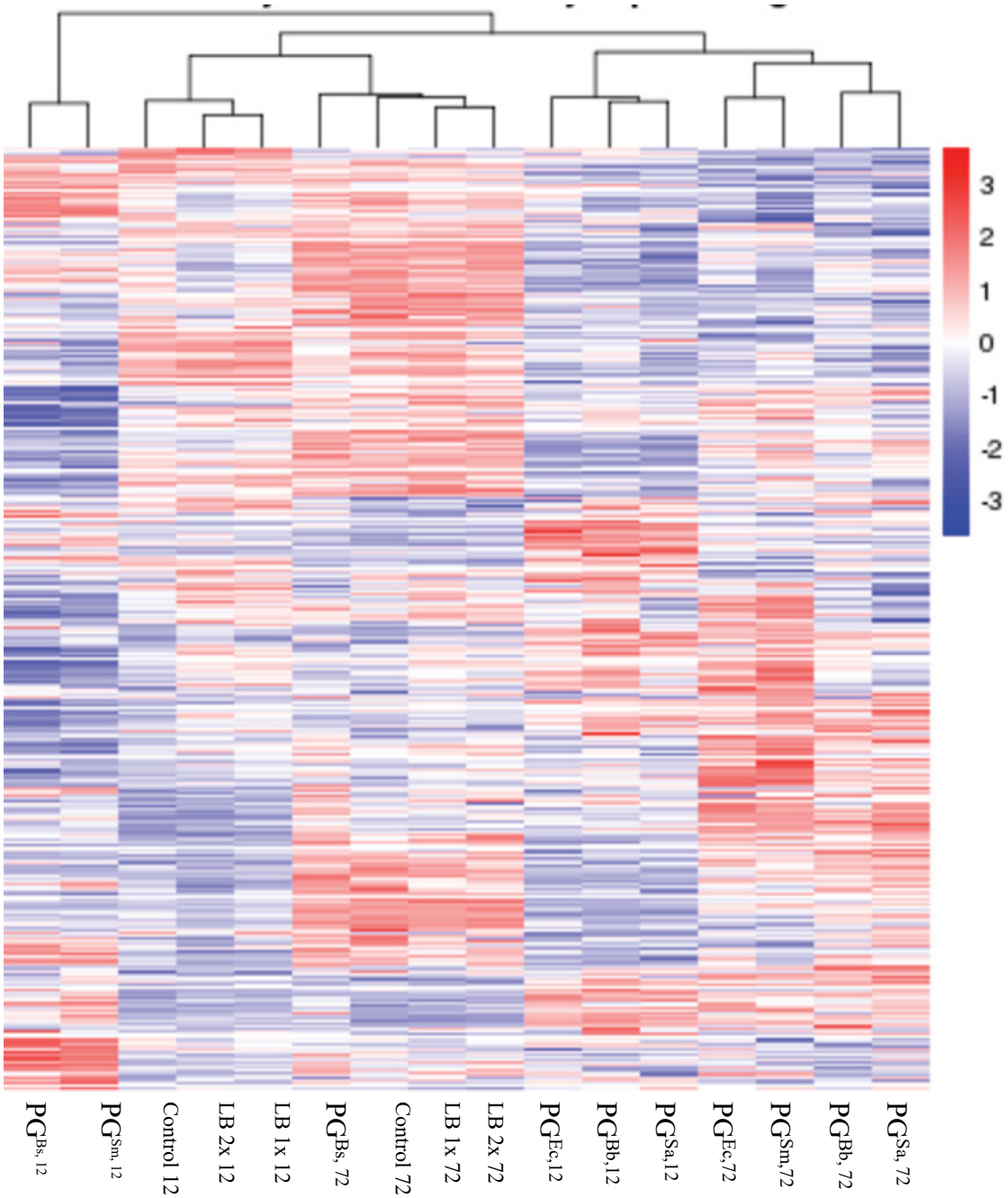

Figure 6: Cluster Analysis of Differentially Expressed Genes. Cluster analysis was performed using log10(FPKM+1). Red represents genes with high levels of expression while blue represents genes with low levels of expression. LB1x: Live Borrelia 500cells/mL LB 2x: Live Borrelia 5000 cells/mL.

Figure 7: GO Enrichment Analysis Results for the PBMCs Stimulated with PG^{Bb} or Live *Borrelia* at 5000 cells/mL for 12 and 72 hours.

A

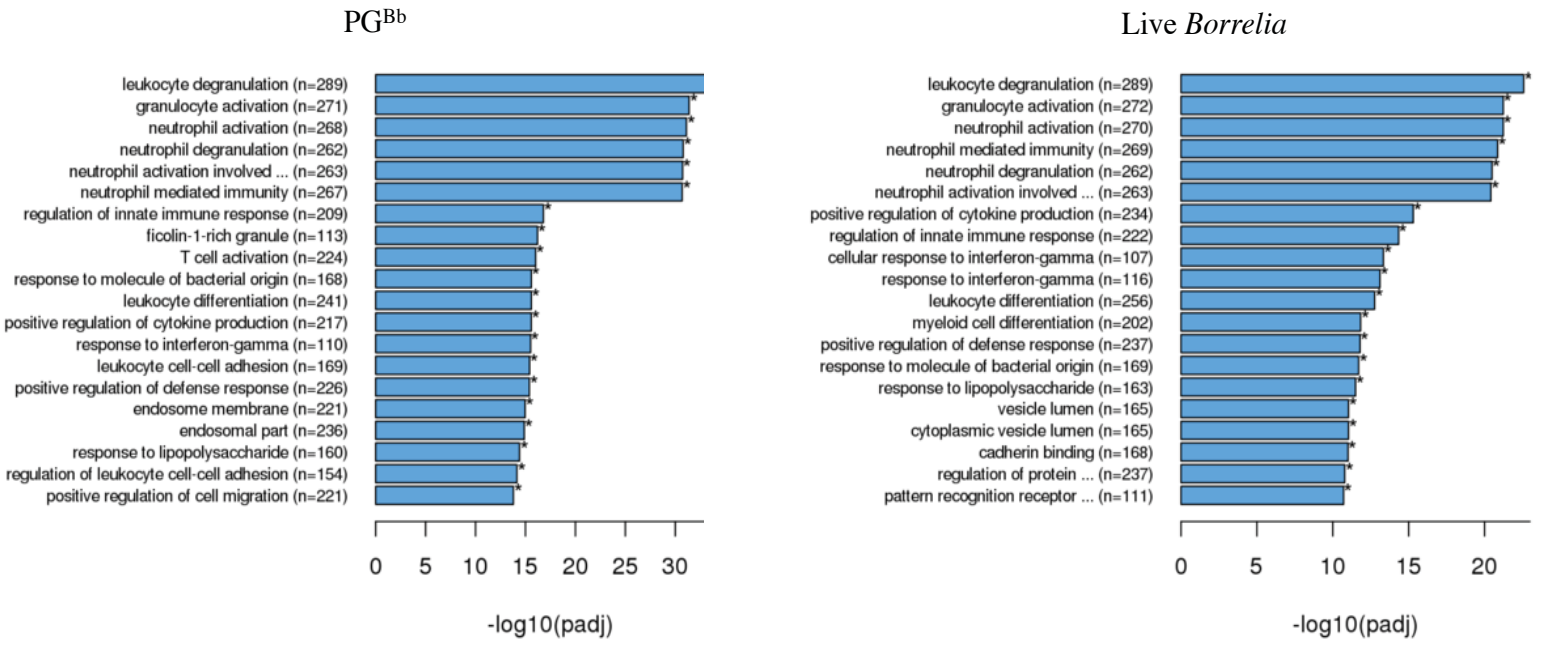

B

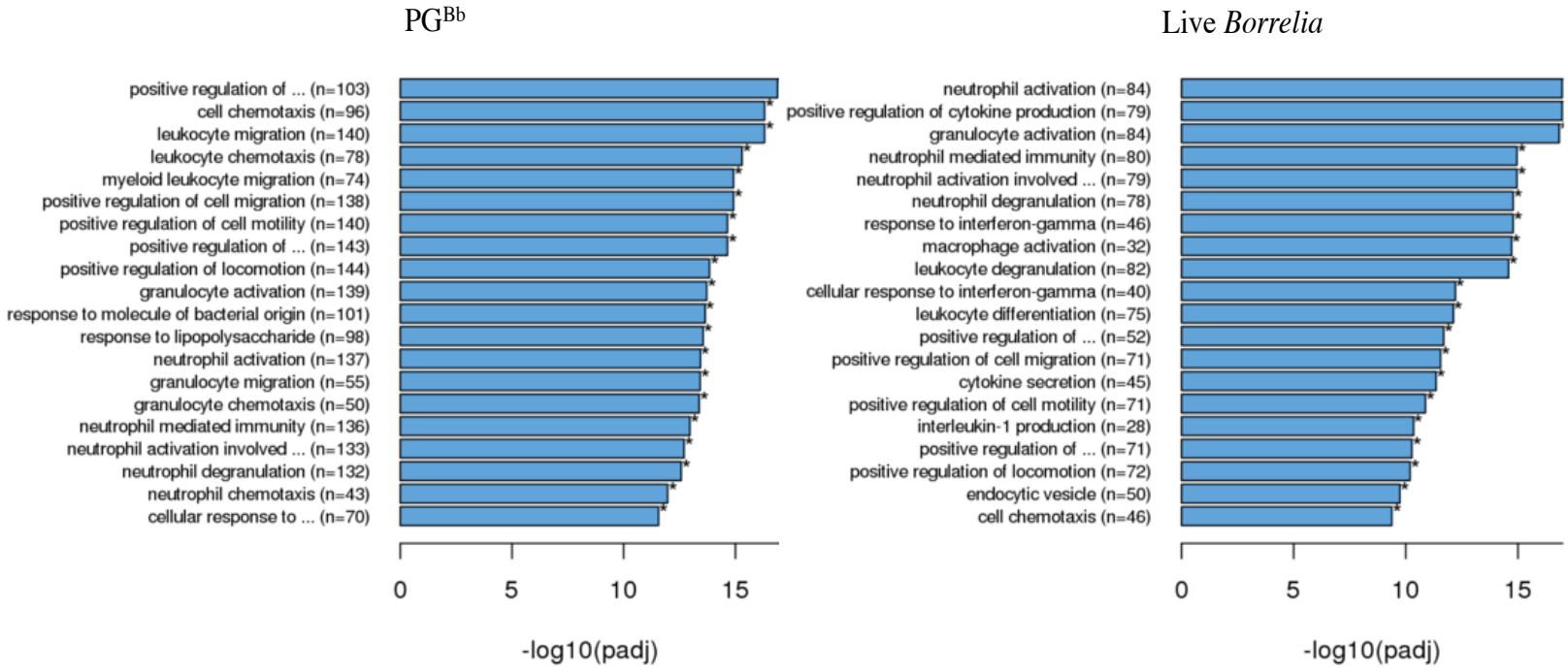

Figure 7: GO Enrichment analysis results for the PBMCs stimulated with PG^{Bb} or live *Borrelia* at 5000 cells/mL at 12 and 72 hours. Top 20 GO results are reported, those with a padj value of <0.05 represent significant findings. **(A)** GO analysis for PBMCs stimulated with bacterial for 12 hours. **(B)** GO analysis for PBMCs stimulated with bacterial PG for 72 hours.

Figure 8: KEGG Enrichment Analysis Results for the PBMCs stimulated with PG^{Bb} or Live *Borrelia* at 5000 cells/mL for 12 and 72 Hours.

A

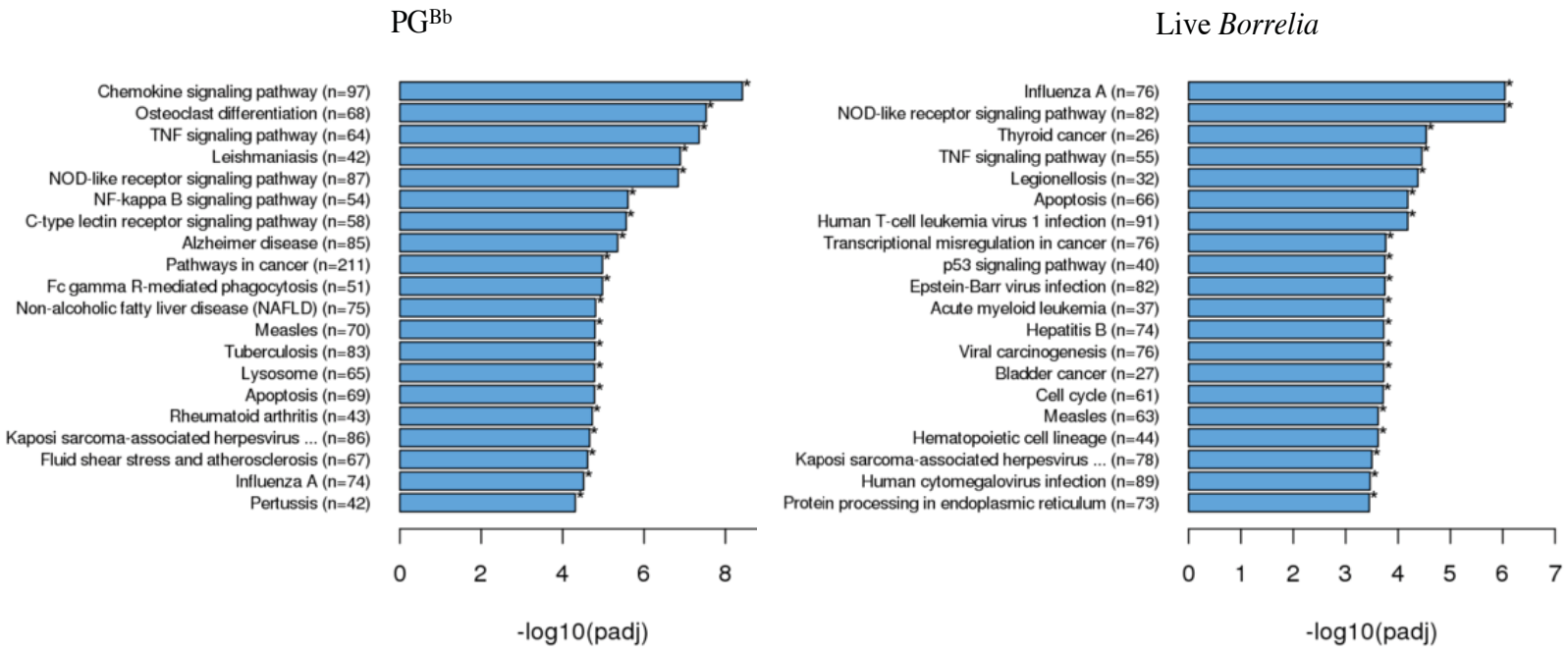

B

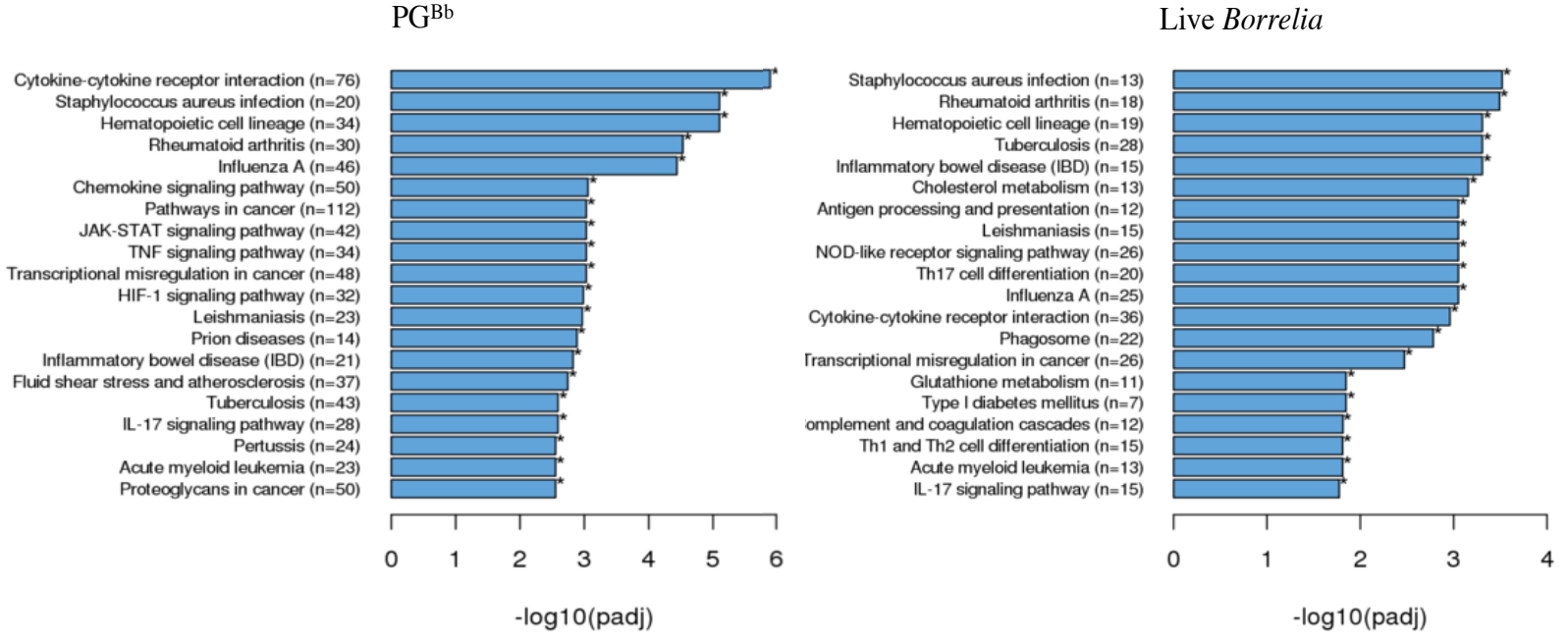

Figure 8: KEGG Enrichment Analysis Results for the PBMCs Stimulated with PG^{Bb} or Live *Borrelia* at 5000 cells/mL for 12 and 72 Hours. Top 20 KEGG results are reported, those with a padj value of <0.05 represent significant findings. **(A)** KEGG analysis for PBMCs stimulated with bacterial for 12 hours. **(B)** KEGG analysis for PBMCs stimulated with bacterial PG for 72 hours

Figure 9: Gene Expression Analysis in PBMCs Stimulated with Bacterial PGs for 12 and 72 Hours.

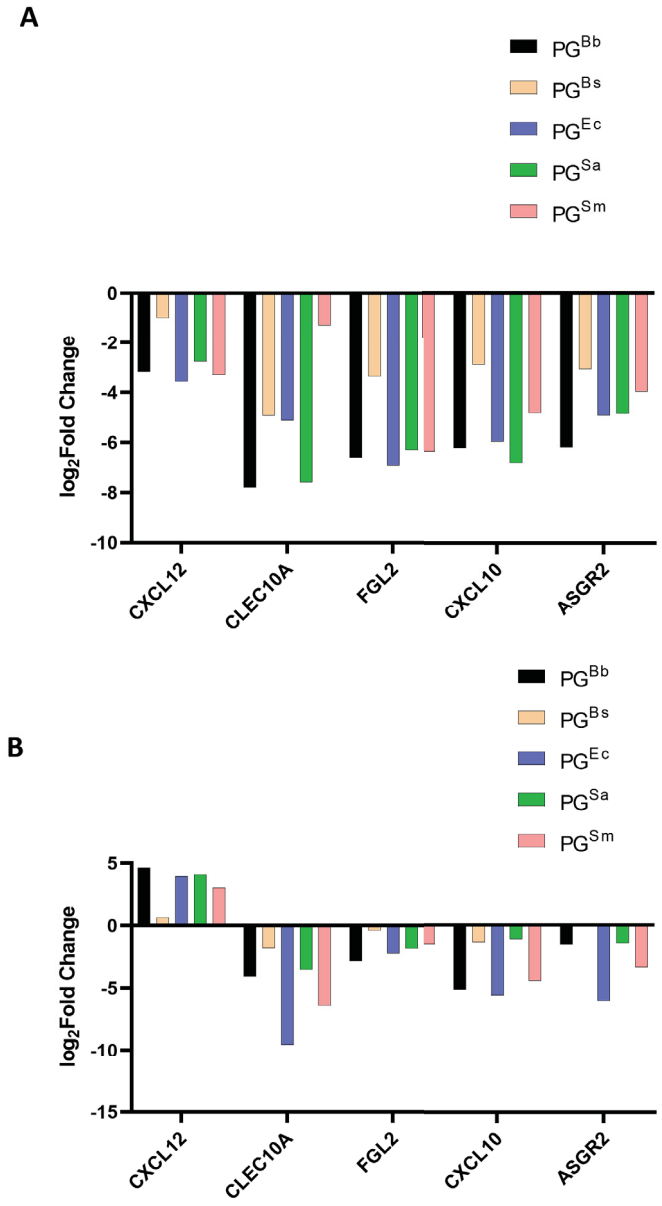

Figure 9: Gene Expression Analysis in PBMCs Stimulated with Bacterial PGs for 12 and 72 hours. Y-axis is $\log_2$Fold change in gene expression compared to controls, PBMC stimulated with PBS. **(A)** Genes significantly downregulated in response to $PG^{Bb,}$ $PG^{Ec,}$ PG^{Bs}, PG^{Sm} and PG^{Sa} for 12 hours. **(B)** Genes significantly downregulated in response to $PG^{Bb,}$ $PG^{Ec,}$ PG^{Bs}, PG^{Sm} and PG^{Sa} for 72 hours.

Figure 10: Gene Expression Analysis in PBMCs Stimulated with Live *Borrelia* at 5000 cells/mLfor 12 and 72 Hours

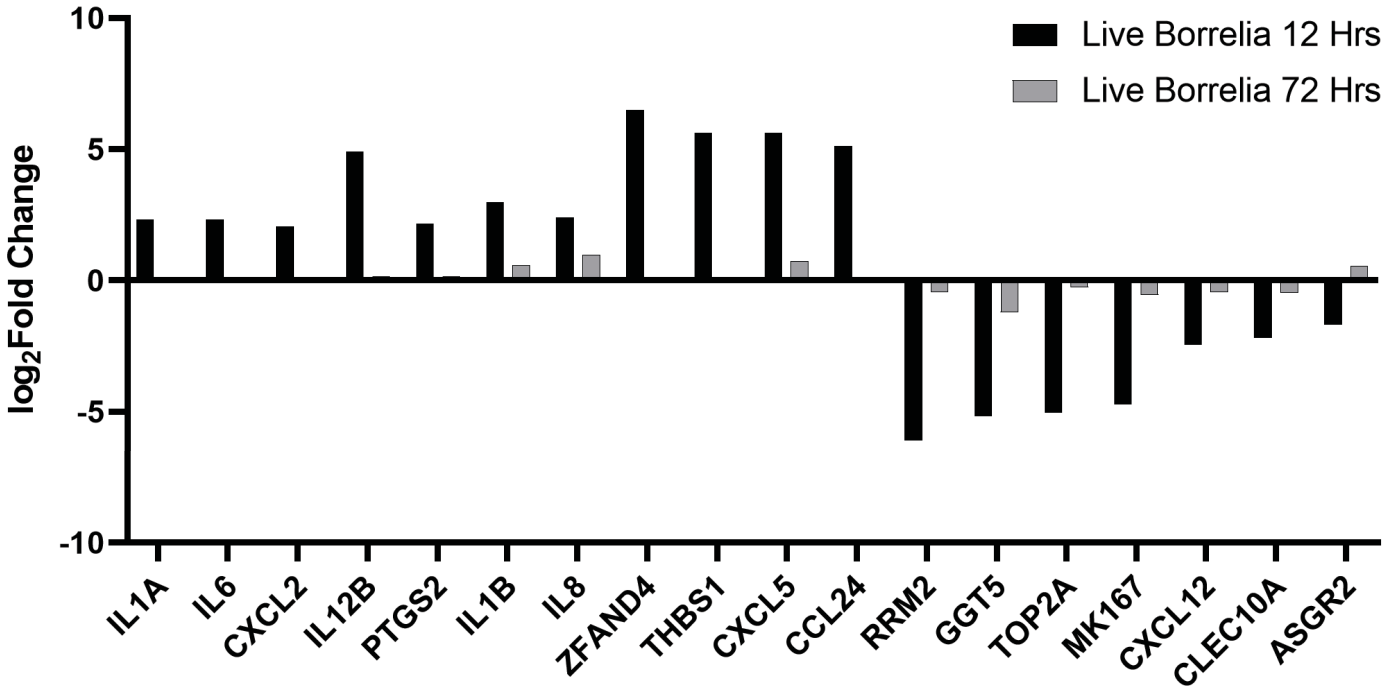

Figure 10: Gene Expression Analysis in PBMCs stimulated with Live *Borrelia* at 5000 cells/mL for 12 and 72 Hours. $\log_2$Fold change in gene expression compared to controls, PBMC stimulated with PBS. Genes listed are those of interest relative to those up/down regulated compared to PBMCs stimulated with PG, and also those that were uniquely expressed by cells stimulated with live *Borrelia.*

References

1. Glauner B, Holtje JV, Schwarz U. The composition of the murein of Escherichia coli. J Biol Chem. 1988;263(21):10088-95.
2. Vollmer W, Blanot D, de Pedro MA. Peptidoglycan structure and architecture. FEMS Microbiol Rev. 2008;32(2):149-67.
3. Slade HD, Slamp WC. Peptidoglycan composition and taxonomy of group D, E, and H streptococci, and Streptococcus mutans. J Bacteriol. 1972;109(2):691-5.
4. Girardin SE, Travassos LH, Herve M, Blanot D, Boneca IG, Philpott DJ, et al. Peptidoglycan molecular requirements allowing detection by Nod1 and Nod2. J Biol Chem. 2003;278(43):41702-8.
5. Baranwal G, Mohammad M, Jarneborn A, Reddy BR, Golla A, Chakravarty S, et al. Impact of cell wall peptidoglycan O-acetylation on the pathogenesis of Staphylococcus aureus in septic arthritis. Int J Med Microbiol. 2017;307(7):388-97.
6. Monteiro JM, Covas G, Rausch D, Filipe SR, Schneider T, Sahl HG, et al. The pentaglycine bridges of Staphylococcus aureus peptidoglycan are essential for cell integrity. Sci Rep. 2019;9(1):5010.
7. Jutras BL, Lochhead RB, Kloos ZA, Biboy J, Strle K, Booth CJ, et al. Borrelia burgdorferi peptidoglycan is a persistent antigen in patients with Lyme arthritis. Proceedings of the National Academy of Sciences. 2019:201904170.
8. Quintela JC, Garcia-del Portillo F, Pittenauer E, Allmaier G, de Pedro MA. Peptidoglycan fine structure of the radiotolerant bacterium Deinococcus radiodurans Sark. J Bacteriol. 1999;181(1):334-7.

9. Zhang X, Rimpilainen M, Simelyte E, Toivanen P. What determines arthritogenicity of bacterial cell wall? A study on Eubacterium cell wall-induced arthritis. Rheumatology (Oxford). 2000;39(3):274-82.
10. Novogene Co. L. Methods_MedTR [cited 2020]
11. database Gthg. 2016 [Available from: www.genecards.org.
12. Ammitzboll CG, Thiel S, Jensenius JC, Ellingsen T, Horslev-Petersen K, Hetland ML, et al. M-ficolin levels reflect disease activity and predict remission in early rheumatoid arthritis. Arthritis Rheum. 2013;65(12):3045-50.
13. Corrado A, Maruotti N, Cantatore FP. Osteoblast Role in Rheumatic Diseases. Int J Mol Sci. 2017;18(6).
14. van der Heijden IM, Wilbrink B, Tchetverikov I, Schrijver IA, Schouls LM, Hazenberg MP, et al. Presence of bacterial DNA and bacterial peptidoglycans in joints of patients with rheumatoid arthritis and other arthritides. Arthritis Rheum. 2000;43(3):593-8.
15. Hannu T. Reactive arthritis. Best Pract Res Clin Rheumatol. 2011;25(3):347-57.
16. Bockenstedt LK, Gonzalez DG, Haberman AM, Belperron AA. Spirochete antigens persist near cartilage after murine Lyme borreliosis therapy. J Clin Invest. 2012;122(7):2652-60.
17. Selmi C, Gershwin ME. Diagnosis and classification of reactive arthritis. Autoimmun Rev. 2014;13(4-5):546-9.
18. Steere AC. Lyme disease. N Engl J Med. 2001;345(2):115-25.
19. Lochhead RB, Ordonez D, Arvikar SL, Aversa JM, Oh LS, Heyworth B, et al. Interferon-gamma production in Lyme arthritis synovial tissue promotes differentiation of

fibroblast-like synoviocytes into immune effector cells. Cell Microbiol. 2019;21(2):e12992.

20. Prevention CfDCa. Signs and Symptoms of Untreated Lyme Disease 2019 [Available from: https://www.cdc.gov/lymesigns_symptoms/index.html

ATTRIBUTION

The work in the following chapter was aided by the work of several colleagues. A brief overview of the work attributed by them is listed below.

Chapter III: NapA is a Peptidoglycan Associating Protein in *B. burgdorferi*

Aaron Brock, Ph.D student in the Jutras lab, helped plan and perform experiments as well as aid in data analysis.

Tanner DeHart, undergraduate student in the Jutras lab, helped plan and perform experiments as well as aid in data analysis.

Nick Cramer, at the time an undergraduate student in the Jutras lab, helped plan and perform experiments as well as aid in data analysis.

Brittany Boribong, Ph.D candidate in the Jones lab, planned, performed and analyzed data involved with the neutrophil chemotaxis studies.

Katherine Lee, lab manager in the Jones lab, planned, performed and analyzed data involved with the neutrophil chemotaxis studies.

Yunjie Chang, Ph.D and postdoctoral associate in the Liu Lab, planned and performed Cryo-Electron Microscopy (Cryo-EM).

CHAPTER III

NapA is a Peptidoglycan Associating Protein in *B. burgdorferi*

Introduction

Borrelia burgdorferi PG is a potent antigen and is implicated in the course of Lyme disease (1). A recent discovery, covered in this section, has implicated other remnants of the bacterial cell envelope as likely contributors to disease pathology. How these factors are connected, the consequences of their interplay, and other components that may contribute to the development and persistence of Lyme disease, and more particularly Lyme arthritis (LA), are not known.

Peptidoglycan position within the periplasm is critical to its protective properties. It is perhaps not surprising then that most diderms produce highly conserved proteins that precisely position PG relative to the other envelope components. Bacteria unable to produce these peptidoglycan-associated proteins (PAPs), have severe defects in cell 1) growth; 2) division; 3) morphology; 4) communication; and 5) ability to withstand exogenous stress (2, 3). Interestingly, many of these seemingly structural cell-wall components moonlight as virulence factors that contribute to bacterial pathogenicity (2, 4, 5). Prior to the studies outline here, there have been no PAPs reported in *B. burgdorferi.*

As mentioned, cross-linking peptides in the PG cell-wall contain the atypical diamine L-Ornithine (6, 1). Further, the typical proteins which are associated with PG and provide both structural integrity and spatial continuity within the cell envelope, appear to be lacking. This chapter will describe the first identification of a *B. burgdorferi,* PAP previously implicated as an immunomodulatory factor and determine its function in the cell envelope homeostasis. In addition, this work provides evidence for a unique PG-PAP relationship that likely contributes to the pathogenic properties of *B. burgdorferi* PG.

Methodology

Bacterial Strains, Eukaryotic Cells, and Growth Conditions.

Both *B. burgdorferi* strains used in this study were generously provided by Frank Gheradini (NIH). A laboratory clone of the *B. burgdorferi* B31 type strain, termed 5A11(7) served as the wild-type parental control. The *napA* mutant was produced in the same 5A11 background and was created by allelic replacement as described previously (8). Barbour-Stoenner-Kelly II (BSK-II) medium containing 6% heat inactivated rabbit serum was used to culture *B. burgdorferi* at 37 °C under 5% CO_2.

Fresh, mixed donor human peripheral blood mononuclear cells (PBMCs) (Zen-Bio) were re-suspended in PBMC media (Zen-Bio) overnight prior to stimulations. Human NOD2 reporter cells, which were used to detect PG in OMVs (see below), were purchased from Invivogen and cultured as recommended by the manufacturer. Human promyelocytic leukemia cells (HL-60 CCL-240, American Type Culture Collection ATCC, Manassas, VA) were cultured in complete media comprising of Iscove's Modified Dulbecco's Medium (IMDM, ATCC, Manassas, VA) supplemented with 10% fetal bovine serum (FBS, ATCC, Manassas, VA) at 37°C in 5% CO2, according to ATCC instructions. HL-60 cells were differentiated into a neutrophil-like state with 1.5% dimethyl sulfoxide (DMSO, Sigma-Aldrich, St. Louis, MO) to 1.5×10^5 cells/mL for five days. Differentiated HL-60 cells (dHL-60 cells) were stained with Hoechst solution [20 mM] for 10 minutes (Thermo Fisher Scientific, Waltham, MA) at 37°C and 5% CO2 and spun down and re-suspended into a concentration of 5.0×10^7 cells/mL immediately before use in the migration assay.

B. burgdorferi DNA Purification and genome sequencing.

Low-passage, 40 mL cultures of each strain, were propagated to late-log (10^8 cells/mL) exponential growth and harvested. After washing bacterial pellets three times with PBS, cells were lysed by sonication and DNA was extracted by standard phenol:chloroform methods. Crude DNA extracts were then purified using Zymo Research (Irvine, California) genomic DNA purification kit.

Whole genomic sequencing was performed by Microbial Genome Sequencing Center (MiGS, Pittsburgh, Pennsylvania), who provided >450X coverage for each sample. Unicycler was used to process and assemble all sequence data. Results were compared to the published type strain (9) and parent of the wild type derivative (5A11) used in these studies.

Peptidoglycan Purification.

B. burgdorferi PG was purified as described previously (1) but was typically from 1L of culture. For comparative studies that included PAPs, one half of the crude PG material was digested overnight with 300 μg/mL chymotrypsin (Sigma-Aldrich) while the other half was not treated. Both samples were heat treated 24 hours later to inactivate chymotrypsin and subjected to 250 U/μL Benzonase Nuclease (Sigma-Aldrich) for 4 hours. After collecting PG material and washes with water, both samples were digested with Mutanolysin (10,000 U/mL) overnight. The concentration of the purified *B. burgdorferi* PG was determined using dry weight prior to drying via SpeedTrap vacuum concentrator. *B. burgdorferi* PG was re-suspended in phosphate buffered saline (Thermo-Fisher) prior to use.

Cellular fractionation.

Periplasmic fractions from *napA*/5A11 and 5A11 parental cultures were isolated essentially as previously described (10). Each strain was cultured in 100 mL of BSKII supplemented with 6% rabbit serum to a final density of 2.5 x 10^7 cells/mL. Bacteria were harvested at 3,000 x g for 20 minutes and washed three times with PBS. Each pellet was resuspended in a 6 mL solution containing 0.2M Tris (pH 8). One milliliter of each suspension was reserved at used as whole cell lysate in western blot analysis. To the remaining 5mL, 1M sucrose, and 1mM EDTA were added (final concentration v/v). Lysozyme was added to a final concentration of 5mg/mL and the solution was rocked for 15 minutes at room temperature. Spheroblasts were created by adding 20 mL of ddH_2O and the entire volume was centrifuged at 200,000 x g for 1 hour at 4°C. Supernatants contained periplasmic contents and were concentrated prior to assaying by western blot.

Immunoblots.

All antibodies used in this study have been previously characterized. Anti-FlaB (11) loading control, and anti-NapA (12) were graciously provided by Melissa Caimano and Frank Gheradini, respectively. Rabbit anti-serum raised against rOspA was purchased from Rockland Inc and was previously validated, while anti-BpuR (13, 14, 15) was produced and provided by Brian Stevenson. Polyclonal anti-PG rabbit serum was recently validated and provided by the Christine Jacobs-Wagner lab. Dilutions for western blots were as follows: Anti-FlaB (1:1000); anti-NapA (1:8000); anti-OspA (1:1000); anti-BpuR (1:160); anti-PG (1:90). A 1:8000 dilution of rabbit IgG:HRP (Jackson labs) was used to detect all primary antibodies, with the exception of FlaB, which was detected with rat IgG:HRP (Jackson labs), used at the same dilution. All

secondary antibodies were detected by chemiluminescence using SuperSignal West Pico PLUS (Thermo Scientific) detection reagents and imaged with a Syngene G:box (Imgene Technologies).

Immunofluorescence.

The immunofluorescence procedure for NapA and PG was identical to that previously described (16). Briefly, pre and post-trypsin treated PG preparations were spotted onto poly-L-lysine-coated slides. After washing with PBS supplemented with 0.05% Tween 20 (PBS-T) to remove unbound material, samples were blocked with 2% BSA in Seablock (Abcam) for 2 hours. Anti-NapA (1:800) was co-incubated with 5 µg/mL WGA:Alexa 350 on each sample for 1 hour, and washed 15 times with PBS-T. Anti-NapA was detected with the rabbit IgG:Cy3 conjugated antibody (Jackson lab), diluted 1:400. Control reactions included secondary antibody, without primary. Samples were treated with SlowFade and imaged as described below.

PBMC Stimulations.

Pooled, cryo-preserved PBMCs were seeded in 12-well plates at 2 x 10^6 cells/well in Lymphocyte culture media (Zen-Bio), pre-equilibrated to 37 °C under 5% CO_2. Cells rested for 18 h under these conditions prior to stimulation. Following stimulation for 18 or 72 h with 25 μg/mL of *B. burgdorferi* PG, the cells were harvested by centrifugation at 800 x g for 5 min at 15 °C. The supernatants were collected, aliquoted, and kept at -80°C prior to cytokine analysis. Cytokine analyses were performed on stimulated PBMC supernatants, diluted 1:4, according to the manufacturers (Abcam ELISA Kit IL-17A/F). Cytokine analysis was tested for statistical significance by an unpaired Student's T Test or One-way ANOVA. Unless stated in the text, statistical significance was set at $p < 0.05$

Microscopy and Image Acquisition.

Samples were immobilized by poly-L-lysine-coated slides. Epifluorescence microscopy was performed on a Zeiss Axio Observer equipped with a Hamamatsu Orca-Flash 4.0 V3 Digital CMOS camera, Colibri 7, and an oil-immersion phase-contrast objective Plan Apochromat 100x/1.45 N.A. (Nikon). Phase contrast and epifluorescence exposures were 100ms and 500 ms, respectively.

Microscopy analysis.

Data and statistical tests were performed using Graph Pad Prism 6.0 Software Inc. Automated sacculi detection was achieved using Oufti (17) on inverted WGA signal. Sacculi were detected using a subpixel logarithmic algorithm that was optimized for our images. The localization of NapA was identified by a Gaussian fit to the NapA signal for each cell mesh in the population (spotDetection via Oufti). The NapA locations were then normalized and plotted relative to NapA signal intensity. NapA locations were then binned; shaded region (18) represents the standard deviation for each bin. Data attained from cell meshes were graphed using MatLab 2019a. The codes used to generate Fig. 2E are listed in the supplementary material.

Cryo-Electron Tomography.

Frozen-hydrated specimens were prepared as previously described (19). Briefly, *B. burgdorferi* culture was mixed with 10 nm colloidal gold and was then deposited onto freshly glow-discharged, holey carbon EM grids for 1 min. Grids were blotted with filter paper and then rapidly frozen in liquid ethane, using a homemade gravity-driven plunger apparatus. Frozen-hydrated specimens were imaged at -170 °C using a Titan Krios electron microscope

(Thermo Fisher) equipped with a field emission gun and a K2 Summit direct detector device (Gatan). The microscope was operated at 300 kV with a magnification of 53,000 ×, resulting in an effective pixel size of 2.7 Å at the specimen level. SerialEM (20) was used to collect tilt series with a cumulative dose of ~60 $e^{-}/Å^{2}$. IMOD (92) was used for alignment and reconstruction.

Stress Tests and Colony Forming Units.

Initial studies geared towards understanding both permissive and restrictive growth conditions upon stress were performed in microplates with serial dilutions. Each strain was cultured to ~1 x 10^{6} cells/mL and subsequently back diluted to a final concentration of 1 x 10^{4} cells/mL in fresh BSKII containing cell-wall stress. Lysozyme and NaCl were serially diluted 1:2. The final concentration of Lysozyme ranged from 2 mg/mL to 0 mg/mL, while NaCl varied from 0.5 M to 0.4 mM. Both microtiter plates contained 4 wells of uninoculated media, which served as a negative control. These 96 well plates were allowed to incubate at 37°C under 5% CO_2 for 6 days. Afterwards, they were placed at ambient conditions for 2 hours before being imaged.

Colony Forming Units.

Parental and NapA mutant cultures were grown to ~6.5 x 10^{6} cells/mL and back diluted to a final starting concentration of 10^{6} cells/mL. Each culture was stressed with Lysozyme (0.37 mg/mL) or NaCl (0.111 M) for 24 hours without additional antibiotic selection. Afterwards, each culture was plated using standard methods (21) and cultured at 37 °C under 5% CO_2. CFUs were determined for strain 5A11 after 3 weeks; *napA* mutant CFUs were counted after 6 weeks.

Neutrophil Migration.

The microfluidic competitive chemotaxis-chip (μC^3) (22) was used to perform each migration assay. This device allowed for the creation of a dual gradient through two opposing chemoattractant reservoirs. The central cell-loading chamber is connected to the two reservoirs by perpendicular cell migration ladders (measured 10 μm wide × 10 μm tall). Device fabrication was as previously(22). Briefly, two layers of photoresist (SU8, MicroChem), the first one 10 μm thin (corresponding to the migration channels) and the second one 70 μm thick (corresponding to the neutrophil loading chamber) were patterned on one silicon wafer sequentially using two photolithographic masks and processing cycles according to the instructions from the manufacturer. The wafer with patterned photoresist was used as a mold to produce polydimethylsiloxane (PDMS) (Sylgard 184, Elsworth Adhesives, Wilmington, MA) devices, which were then bonded to the base of glass-bottom 6-well plates (MatTek Corp., Ashland, MA), using an oxygen plasma machine (Nordson March, Concord, CA). Prior to each migration assay, the device was primed with fibronectin (Sigma-Aldrich, St. Louis, MO) (11 μg/mL). After priming with fibronectin, each device was covered in 4 mL complete media. Samples were loaded into one chemoattractant reservoir of each corresponding device using a trimmed gel loading pipette tip. Formylmethionine-leucyl-phenylalanine (fMLP, Sigma-Aldrich, St. Louis, MO) (10 nM) and Leukotriene B4 (LTB4, Cayman Chemical, Ann Arbor, MI) (100 nM) served as positive controls in the chemotaxis assay and were loaded in the same manner. The second chemoattractant reservoir was filled with complete media to measure chemorepulsion from the sample. Complete media in both reservoirs served as a negative control in the chemotaxis assay. dHL-60 cells were loaded into the central cell-loading chamber in the ladder device with a gel loading pipette tip. The media was removed and replaced with new complete media after the dHL-60 cells were loaded.

Chemotaxis imaging and measurements.

Each assay was visualized on a fully automated Nikon TiE microscope using a Plan Fluor 10X Ph1 DLL (NA = 0.3) lens with a biochamber heated to 37°C with 5% CO_2. Image capture was performed using NIS-elements (Nikon Inc., Melville, NY). Experiments were run under the microscope for 5 hours with brightfield and fluorescent images taken at 2-minute intervals. Image analysis of cell migration counts was analyzed automatically using ImageJ (NIH). Cell tracking was conducted using an automated tracker, TrackMate (23) (custom tracking and analysis codes are available for download at https://github.com/boribong/Single-Cell-Migration-Tracking) and ImageJ software (NIH). Cell migration parameters have been defined previously (94).

Statistical Analysis of dHL-60 Cell Chemotaxis towards NapA.

All experiments were performed and replicated at least three times, unless otherwise stated. Statistical analysis was performed using Prism software (GraphPad Software, La Jolla, CA). Data expressed as means ± standard deviations. To compare the migration between the different 5A11 and 5A11/*napA* samples, we used a one-way ANOVA and Turkey's Multiple Comparison test. To compare the migration toward or away within the different 5A11 and 5A11/*napA* samples, we used a Student's *t*-test. Differences were considered statistically significant for $p < 0.05$.

Outer Membrane Vesicle Analysis.

Outer membrane vesicles (OMVs) were isolated from *B. burgdorferi* parental and NapA mutant strains using a modified protocol from G. Mordukhovich (25). Briefly, 80 mL BSK-II media culture that had hosted both the strains during growth was vacuum filtered through 0.22 μM filter prior to ultracentrifugation at 40,000 x g at 4 °C for 45 min. The pelleted material was re-

suspended in 1 mL of water and added to the top of an Opti-prep (Sigma-Aldrich) gradient composed of 45%, 40%, 35%, 30%, 25% and 20% layers diluted in 1X HEPES buffer. The gradient containing the OMV sample was ultra-centrifuged at 215,000 x g for 5 hrs at 4 °C. Each layer was removed and assayed for contents as described in the text.

Results

Identification of PAPS.

Despite their apparent paucity (9, 24), we hypothesized that *B. burgdorferi* does, indeed, produce (PAPs) that may be functionally akin to Braun's lipoprotein and/or outer membrane proteins (Omps), but are not easily identifiable using standard *in silico* homology searches. To test our hypothesis without any a priori assumptions, we purified PG^{Bb} using standard methods (1, 16). An initial purification step solubilizes most cellular components using 5% boiling sodium dodecyl sulfate (SDS). Following solubilization, PG as well as PG-associated material was collected. After washing to remove SDS, sacculi were treated with trypsin, which cleaves PAPs (Fig 11A). Intact PG was removed from liberated PAP peptides, and fragments were identified by LC-MS (Fig 11A). In addition, we performed more rigorous sample processing (see methods) and applied inclusion/exclusion criteria to curtail potential hits. Specifically, peptides from proteins that 1) were present in multiple biological replicates; 2) consistently had MASCOT scores > 30, and; 3) were identified regardless of processing method (Fig. 10A) were considered further. Using these exclusion criteria BB0690 (MASCOT score 301 +/- 76, Table 8.1) was the top PAP candidate.

BB0690 has many names. Earlier studies identified BB0690 bioinformatically as a homologue of Dps (DNA binding protein from starved bacteria) and demonstrated that, like Dps, its production is regulated and induced by stress (8, 12, 26, 27). Unlike Dps produced by most

bacteria, BB0690 lacks the DNA-binding domain and does not bind DNA (8). Curious, since the main function of Dps is to decorate DNA and protect heritable material from oxidative stress (27, 28). Subsequent studies demonstrated that BB0690 does play a role in oxidative stress by sequestering metal ions copper and iron, and thereby earned the name BicA (*Borrelia* iron copper binding protein A) (29). Perhaps the most well studied phenomena associated with BB0690 is its ability to attract neutrophils and modulate innate immune responses (28, 30-32) which precipitated the alternative moniker NapA (Neutrophil attracting protein A). We contend that the basic function of BB0690 is not well understood. However, for simplicity, we refer to BB0690 as NapA throughout the remainder of this section.

Sub-cellular localization of *B. burgdorferi* NapA.

Despite the paradoxical role of NapA acting to protect *B. burgdorferi* against metal-stress (8, 29, 33) but yet does not bind DNA (8), the sub-cellular localization of NapA has never been determined. To begin, we first validated the specificity of polyclonal anti-NapA serum (12) raised in rabbits in two strains— a fully infectious derivative of the B31 type strain (5A11) and a mutant strain in which the *napA* locus has been replaced by a kanamycin resistance cassette *aphI1* (5A11/*napA*). Within the expected size range, anti-NapA yielded a single band in parent strain 5A11, which was absent in 5A11/*napA* (Fig. 11B). Comparative, whole genome sequencing results of 5A11 and 5A11/*napA* indicated that the resistance cassette, *aphI1,* completely replaced the *napA* locus in the mutant, but no additional mutations were present (Tables 9.1 and 9.2). Upon strain and reagent validation, we fractionated 5A11 parental and 5A11/*napA* mutant lysates and probed periplasmic contents by western blot. As expected for a PAP, NapA was readily detectable in the periplasm, similar to flagellar filament protein FlaB (Fig. 11C). Outer surface protein OspA, and

DNA/RNA-binding protein BpuR (1, 13, 14) were not detected in periplasmic fraction, indicating that NapA signal was not due to contamination during sample fractionation (Fig. 11C).

Some PAPs traverse the OM and can be detected on the bacterial surface (34, 2). Such localization would be noteworthy for a protein thought to influence immune cell chemotaxis (30-32). To determine if NapA was surface-exposed, we incubated live parental and *napA* mutant cells with Proteinase K, which would cleave proteins on the cell surface rendering them undetectable by western blot. NapA was detected in wild type 5A11 cells, regardless of treatment, whereas surface exposed OspA was readily cleaved and no longer detectable in both Proteinase K treated samples (Fig. 11D). We conclude that NapA is located in the periplasm of *B. burgdorferi*.

NapA is associated with the PG of *B. burgdorferi*.

To determine if NapA is associated with PG, we developed a strategy based on the concept of our screen (Fig. 11A). Parental and *napA* mutant strains were cultured to mid-log exponential growth, cellular components were solubilized with boiling SDS and insoluble material was collected. One half of the insoluble material was removed, and the remainder treated with trypsin, as is typical for PG purification. A dilution series of each sample was spotted on nitrocellulose and probed for NapA and PG. Dot blots demonstrated that PG was present in all samples tested (Fig. 12A), indicating that each sample was processed similarly and contained relatively equal amounts of cell-wall material. Much like PG, NapA signal was clearly present, and reduced with each dilution, but only in material purified from parental cells, prior to trypsin treatment (Fig. 12A). These data support the notion that, even after harsh treatment in boiling detergent, NapA is associated with PG^{Bb} . To further assess their relationship, we used immunofluorescence on separate, biological replicate samples, prepared as described above. To circumvent anti-serum

incompatibility issues (rabbit Anti-PG/NapA), we used Wheat Germ Agglutinin (WGA) conjugated to Alexa-350 to detect PG^{Bb}. Wheat Germ Agglutinin is known to bind Glc*NA*c— a ubiquitous PG sugar. Consistent with dot blot results, PG sacculi were clearly present, at relatively equal abundance, pre and post trypsin treatment in both parental and *napA* mutant strains (Fig. 12B). Peptidoglycan remained intact and WGA-PG derived signal was relatively uniform, with the possible exception of sacculi poles (Fig. 12B and 12C), suggesting that neither sample preparation nor the presence of NapA impacted PG signal (Fig. 12B and 12C). Prior to trypsin digestion, NapA appears to be scattered throughout the PG sacculus (Fig. 12B and 12C). Population level analysis of NapA signal, normalized by total sacculi area, was greater than 5-fold above background (Fig. 12D). While NapA signal appeared to display discrete patterning (Fig. 12B and 12C), population level assessment of relative position indicated that NapA is approximately equally distributed throughout PG sacculi (Fig. 12E). Taken together, our immunoblotting and immunofluorescence studies confirm that NapA is a PAP in the Lyme disease spirochete.

NapA provides structural and physiological integrity to the cell-wall.

Since NapA is in the periplasm and decorates the PG sacculus of *B. burgdorferi,* we speculated that NapA-mediated protection from exogenous stress may be at the level of cell envelope integrity. If cell envelope integrity is compromised in a NapA deficient bacterium, then any cell-wall stress should produce a phenotype, not just oxidative stress (12, 29). To evaluate this, we first incubated 5A11 and 5A11/*napA* cells with increasing amounts of NaCl and Lysozyme, which cause osmotic and PG specific stress, respectively. We monitored microtiter plates for changes in pH— an indirect measurement of growth (35, 36). Wild-type cells were more than 8

times more resistant to NaCl-induced stress (Fig. 13A, right). Similarly, titrations of Lysozyme, which attacks the 1-4 glycosidic linkage in PG between glycan sugars, Glc*NA*c and Mur*NA*c, ablated 5A11/*napA* growth at 5-6 times less enzyme than the wild-type bacteria (Fig. 13A, left).

Our data hint at a cell-wall defect in NapA deficient bacteria, however our microtiter plate assay also suggested a growth defect (Fig. 13A). Indeed, direct culture enumeration indicated that NapA deficient bacteria replicate 1.9 times slower than the parental strain (Fig. 13B). Since data presented in Figure S1A were end-point measurements after 6 days, we reasoned that the growth defect could account for the apparent differences in susceptibility to cell-wall stresses. To circumvent these issues, we performed stress tests on both strains at a single, previously optimized concentration of NaCl and Lysozyme (Fig. 13A) for 18 hours in liquid broth (see methods). Each strain, and treatment, were then diluted in plating media lacking stress and colony forming units (CFUs) were determined. Wild-type CFUs were calculated after 3 weeks and, to compensate for growth defects, compared to results obtained from the *napA* mutant bacteria after 6 weeks (Fig. 13A). Even after accounting for growth rate defects, mutant bacteria were 2-4 logs lower in CFUs (Fig. 14A), indicating that NapA plays a basic role in cell envelope integrity and homeostasis. Our data are consistent with earlier studies that NapA provides protection from exogenous stress (8, 12, 29). However, we surmise that NapA protects *B. burgdorferi* from all cell-wall stresses, potentially by reinforcing PG.

The distribution of NapA throughout the PG sacculi (Figs. 12B, 12C, and 12E) suggested that NapA may help bolster the PG, and that this association is essential to overall cell-wall integrity (Fig. 14A and 14B). Mechanistic insights were provided by comparative Cryo-Electron Microscopy (Cryo-EM) analysis of *napA* mutant and parental strains. Bacteria unable to produce NapA possessed compromised PG— appearing discontinuous, thinner, and more ruffled in

shape— relative to the thicker, more electron dense PG layer of the parental strain (Fig. 14B). Analysis of multiple micrographs, along the cell body, from each strain demonstrated that both were true. The thickness of PG sacculi in mutant bacteria was, on average, roughly half (0.53) that of wild type cells (Fig. 14C). Integrated average PG pixel intensity values, normalized by sampling area, were also significantly less in the *napA* mutant strain (Fig. 14D). These data clearly delineate the role of NapA in cell envelope integrity and provide critical insights into the mechanism by which it protects the cell from stress.

NapA and PG fragments are secreted in *B. burgdorferi* Outer Membrane Vesicles.

Bacterial elongation requires PG synthesis. Newly synthesized PG multimers are incorporated into the existing structure, resulting in expansion, but at a cost. Each incorporation event requires that incisions are made to provide substrates for transglycosylation reactions. Most diderms typically recycle excised PG monomers back into the cytoplasm for reuse. *B. burgdorferi* lacks the transporters and enzymes necessary for PG recycling. The result— approximately 45% of *B. burgdorferi* PG is shed per generation from the periplasm into the extracellular environment (1). How these PG fragments cross the outer membrane boundaries of the cell envelope is not known.

We postulated that PG and, due to their association, potentially NapA, could be released from the periplasm in Outer Membrane Vesicles (OMVs). *B. burgdorferi* produces OMVs, not only under stress, but also under regular homeostatic conditions (37). A comprehensive *B. burgdorferi* OMV proteome has not been published, and if available, typical data mining would overlook PG^{Bb} or muropeptides fragments. To extend upon our findings and query OMVs for specific occupants, we cleared mid-log exponential cultures of cells by centrifugation and filtered

spent culture media. After ultra-centrifugation to enrich for OMVs, we used a density gradient to further purify supernatant contents (25). Gradient fractions 1 and 2, from each strain, contained OspA (Fig. 15A), an abundant outer membrane protein known to be released in OMVs (38). Probing the same fractions for NapA yielded similar results, indicating that the full-length protein was indeed in *B. burgdorferi* OMVs isolated from wild type cells (Fig. 15A).

Given the NapA-PG association, we reasoned that released muropeptides and/or fragments of polymeric PG could, too, be included in OMVs. Given the large distribution of potential PG sizes, we opted for dot blot analysis of density fractions and co-immunoblotting with anti-PG and anti-NapA. PG could be detected in the fractions containing OMVs, in both parental and *napA* mutant preparations (Fig. 15B), indicating that NapA is not required for PG to be released in OMVs. Although, our results suggest that more PG is present in NapA-containing OMVs (Fig. 15A and 15B). We further confirmed that *B. burgdorferi* OMVs contain PG by a ligand-receptor reporter assay. Each density fraction was incubated with a hNOD2 receptor reporter cell line, which, when exposed to PG containing Muramyl-L-Alanine-D-Glutamine (MDP), activates the secretion of alkaline phosphatase. Both OMV fractions 1 and 2 caused significant hNOD2 activation (Fig. 15C). Once again, OMVs produced by wild-type cells contain significantly more PG than the *napA* mutant OMVs (Fig. 15C). Using titrations of known concentrations of MDP, we back calculated the average amount of PG in OMVs to be ~6.10×10^{-2} and ~1.91×10^{-2} pg of MDP per cell of wild-type and mutant, respectively. Concentration aside, we also note that OMV contents activated a cytoplasmic receptor which indicates that 1) *B. burgdorferi* OMVs lysed during the experiment or 2) they are capable of fusing with eukaryotic membranes and expelling their contents, as reported for other bacteria (39, 37).

NapA-associated PG acts as a molecular beacon, augmenting the immunomodulatory properties of the *B. burgdorferi* cell wall.

B. burgdorferi PG was recently shown to be a persistent antigen in the synovium of LA patients and is capable of inducing both inflammation and arthritis (1). We note that these studies were performed using purified PG^{Bb}, which includes a trypsin digestion step to cleave any linked proteins. Since, in its natural biological state PG is associated with NapA, we questioned whether the combination may augment the inflammatory response. Here, we focused on IL-17 since 1) PG^{Bb} only modestly increased IL-17 secretion (1); 2) IL-17 is markedly over-represented in LA patients (1, 40); and 3) previous studies have found that recombinant NapA can stimulate an T_H1/T_H17 response (28, 32). Using OMVs containing NapA-PG is complicated by package contents and casing. Instead, we used the same pre trypsin treated PG samples as above, prepared from wild-type and mutant *napA* cultures. Relative to *napA* mutant derived PG preparations, wild-type PG caused human peripheral blood mononuclear cells (PBMCs) to secrete ~9-fold more IL-17 (Fig. 15D), which highlights two important points: 1) The NapA-PG association has immunological consequences and 2) while it is possible that other proteins are associated with *B. burgdorferi* PG (Table 8.1), NapA alone is sufficient to augment the PG-induced IL-17 response (Fig. 15D).

Since NapA-PG produced higher levels of IL-17 it may also act as a molecular beacon for neutrophils, naturally. To determine the chemoattractant capabilities of NapA-PG, we performed a comparative study using real-time neutrophil tracking in a microfluidic chamber. In this system, neutrophils flow into a central chamber that is flanked by reservoirs on each side (Fig 15E). Migratory bait is added to one reservoir and compared to the adjacent media-containing reservoir. Migration towards a potential stimulus was monitored by phase-contrast epifluorescent

microscopy for 5 hours. Percent migration was determined by the number of cells that reached a flanking reservoir. The only PG bait that acted as a significant chemoattractant was NapA-associated PG (16.03 ± 1.93%)(Fig. 15F); similar to that of known attractants LTB_4 (25.89 ± 3.52%) and fMLP (35.94 ± 5.42%) (22). None of the other PG preparations caused significant attraction or repulsion (Fig 15F). Since data presented are the combined results of three biological replicates, we conclude that NapA alone, is both necessary and sufficient to cause neutrophil migration toward PG^{Bb}.

Discussion

The studies outlined here provide the first evidence for a PAP in *B. burgdorferi*. We report that NapA exists in the periplasm but is not surface exposed (Fig. 10). Molecular and cellular studies demonstrate a NapA-PG interaction and that this association is important in stabilizing the *B. burgdorferi* cell envelope (Figs. 12 and 14). NapA-PG is not only important for the physical and physiological homeostasis, but the nature of the interaction has pathogenic consequences—increased IL-17 production and neutrophil attraction (Fig. 15). Here the findings are discussed in the context of Lyme disease, spirochete biology and pathogenesis, in addition to bacterial evolution.

The natural life cycle of *B. burgdorferi* is complex and involves establishing residency in very different hosts—the tick vector, and dozens of potential vertebrate hosts (41). Earlier studies have shown that *napA* is dispensable for mouse infection but required for tick survival (8). Bacteria unable to produce NapA are more susceptible to stress — particularly PG-specific stress (Fig. 14). With the exception of host blood, it is not clear what stressors would be present in the tick mid-gut or how NapA ameliorates the osmoprotective properties of PG. *Ixodes scapularis,* however,

does produce the *B. burgdorferi* PG-specific hydrolyzing enzyme Dae2 (42, 43), which could function more effectively in the absence of NapA-linked PG. Further studies are required to elucidate the nature of the NapA-PG interaction since disrupting their association would likely be an effective mode of pathogen control in ticks.

Cell elongation requires both PG anabolism and catabolism. Excised muropeptides accumulate outside the cell and are involved in the pathogenesis of LA (1). Until now, there has been no mechanism to explain how released PG crosses the *B. burgdorferi* outer membrane. Here, we show that one route of PG release is through OMVs (Fig 15). OMVs also contain NapA (Fig.15). Based on our cellular reporter assay, OMV contents can end up inside eukaryotic cells (Fig. 15C). Several mechanisms have been proposed, including endocytosis and membrane fusion. Two-way lipid exchange has been shown to occur following internalization of *B. burgdorferi* OMVs (39), which supports the notion that OMVs may also be used for exchange of periplasmic contents such as NapA and other potentially pathogenic material. Of course, it is also possible the OMVs lyse, spilling their contents into the extracellular space of host systems. Regardless of the possible mechanism, NapA-linked PG augments the helper T cell response caused by PG alone, inducing higher levels of IL-17 (Fig. 15D). These findings are in line with studies using rNapA, which has been implicated in LA (28, 32). While other PAPs are likely (Table 8.1), these effects can be solely attributed to NapA-PG.

Neutrophils are akin to a platoon on the front lines— controlling the environment, initiating a response, and recruiting backup. During the initial stages of infection, neutrophils phagocytize *B. burgdorferi*, utilize lethal enzymes, and destroy bacterial cells using neutrophil extracellular traps (NETs)(44-46). This initial attraction may be due to NapA-linked PG released from *B. burgdorferi* during growth, as our migration studies indicate that NapA-PG attracts neutrophils

and that PG alone does not. Although neutrophils are recruited to the site of the tick bite — and function to recruit other immune cells — later symptoms of the disease are often disseminated to other organ systems including the joints, heart, and central nervous system, indicating that the initial assault is not enough to stop the infection from spreading. One method of diversion may be the use of NapA-PG containing OMVs that attract neutrophils to themselves, leaving *B. burgdorferi* to disperse to other parts of the body. In another light, the NapA-PG in these OMVs may also represent a more biologically relevant PG. Purified NapA has been shown to provoke inflammation in rat synovial tissue via the recruitment of immune cells (32). In a similar manner, trypsin treated PG^{Bb} has been shown to induce arthritis in the mouse model (1). Therefore, the coordinated effect of both NapA and PG within the synovial tissue could exacerbate arthritis severity since the two have been tested individually but not simultaneously. These results, in conjunction with the chemotactic properties of NapA-PG, create a unique situation in which a structural protein moonlights as a molecular beacon for immune cells— attracting them to an abundant inflammatory molecule.

Dps homologues are produced by virtually all bacteria (47). NapA shares structural and amino acid sequence homology to Dps (27,31) (Fig. 16). However, there are notable differences which may extend to other proteins that have evolved to perform altered functions. 1) Dps production is highly upregulated in stressed conditions, and 2) acts by shielding DNA for oxidative damage, a ubiquitous function that appears to be highly conserved across diverse taxa (26). NapA, on the other hand, does not bind DNA (8) and its role in cellular homeostasis is in the periplasm (Fig 11). NapA production does appear to increase under oxidative stress (11), but others have argued that basal production is considerable in culture and increased NapA expression by metal stress is negligible (48). Our findings are in line with the latter— we detect considerable NapA

under exponential growth, which would make sense for a structural protein. At the amino acid level, *B. burgdorferi* NapA has two distinct features that separate it from other Dps homologues. First, much like *H. pylori*, *B. burgdorferi* NapA has a truncated N-terminus that lacks the Lys-rich residues implicated in DNA binding (8, 49, 50). Unlike *H. pylori* NapA, the *B. burgdorferi* homologue has an extended C-terminus, which is rich in Cysteine residues (Fig. 16B and 16C). The latter is intriguing since Cysteine is known to be important in Protein-PG interactions (51, 52). *In silico* analysis indicates that this feature is unique to *Borreliae*; other spirochetes do not appear to have the same extended Cys-rich region (Fig. 16B and 16C). Regardless of the divergence among spirochetes, our findings highlight the ingenuity of bacteria in which a protein can evolve mechanistically, while maintaining the same basic biological function.

Table 8. 1 Summary LC-MS results from PAP screen

Accession	Name/Function	MW (kDa)	MASCOT mean (+/-STD)	Exp
BB0476	Elongation Factor Tu	43.6	1134 (343)	T^+
BB0744	Borrelia P83/P100 antigen	79.9	599 (238)	T^+
BB0690	NapA/Neutrophil attracting	21.3	301 (76)	T^+/M^+
BB0073	OM Protein/Unknown	21.5	199 (47)	T/M

T^+ Present with MASCOT score >30 in replicate Trypsin experiments
T Present with MASCOT score >30 in one Trypsin experiment
M^+ Present with MASCOT score >30 in replicate Mutanolysin/Trypsin experiments
M Present with MASCOT score >30 in one Mutanolysin/Trypsin experiments

LC-MS results from biological replicates of PG-associated protein analysis following trypsin cleavage (T) or Mutanolysin treatment, followed by trypsin (M). Data are organized by mean MASCOT score.

Table 9. 1 Parental clone 5A11 mutations relative to B31 reference genome

Mutation	Event	Coordinate	Location	Result
S	G→T	10,883	Coding-OspB	G199V
S	C→A	28,269	Coding-BBN41	Q82K
S	C→T	17,924	Intergenic	—
A	+C	3,140	Intergenic	—
S	G→A	56,157	Coding-BB0059	V42I
A	+A	138,870	Intergenic	—
A	+T	366,152	Intergenic	—
A	+A	422,314	Intergenic	—
D	-G	515,969	Intergenic	—
D	-C	516,002	Intergenic	—
D	-G	516,098	Intergenic	—
S	T→A	528,031	Intergenic	—
A	+G	532,509	Intergenic	—
A	+T	540,032	Intergenic	—
S	T→G	747,897	Intergenic	—
A	+A	862,670	Intergenic	—

S Substitution
A Addition
D Deletion

All mutations that differ from the B31 type strain are shown with the exception of the hypervariable *vlsE* expression locus.

Table 9. 2 5A11/napA mutations relative to B31 reference genome

Mutation	Event	Coordinate	Location	Result
S	G→T	10,883	Coding-OspB	G199V
S	C→A	28,269	Coding-BBN41	Q82K
S	C→T	17,924	Intergenic	—
A	+C	3,140	Intergenic	—
S	G→A	56,157	Coding-BB0059	V42I
A	+A	138,870	Intergenic	—
A	+T	366,152	Intergenic	—
A	+A	422,314	Intergenic	—
D	-A	424,631	Intergenic	—
D	-G	515,969	Intergenic	—
D	-C	516,002	Intergenic	—
D	-G	516,098	Intergenic	—
S	T→A	528,031	Intergenic	—
A	+G	532,509	Intergenic	—
A	+T	540,032	Intergenic	—
D	Allele exchange	731,203-731,758	Coding-NapA	*napA*$^{-}$
S	T→G	747,897	Intergenic	—
A	+A	862,670	Intergenic	—

S Substitution
A Addition
D Deletion

All mutations that differ from the B31 type strain are shown with the exception of the hypervariable *vlsE* expression locus.

Figure 11: Identification of peptidoglycan-associated proteins (PAPs) in *B. burgdorferi*

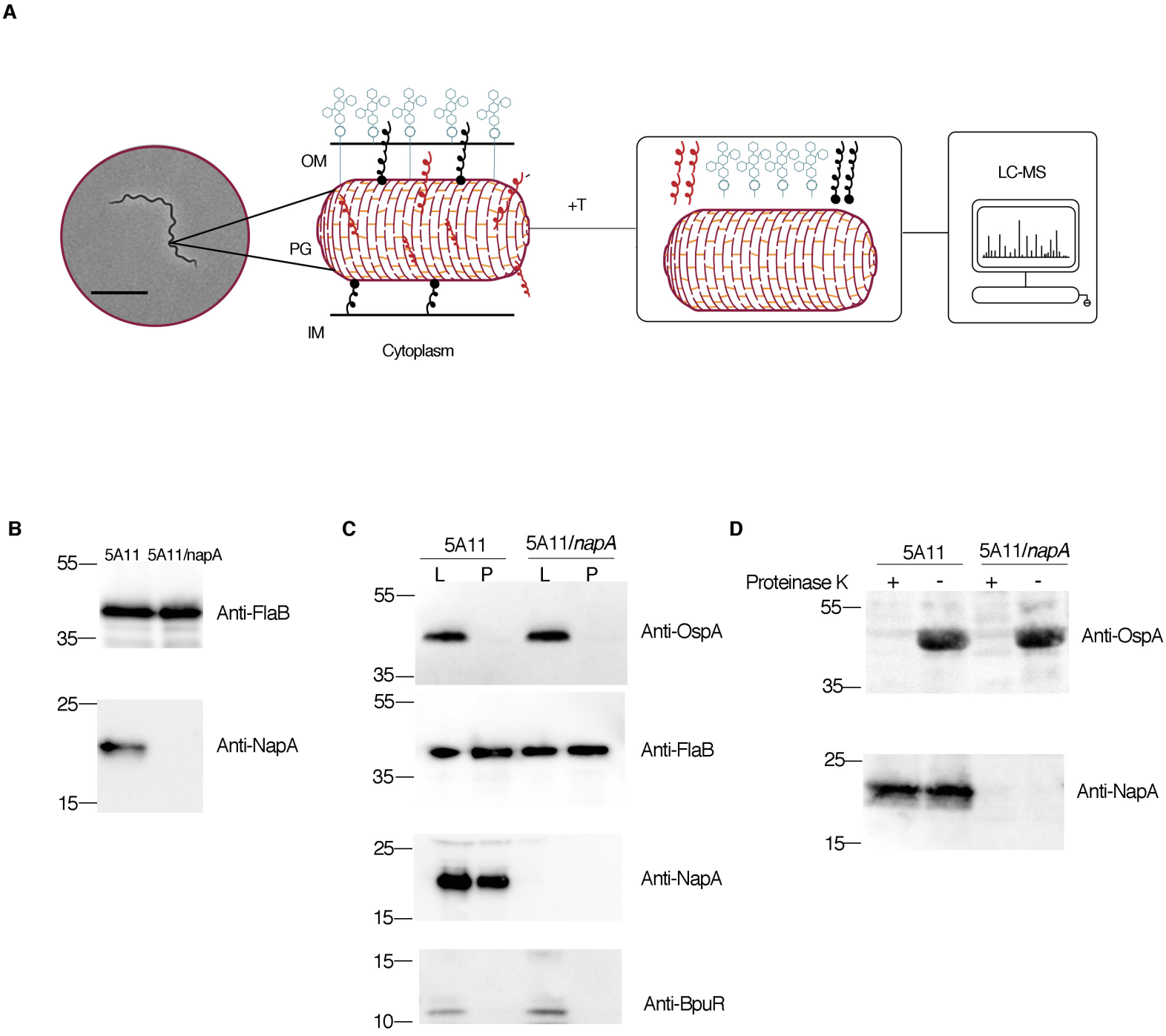

Figure 11: (A) Peptidoglycan was isolated from live *B. burgdorferi* (phase-contrast micrograph, scale bar 5um) and treated with trypsin. Peptides from each preparation were identified by LC-MS. Data presented in Table S1 were from two biological replicates, for each method. (B-D) Sub-cellular localization of putative PAP NapA. (B) Western blot analysis of whole cell lysates prepared from the parental, wild-type strain (5A11) and *napA* mutant (5A11/*napA)*. Each preparation was assayed by western blot for NapA (below) and the constitutive protein FlaB (above). The latter served as a loading control. (C) Whole cell lysates (L) or periplasmic (P) fractions were prepared for wild-type and *napA* mutant bacteria and probed by western blot for outer membrane protein OspA, periplasmic protein FlaB, or cytosolic DNA/RNA binding-protein BpuR. Like FlaB, NapA was found in the periplasmic fraction. (D) Surface proteolysis assay using proteinase K. Live, intact wild-type and mutant bacteria were treated with proteinase K (+) or untreated mock control (-) and lysates were probed by western blot for surface exposed outer membrane protein OspA or NapA.

Figure 12: NapA is a PAP

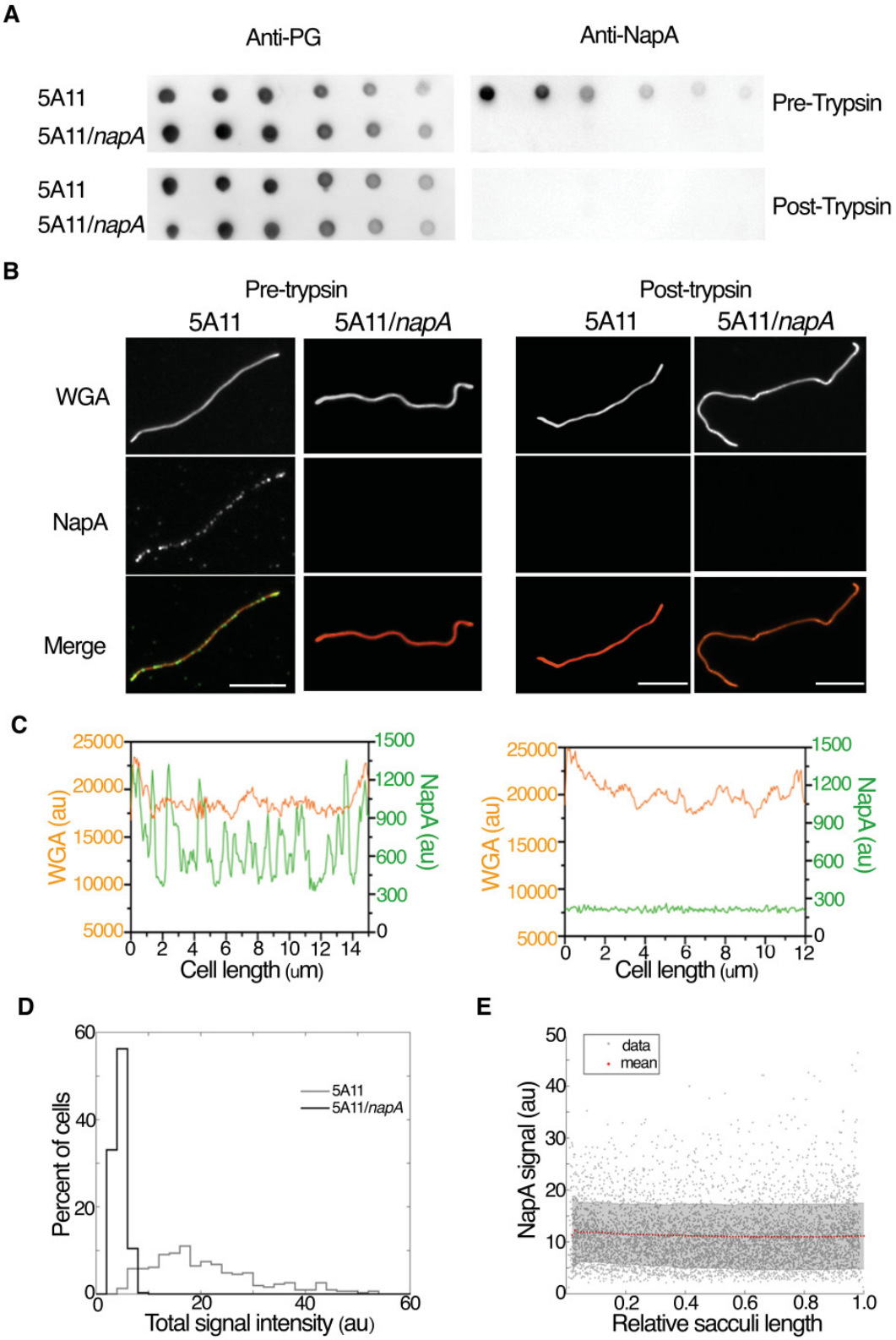

Figure 12: (A) Dot blot analysis of PG. Wild-type (5A11) and *napA* mutant (5A11/*napA*) bacteria were cultured to mid-log exponential growth, cells were harvested, and PG was purified. Prior to trypsin treatment, one half of each sample was removed. Serial dilutions of each pre and post trypsin preparation were spotted on nitrocellulose and probed for PG (Anti-PG, left) or NapA (Anti-NapA, right). (B) The same samples, prepared in A, were used for immunofluorescence studies. Whole PG sacculi were visualized by epifluorescence microscopy using wheat germ agglutinin (WGA) conjugated to Alexa Fluor 350. NapA was detected using anti-NapA antibody and anti-rabbit IgG conjugated to Alexa Fluor 488. Scale bars = 5um. (C) Fluorescent intensity line scan analysis of WGA (left y-axis) and NapA (right y-axis) in arbitrary units (au). Data presented were collected from pre trypsin treated cells in B. (D) Population-level analysis of integrated fluorescent signal intensities of NapA from sacculi isolated from 5A11 (n=310) and 5A11/*napA* (n=345). (E) Demograph analysis of NapA signal from wild-type sacculi, pre-trypsin treatment. Sacculi were organized based on cell length. NapA signal is shown along the length of each sacculi (n = 310) and shown as heat-map in arbitrary units from 0-1 (right).

Figure 13: Lysozyme and NaCl stress tests

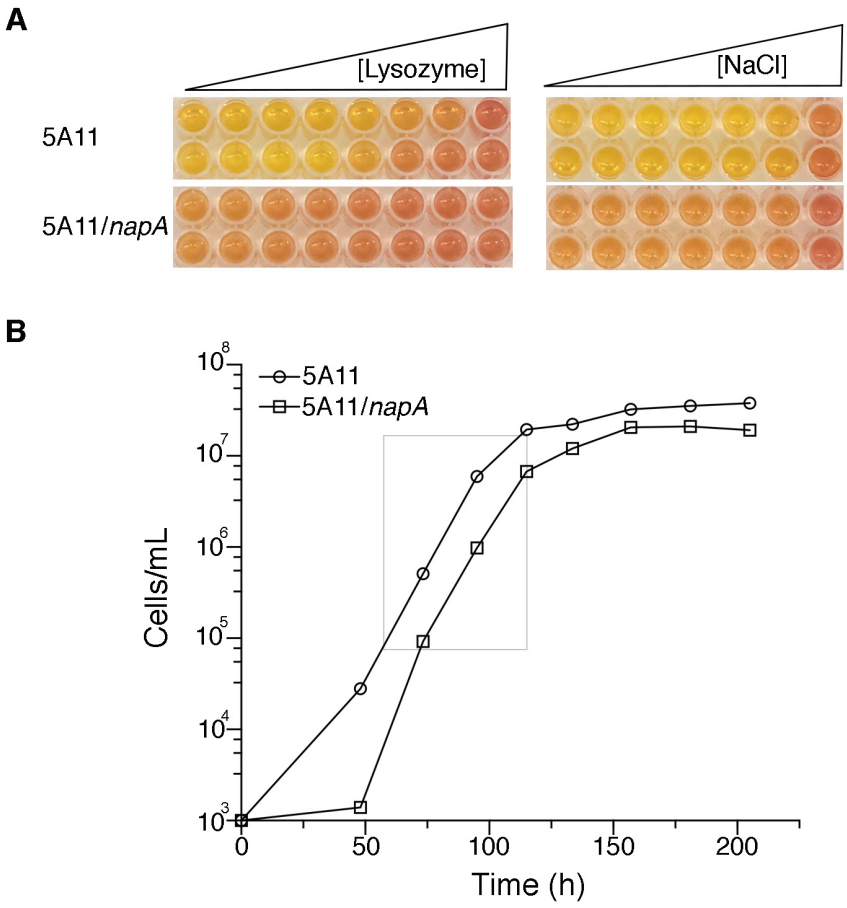

Figure 13: A) Both 5A11 and 5A11/*napA* strains were grown to 1 x 10^4 cells/mL in BSK II at 37 ^oC media prior to adding increasing amounts of Lysozyme (2 mg/mL to 0) (left) or NaCl (0.5 M to 0.4mM) (right). Cells were allowed to grow for one week in a 96 well plate prior to growth analysis using spectrophotometry. (B) Growth curves. 5A11 and 5A11/*napA* were grown at a starting concentration of 1 x 10^3 cells/mL in BSK II media. Cells were enumerated roughly every 24 hours for 10 days with the exception of the first count which occurred 48 hours after inoculation.

Figure 14: Cell envelope stress and defects of NapA deficient bacteria.

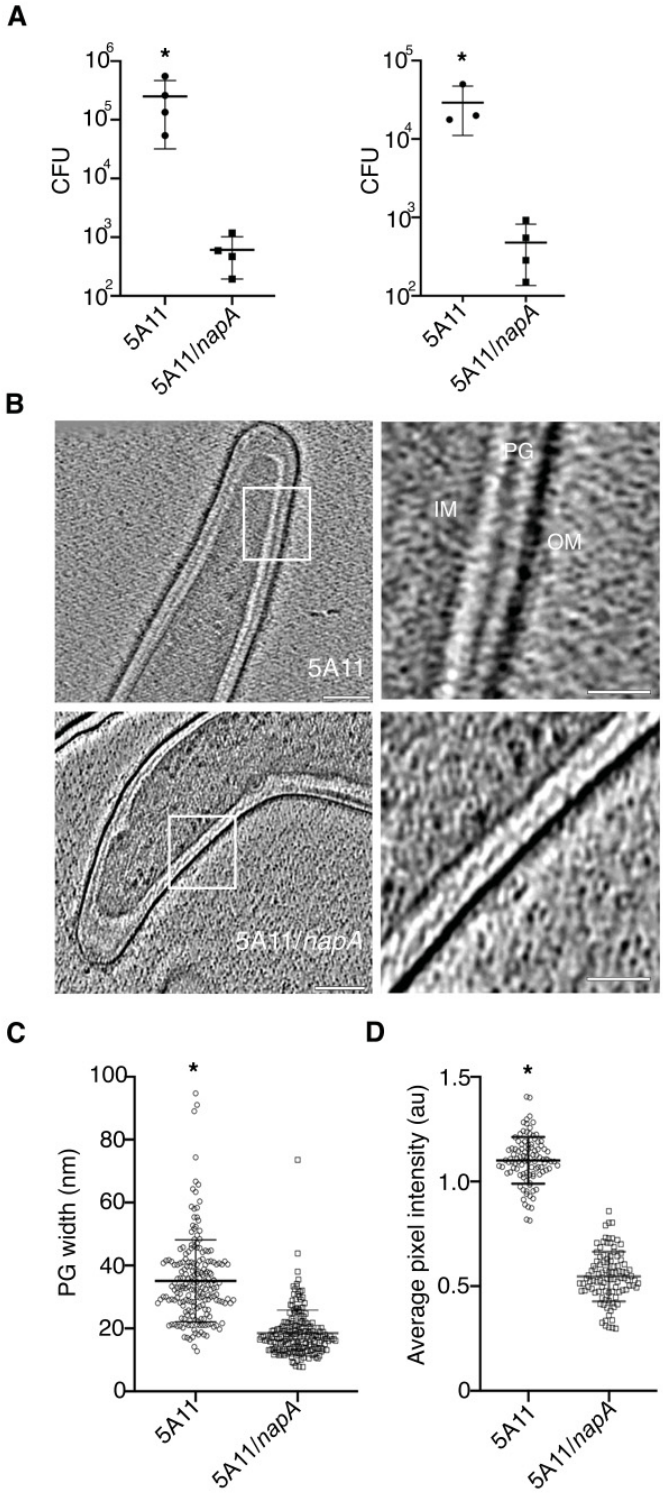

Figure 14: (A) Osmotic and lysozyme susceptibility in wild-type (5A11) and *napA* mutant (5A11/*napA*) bacteria. Following exposure to 0.111 M NaCl (left) or 0.37 mg/mL Lysozyme (right) for 18 hours, each strain was diluted in fresh media and plated. Three (wild-type) or six (mutant) weeks later, CFUs were determined. Bars shown are the mean (+/-) SD from 4 experimental BSK II plates with either strain. P-value determined using unpaired t-test, * = P <0.05. (B) Cryo-electron micrographs of the inner membrane (IM), peptidoglycan (PG) and outer membrane (OM) of the 5A11 (top) and 5A11/*napA* (bottom) strains. Scale bar 100 nm. (C) Population-level analysis of average PG width (in nm, left) and (D) average PG pixel intensity (au), normalized by sampling area. Note that measurements collected in C and D excluded PG from 10% of each cell pole since these areas are thicker and more variable.

Figure 15: NapA-PG is released in outer-membrane vesicles and together act as a neutrophil chemoattractant

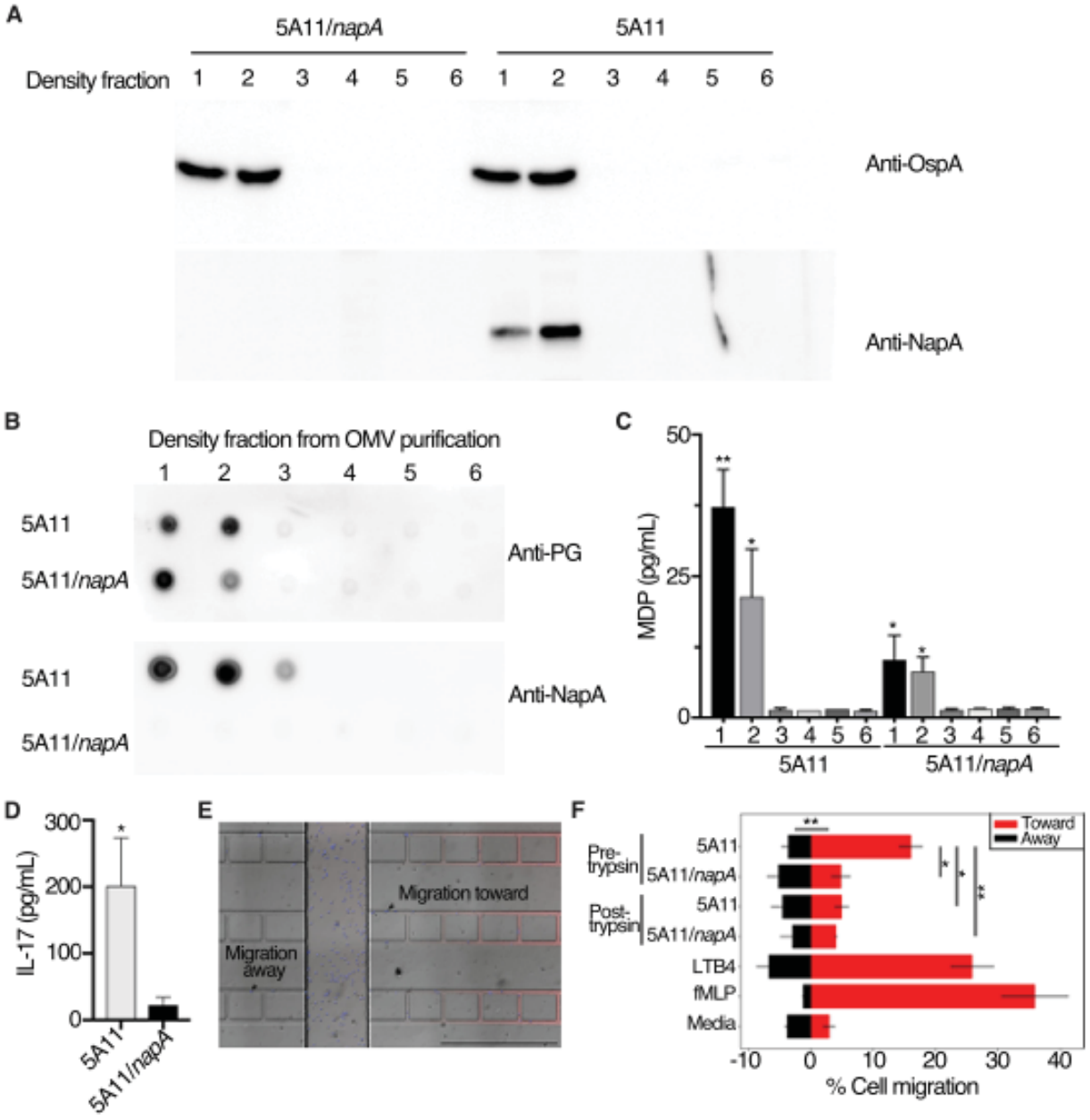

Figure 15: (A) Crude preparations of Outer-membrane vesicles (OMVs), collected from wild-type (5A11) and *napA* mutant (5A11/*napA*), were further purified by density gradient and probed for contents by western blot. OspA (above) and NapA (below) was present in OMV fractions 1 and 2. (B) The same density gradient fractions, prepared in A, were probed for PG (above) and NapA (below) by dot blot analysis. (C) Reporter assay to query each density gradient fraction for PG containing Muramyl dipeptide (MDP). Human NOD2 reporter cell line (Invivogen) was used to measure the amount of MDP in each density fraction (from panels A-C). Serial dilutions of purified MDP was used to for standards curves to back calculate the amount of MDP in each fraction. Bars shown are the mean (+/-) SD. P-value determined using unpaired Student's t-test, * = $p < 0.05$ and indicates significant difference between 5A11 density gradient layer 1 and layers 3-6. ** = $p < 0.05$ between 5A11 and 5A11/*napA* gradients layers 1 and 2 for both, samples respectively. (D) IL-17 production by human peripheral blood mononuclear cells (PBMCs). Three pools of eight mixed donor PBMCs samples were stimulated with 10 ug/mL of PG, prior to trypsin treatment, from wild-type and *napA* mutant bacteria. Culture supernatants, from each stimulation, were assayed for IL-17 by ELISA (Abcam). Normalized, mean values (+/-SD) are shown. Statistical analysis unpaired Student's t-test, * = $p < 0.05$. (E) Merged Phase-contract/epifluorescence micrograph of microfluidic competitive chemotaxis-chip (μC^3) (94) used to measure dHL-60 cell (blue) migration both toward (red) and away (black) from gradients of each stimulus. Scale bar = 500 μm. (F) dHL-60 cells show a higher percentage of cells migrating toward PG-linked NapA. Reservoirs that flank each maze were loaded with 125 μg/mL of each PG sample, diluted in dHL-60 cell culture media, and compared to opposite reservoir, which contained culture media alone. Controls included media, 10nM of Formylmethionine-leucyl-phenylalanine (fMLP), and 100nM

of Leukotriene B4 (LTB4). Data were collected over 5 hours, images captured every 2 minutes, while cells were maintained at 37°C under 5% CO_2. Results shown are mean +/- SD of three biological replicate experiments. To evaluate differences between responses ANOVA were performed with Turkey's correction for multiple comparisons (* = $p < 0.05$, ** = $p < 0.005$).

Figure 16: Phylogenetic Analysis of NapA

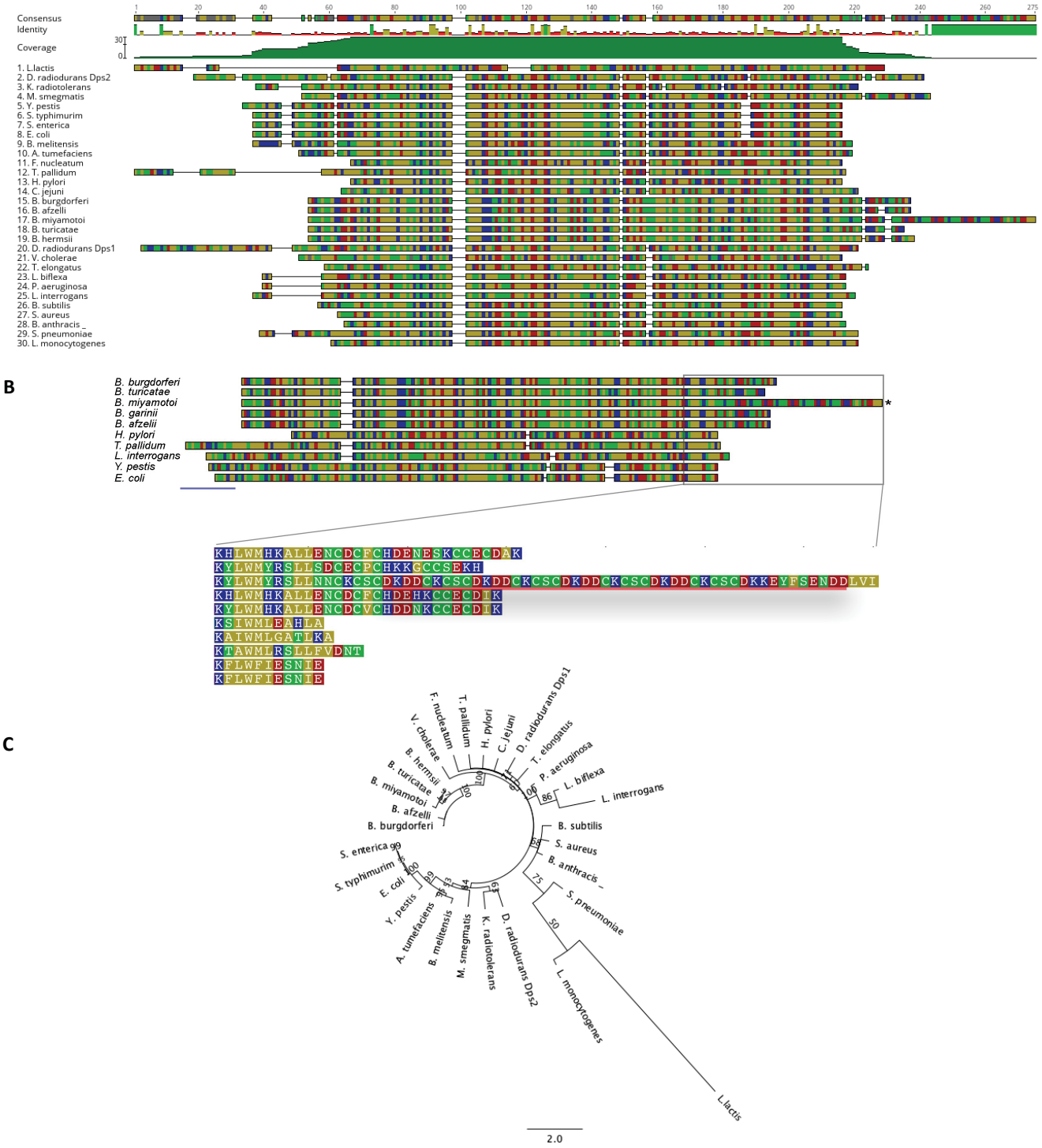

Figure 16: Phylogenetic analysis of Dps/NapA. (A) Phylogenic analysis of Dps/NapA homologues in *Borreliae, Helicobacter pylori, Treponema pallidum, Leptospira interrogans, Yersinia pestis, and Escherichia coli*. (B) Amino acid alignment of Dps/NapA homologues from bacteria in A. The Lysine-rich DNA binding domain is underlined (blue) (C) Zoomed in amino acid sequence of the C-terminus of Dps/NapA homologues. Note that the extended C-terminus contains several Cysteine residues and the repeat sequence DDCKCSC (red underline) found in *B. miyamotoi*.

References

1. Jutras BL, Lochhead RB, Kloos ZA, Biboy J, Strle K, Booth CJ, et al. Borrelia burgdorferi peptidoglycan is a persistent antigen in patients with Lyme arthritis. Proceedings of the National Academy of Sciences. 2019:201904170.

2. Kovacs-Simon A, Titball RW, Michell SL. Lipoproteins of bacterial pathogens. Infect Immun. 2011;79(2):548-61.

3. Cascales E, Bernadac A, Gavioli M, Lazzaroni JC, Lloubes R. Pal lipoprotein of Escherichia coli plays a major role in outer membrane integrity. J Bacteriol. 2002;184(3):754-9.

4. Haake DA. Spirochaetal lipoproteins and pathogenesis. Microbiology-Uk. 2000;146:1491-504.

5. Henderson B, Martin A. Bacterial virulence in the moonlight: multitasking bacterial moonlighting proteins are virulence determinants in infectious disease. Infect Immun. 2011;79(9):3476-91.

6. Beck G, Benach JL, Habicht GS. Isolation, preliminary chemical characterization, and biological activity of Borrelia burgdorferi peptidoglycan. Biochem Biophys Res Commun. 1990;167(1):89-95.

7. Purser JE, Norris SJ. Correlation between plasmid content and infectivity in Borrelia burgdorferi. Proc Natl Acad Sci U S A. 2000;97(25):13865-70.

8. Li X, Pal U, Ramamoorthi N, Liu X, Desrosiers DC, Eggers CH, et al. The Lyme disease agent Borrelia burgdorferi requires BB0690, a Dps homologue, to persist within ticks. Mol Microbiol. 2007;63(3):694-710.

9. Fraser CM, Casjens S, Huang WM, Sutton GG, Clayton R, Lathigra R, et al. Genomic sequence of a Lyme disease spirochaete, Borrelia burgdorferi. Nature. 1997;390(6660):580-6.

10. Thein M, Sauer G, Paramasivam N, Grin I, Linke D. Efficient subfractionation of gram-negative bacteria for proteomics studies. J Proteome Res. 2010;9(12):6135-47.

11. Caimano MJ, Eggers CH, Gonzalez CA, Radolf JD. Alternate sigma factor RpoS is required for the in vivo-specific repression of Borrelia burgdorferi plasmid lp54-borne ospA and lp6.6 genes. J Bacteriol. 2005;187(22):7845-52.

12. Seshu J, Boylan JA, Gherardini FC, Skare JT. Dissolved oxygen levels alter gene expression and antigen profiles in Borrelia burgdorferi. Infect Immun. 2004;72(3):1580-6.

13. Jutras BL, Chenail AM, Carroll DW, Miller MC, Zhu H, Bowman A, et al. Bpur, the Lyme disease spirochete's PUR domain protein: identification as a transcriptional modulator and characterization of nucleic acid interactions. J Biol Chem. 2013;288(36):26220-34.

14. Jutras BL, Jones GS, Verma A, Brown NA, Antonicello AD, Chenail AM, et al. Posttranscriptional self-regulation by the Lyme disease bacterium's BpuR DNA/RNA-binding protein. J Bacteriol. 2013;195(21):4915-23.

15. Jutras BL, Savage CR, Arnold WK, Lethbridge KG, Carroll DW, Tilly K, et al. The Lyme disease spirochete's BpuR DNA/RNA-binding protein is differentially expressed during the mammal-tick infectious cycle, which affects translation of the SodA superoxide dismutase. Mol Microbiol. 2019;112(3):973-91.

16. Jutras BL, Scott M, Parry B, Biboy J, Gray J, Vollmer W, et al. Lyme disease and relapsing fever Borrelia elongate through zones of peptidoglycan synthesis that mark division sites of daughter cells. Proc Natl Acad Sci U S A. 2016;113(33):9162-70.

17. Paintdakhi A, Parry B, Campos M, Irnov I, Elf J, Surovtsev I, et al. Oufti: an integrated software package for high-accuracy, high-throughput quantitative microscopy analysis. Mol Microbiol. 2016;99(4):767-77.

18. R. C. raacampbell/shadedErrorBar 2020 [Available from: https://www.github.com/raacampbell/shadedErrorBar.

19. Chang Y, Moon KH, Zhao X, Norris SJ, Motaleb MA, Liu J. Structural insights into flagellar stator-rotor interactions. Elife. 2019;8.

20. Kremer JR, Mastronarde DN, McIntosh JR. Computer visualization of three-dimensional image data using IMOD. J Struct Biol. 1996;116(1):71-6.

21. Zuckert WR. Laboratory maintenance of Borrelia burgdorferi. Curr Protoc Microbiol. 2007;Chapter 12:Unit 12C 1.

22. Boribong BP, Lenzi MJ, Li L, Jones CN. Super-Low Dose Lipopolysaccharide Dysregulates Neutrophil Migratory Decision-Making. Front Immunol. 2019;10:359.

23. Tinevez JY, Perry N, Schindelin J, Hoopes GM, Reynolds GD, Laplantine E, et al. TrackMate: An open and extensible platform for single-particle tracking. Methods. 2017;115:80-90.

24. Casjens S, Palmer N, van Vugt R, Huang WM, Stevenson B, Rosa P, et al. A bacterial genome in flux: the twelve linear and nine circular extrachromosomal DNAs in an infectious isolate of the Lyme disease spirochete Borrelia burgdorferi. Mol Microbiol. 2000;35(3):490-516.

25. Mordukhovich G, Bahar O. Isolation of Outer Membrane Vesicles from Phytopathogenic Xanthomonas campestris pv. campestris. Bio-Protocol. 2017;7(5).

26. Calhoun LN, Kwon YM. Structure, function and regulation of the DNA-binding protein Dps and its role in acid and oxidative stress resistance in Escherichia coli: a review. J Appl Microbiol. 2011;110(2):375-86.

27. Haikarainen T, Papageorgiou AC. Dps-like proteins: structural and functional insights into a versatile protein family. Cell Mol Life Sci. 2010;67(3):341-51.

28. Cooksley C, Jenks PJ, Green A, Cockayne A, Logan RP, Hardie KR. NapA protects Helicobacter pylori from oxidative stress damage, and its production is influenced by the ferric uptake regulator. J Med Microbiol. 2003;52(Pt 6):461-9.

29. Wang P, Lutton A, Olesik J, Vali H, Li X. A novel iron- and copper-binding protein in the Lyme disease spirochaete. Mol Microbiol. 2012;86(6):1441-51.

30. Codolo G, Amedei A, Steere AC, Papinutto E, Cappon A, Polenghi A, et al. Borrelia burgdorferi NapA-driven Th17 cell inflammation in lyme arthritis. Arthritis Rheum. 2008;58(11):3609-17.

31. Codolo G, Papinutto E, Polenghi A, D'Elios MM, Zanotti G, de Bernard M. Structure and immunomodulatory property relationship in NapA of Borrelia burgdorferi. Biochim Biophys Acta. 2010;1804(12):2191-7.

32. Codolo G, Bossi F, Durigutto P, Bella CD, Fischetti F, Amedei A, et al. Orchestration of inflammation and adaptive immunity in Borrelia burgdorferi-induced arthritis by neutrophil-activating protein A. Arthritis Rheum. 2013;65(5):1232-42.

33. Troxell B, Ye M, Yang Y, Carrasco SE, Lou Y, Yang XF. Manganese and zinc regulate virulence determinants in Borrelia burgdorferi. Infect Immun. 2013;81(8):2743-52.

34. Zuckert WR. Secretion of bacterial lipoproteins: through the cytoplasmic membrane, the periplasm and beyond. Biochim Biophys Acta. 2014;1843(8):1509-16.

35. Koetsveld J, Draga ROP, Wagemakers A, Manger A, Oei A, Visser CE, et al. In Vitro Susceptibility of the Relapsing-Fever Spirochete Borrelia miyamotoi to Antimicrobial Agents. Antimicrob Agents Chemother. 2017;61(9).

36. Dever LL, Jorgensen JH, Barbour AG. In vitro antimicrobial susceptibility testing of Borrelia burgdorferi: a microdilution MIC method and time-kill studies. J Clin Microbiol. 1992;30(10):2692-7.

37. Schwechheimer C, Kuehn MJ. Outer-membrane vesicles from Gram-negative bacteria: biogenesis and functions. Nat Rev Microbiol. 2015;13(10):605-19.

38. Yang X, Promnares K, Qin J, He M, Shroder DY, Kariu T, et al. Characterization of multiprotein complexes of the Borrelia burgdorferi outer membrane vesicles. J Proteome Res. 2011;10(10):4556-66.

39. Crowley JT, Toledo AM, LaRocca TJ, Coleman JL, London E, Benach JL. Lipid exchange between Borrelia burgdorferi and host cells. PLoS Pathog. 2013;9(1):e1003109.

40. Oosting M, ter Hofstede H, van de Veerdonk FL, Sturm P, Kullberg BJ, van der Meer JW, et al. Role of interleukin-23 (IL-23) receptor signaling for IL-17 responses in human Lyme disease. Infect Immun. 2011;79(11):4681-7.

41. Radolf JD, Caimano MJ, Stevenson B, Hu LT. Of ticks, mice and men: understanding the dual-host lifestyle of Lyme disease spirochaetes. Nat Rev Microbiol. 2012;10(2):87-99.

42. Chou S, Daugherty MD, Peterson SB, Biboy J, Yang Y, Jutras BL, et al. Transferred interbacterial antagonism genes augment eukaryotic innate immune function. Nature. 2015;518(7537):98-101.

43. Oliva Chavez AS, Shaw DK, Munderloh UG, Pedra JH. Tick Humoral Responses: Marching to the Beat of a Different Drummer. Front Microbiol. 2017;8:223.

44. Oosting M, Buffen K, van der Meer JW, Netea MG, Joosten LA. Innate immunity networks during infection with Borrelia burgdorferi. Crit Rev Microbiol. 2016;42(2):233-44.

45. Benach JL, Fleit HB, Habicht GS, Coleman JL, Bosler EM, Lane BP. Interactions of phagocytes with the Lyme disease spirochete: role of the Fc receptor. J Infect Dis. 1984;150(4):497-507.

46. Menten-Dedoyart C, Faccinetto C, Golovchenko M, Dupiereux I, Van Lerberghe PB, Dubois S, et al. Neutrophil extracellular traps entrap and kill Borrelia burgdorferi sensu stricto spirochetes and are not affected by Ixodes ricinus tick saliva. J Immunol. 2012;189(11):5393-

47. Nair S, Finkel SE. Dps protects cells against multiple stresses during stationary phase. J Bacteriol. 2004;186(13):4192-8.

48. Wang G, Hong Y, Olczak A, Maier SE, Maier RJ. Dual Roles of Helicobacter pylori NapA in inducing and combating oxidative stress. Infect Immun. 2006;74(12):6839-46.

49. Grant RA, Filman DJ, Finkel SE, Kolter R, Hogle JM. The crystal structure of Dps, a ferritin homolog that binds and protects DNA. Nat Struct Biol. 1998;5(4):294-303.

50. Karas VO, Westerlaken I, Meyer AS. The DNA-Binding Protein from Starved Cells (Dps) Utilizes Dual Functions To Defend Cells against Multiple Stresses. J Bacteriol. 2015;197(19):3206-15.

51. Braun V, Rehn K. Chemical characterization, spatial distribution and function of a lipoprotein (murein-lipoprotein) of the E. coli cell wall. The specific effect of trypsin on the membrane structure. Eur J Biochem. 1969;10(3):426-38.

52. Braun V, Sieglin U. The covalent murein-lipoprotein structure of the Escherichia coli cell wall. The attachment site of the lipoprotein on the murein. Eur J Biochem. 1970;13(2):336-46.

CHAPTER IV

Conclusions and Future Directions

As we slowly, but surely approach the 50-year mark of science's first diagnosis of Lyme disease and thereafter the discovery of the etiological agent, *B. burgdorferi*, we find that there is still much to learn about this world. The pathogen responsible is incredibly complex and there are numerous laboratory teams racing to find the next missing puzzle piece in the study of its biology. Lyme disease presents in patients in a similarly complex fashion and the factors that directly contribute to the pathogenesis of the disease are still under harsh investigation. This thesis has presented supporting evidence for the hypothesis that the PG^{Bb} is a contributing factor to the immunological reaction seen in the host, and that there may be other factors at play including the presence of other ligands such as the PAP NapA.

The molecular structure of PG is a bacterial signature that can be recognized, read, and even encrypted. Changes in the amino acid sequence of PG have immunological consequences and by using RNA sequencing technology, we have gained insights into this complex relationship. We show here that PG alone is capable of causing an acute pro-inflammatory response in PBMCs and these responses share similarities to the transcriptomic profiles of rheumatic diseases. Osteoclast and osteoblast homeostasis are disturbed in these diseases and interestingly we find the same sorts of pathways augmented when stimulating immune cells with PG^{Bb}. Perhaps LA is yet another example of genetic susceptibility, previously resolved bacterial infection, and some degree of autoimmunity resulting in arthritic symptoms, similar to that of RA, ReA or psoriatic arthritis. The shared clinical manifestations and the common features seen in these pathologies may help to unlock more of what is still unknown in LA.

The identification of a PAP in *B. burgdorferi* provides supporting evidence for the role of PAPs in both structural integrity and cellular response to host immunity. The physical architecture of the cell envelope in the NapA mutant is thinner, ruffled, and discontinuous thereby contributing to its increased susceptibility to stressors. Both PG and NapA are associated with one another and they can both be found in OMVs expelled from the cell under normal homeostatic conditions. The most abundant leukocyte in the body, the neutrophil, is attracted to PG-NapA which can be shed in OMVs, away from the cell itself, perhaps providing yet another mechanism of immune system evasion employed by *B. burgdorferi.*

Taken together these two findings support the role of PG in the pathogenesis of Lyme disease. Through the RNA sequencing studies this thesis work has found supporting evidence for the role of PG^{Bb} in the construction of an acute pro-inflammatory environment, and perhaps we are beginning to see the late stage consequences of PG^{Bb} in disease progression. Through the NapA studies, we have found that PG is associated with NapA both within the cell and when it is released extracellularly. This finding should push future work to consider the role of other ligands such as NapA in these studies because of the immunological implications they may hold. Peptidoglycan associated with NapA is perhaps a more biologically relevant form of the ligand and therefore may stimulate cells to a greater extent than just PG alone, as is supported in the preliminary studies outlined here.

Biological relevance in experimental design is key to understanding the pathogenesis of any disease. The identification of a PAP in *B. burgdorferi* illustrates this point beautifully. The future studies involving the use of PG^{Bb} as an immune system stimulant should consider this and other factors at play in the pathogenesis of Lyme disease. One of these factors that should also be considered is the presence of neutrophils. The cells used for the RNA sequencing analysis were

PBMCs, which traditionally exclude the presence of granulocytes due to the extraction and separation process. Among all of the PGs tested, the GO results strongly suggest that the cells present are producing genes responsible for upregulating 1) neutrophil activation; 2) neutrophil activation as involved in the immune response and; 3) neutrophil mediated immunity (Fig. 3A and 3B). Monocytes and macrophages, found in PBMC samples, release these signals such as CXCL1, CXLC2, and IL-1 to attract neutrophils to the site of infection (1). The monocytes and neutrophils rely on one another to produce and effective assault on the invading pathogen. Without the presence of neutrophils to respond to these messages from other leukocytes, we may be missing a portion of the overall acute response to PG^{Bb}.

The crosstalk between the innate and adaptive immune response is critical for the effective clearance of an invading pathogen. The onset of infection marks the start of the innate immune response and within a few days there is typically evidence of initiation of the adaptive immune response by way of T/B cell activation. Due to the complex course of Lyme disease, it is also vital to take the time to study the long-term effects of circulating PG^{Bb}. The RNA sequencing experiments were meant to capture the beginning of the adaptive immune response and the presence of the genes responsible for the production of CD74 (Class II MHC antigen presentation), IL-17 (Th_{17} differentiation), and IL-4 and IL-13 (induction of T helper cell differentiation to Th_2) (Fig. 3A, Fig. 4A, and Table 4.5) indicate that we captured a snapshot of the adaptive response. However, PG can still be found in the synovial fluid of patients 2-3 months post antibiotic treatment, indicating that a 72-hour time interval is useful, but does not capture the entire course of the disease.

Lastly, it is important to consider that Lyme disease is first and foremost a vector borne illness. The presence of the tick vector in future studies is crucial, especially to the innate arm of

the immune response. Proteins such as Salp14 (a potent anti-coagulant) or TSLPI (a complement inhibitor) found in the tick saliva provide a gateway for *B. burgdorferi* to avoid acute destruction by the immune system (2). If the innate response is compromised to any extent, this ripple effect must also be felt by the adaptive, as the two work in harmony to orchestrate a proper counterattack. Peptidoglycan is not released into the host without the presence of *B. burgdorferi* and *B. burgdorferi* is not inoculated in the host without the presence of the tick, therefore an attempt at encompassing all these factors should be made in future studies.

Both *B. burgdorferi* and the pathogenesis of Lyme disease remain systems under investigation. This thesis has provided supporting evidence for the role of PG^{Bb} as a driver of pro-inflammatory mediators. The transcriptomic profile from immune cells stimulated with PG^{Bb} looks in many ways similar to that of other inflammatory rheumatic diseases and thus may offer insights into future treatments for Lyme arthritis moving forward.

My personal hope is that this work will provide a supporting framework for the next set of studies aimed at continuing the delineation of the role of PG^{Bb} in the pathogenesis of Lyme disease.

References

1. Prame Kumar K, Nicholls AJ, Wong CHY. Partners in crime: neutrophils and monocytes/macrophages in inflammation and disease. Cell Tissue Res. 2018;371(3):551-65.

2. Narasimhan S, Kurokawa C, Diktas H, Strank NO, Cerny J, Murfin K, et al. Ixodes scapularis saliva components that elicit responses associated with acquired tick-resistance. Ticks Tick Borne Dis. 2020;11(3):101369.